Doctoral Dissertation
Doctoral Program in Materials Science and Technology (30th Cycle)

Advanced and Functional Materials for Sodium Secondary Batteries

By

Francesca Colò

******

Supervisor(s):
Prof. Claudio Gerbaldi

Politecnico di Torino
2015-2016-2017

Declaration

I hereby declare that, the contents and organization of this dissertation constitute my own original work and does not compromise in any way the rights of third parties, including those relating to the security of personal data.

Francesca Colò

2017

* This dissertation is presented in partial fulfillment of the requirements for **Ph.D. degree** in the Graduate School of Politecnico di Torino (ScuDo). The public examination will be conducted in English.

Head of the Ph.D. Program in Materials Science and Technology: Prof. Claudio Badini.

To my family…

Acknowledgment

This PhD experience for me was really important for grew up not only professionally, but also as person. For that a hefty thanks to my Supervisor Prof. Claudio Gerbaldi, for the patient, the knowledge which taught me, and the great person that he is. Not least, I want to thanks also all the members of the GAME Lab Group, current and not, with a particular regard to Jijeesh Nair and Federico Bella, for their availability at all the times, insight and technical contributions that have resulted in this thesis. Thanks to Giusy Meligrana, she was the first person that teach me something new in batteries preparation, in particular she teach me how to prepare electrodes, and some procedures of inorganic synthesis, that was really the first think that I done at Politecnico di Torino, before starting the PhD "*journey"*. Thank you to Luca Porcarelli, for support me during my first time in Torino, helping me to know this wonderful city. Thanks to Simone Casino, Simone Zanarini and, Italo Doberdò, which share with me the office space during my first time at Politecnico. A great thanks to Francesca Di Lupo, she was for me very important for my scientific introduction on the labs of the group, and for become a friend.

Thanks to Marisa Falco and Giulia Piana, I cherish to share the lab and office spaces with you.

Thanks also to Prof. Daniel Brandell which gave me the possibility to spend 5 months at Ångströmlaboratoriet at Uppsala University, in his battery group. Thank you also to PhD Stèven Renault, which follow me for the experimental part in Uppsala. I want to thanks also all the thesis students and PhD students known during this period, for the fun and specially because they made me feel at home, despite my dear were so far.

Thank you to my parents, I think that a river of words is not enough…

Thank you to my big brother Enrico, very important in all the time of my life.

Aunt Giorgia and uncle Luciano, what to say? My second parents, my anchor. G. Luca Trasatti, a brother, a friend, an example (also for avoid bosh). Bianca Ciccarelli, thanks for gave me the possibility to met Emanuele, a little/big child.

In the order of birth: Flavio, Valerio, Emanuele, I love you… remember this words: “Aunt Francesca, albeit distant, will be always for you. Always!”

Luca F. Martinat, thank you because you teach me some things that other people couldn’t, in particular life things. Thank you, because you choose me for open your heart. Thank you, because you decide to share a part of your life with me. Thank you because are you.

In the end, but not for importance, I want to thanks all, and I repeat, all, the people who did not believed in me. Now I can say: “I won”! Is so sweat the victory. You know? It’s not whether you get knocked down, it’s whether you get back up.

“I may break my arm, my leg, my neck,
but I will not let that freaking guy go”.
Françoise Pienaar
(Captain of the South African rugby national team 1993-1996)

Abstract

Over the past decades, the relevance of clean and efficient energy production and storage has enormously grown worldwide, primarily driven by concerns over global warming, dwindling fossil-fuel reserves and increasing demand for portable electronics, electric mobility and grid storage systems. Modern energy economy is at a serious risk due to a series of factors, including the continuous increase in the demand for oil, the depletion of non-renewable resources, the dependency on politically unstable oil producing countries and the related CO_2 emissions, which results in global temperature rise with associated dramatic climate changes. Near-future implementation of renewable energy will demand a sudden growth of inexpensive, safe and efficient energy storage systems, thus the extension of batteries to large-scale storage will become essential in addressing the global challenge of clean and sustainable energy.

In such a scenario, particularly for large-scale stationary electric energy storage systems, is crucial to find a valid alternative to lithium, in order to develop battery prototypes with similar characteristics in terms of energy densities and performances, but cheaper than the existing ones, and with a better look at the sustainability of the all of the components of the cells. Amongst the post-LIBs technologies under development, sodium ion batteries (NIBs) appears to be the most appealing and ready-to-use system. Indeed, sodium mineral resources are "unlimited", attainable at low cost, and equally geodistributed. Clearly, technological advances, particularly in materials' science viewpoint, must be effectively implemented: the electrode materials need to have high capacity and durability, while the electrolyte should be a solid membrane capable of high ionic conductivity even at ambient temperature, with good mechanical and interfacial properties and stable performances. In all cases, the materials must be inexpensive, ecologically friendly and safe.

Taking into account the abovementioned challenges and expectations particularly for large-scale energy storage devices in the near future, the target of this PhD Thesis was the study and the development of novel polymer electrolytes and organic electrodes to fabricate high energy, safe and ecofriendly sodium-ion batteries and the assessment of their physico-chemical characteristics and electrochemical behaviour.

The outcome of the work contains six chapters, comprising introductory section and concluding remarks. *Chapter 1* deals with an introductory overview on the global energy scenario, present energy storage systems and future alternatives. *Chapter 2* highlights the basic concepts and fundamentals of batteries and elucidates the different components of sodium-based batteries, comprising a concise explanation of the materials and components relevant to the Na-ion battery technology. *Chapter 3* reviews in details the different sodium ion conducting polymer electrolytes developed by the scientific community during recent years, the state of the art of polymer-based electrolytes is illustrated along with the next future prospective in this field.

The experimental part of this thesis deals with the research work carried out on the development of highly performing electrolyte materials for Na-ion cells. In *Chapter 4* the development of cellulose-based hybrid polymer electrolytes for green and efficient Na-ion batteries is presented. This is the first ever report where the useful characteristics of carboxymethylcellulose sodium salt as additive in a Na^+-ion conducting polymer electrolyte are explored. The same Na-CMC is also used as binder for the active electrode material particles, which enables the overall process including the electrodes and electrolyte preparation to be carried out through very simple, cheap and absolutely eco-friendly water based procedures. The preliminary results of lab scale cell testing in terms of galvanostatic charge/discharge cycling strongly recommend the use of such hybrid solid polymer electrolyte for the development of safe and sustainable Na-ion polymer cells.

Chapter 5 details the experimental results regarding the UV-induced photopolymerization strategies adopted to produce crosslinked quasi-solid polymer membranes, highly suitable as electrolyte separators in Na-ion cells. In particular, the first section demonstrates the possibility of preparing gel-polymer electrolyte membranes using reactive methacrylic-based oligomers, together with different reactive diluents and some organic plasticisers. The prepared polymer membranes are activated by a swelling process to incorporate the sodium salt (source of Na^+ ions) and, finally, fully characterized in both physical and electrochemical point of view. Very high values of ionic conductivity are obtained even at ambient temperature, results almost comparable to the values obtained for liquid electrolytes. These swelled methacrylic-based polymer membranes can provide efficient cycling behaviour as electrolyte separators in Na-ion cells. The second section deals with an innovative approach, in which a rapid one-step process is proposed to prepare quasi-solid polymer electrolyte membranes in a facile and versatile way, so that the maximum advantage of UV-induced photopolymerisation

can be exploited. The poly(ethylene oxide) – PEO based polymer electrolytes are prepared by directly incorporating the Na-X electrolyte solution into the reactive mixtures during preparation. This approach is highly advantageous because it avoids the time consuming swelling step. In fact, in less than 15 minutes, a ready-to-use truly quasi-solid polymer electrolyte membrane can be prepared, showing promising characteristics to be used as a highly ionic conducting, safe separator in sodium based cells. The battery assembled with the crosslinked PEO-based electrolyte can provide a stable specific capacity of 250 mAh g^{-1} at ambient temperature and demonstrates to be very stable upon prolonged galvanostatic cycling at 0.1 mA cm^{-2} for more than 6 months of continuous operation. This rapid technique gives the opportunity to prepare polymer electrolytes in a fast way, which could give easy scale up features if considered for bulk industrial production.

The final part of the PhD thesis work is focused on the development and electrochemical characterization of a carboxylate organic electrode for NIBs, the disodium benzenediacrylate (Na_2BDA). The material was synthesized and optimized during a 6 months' stage of research at the Ångströmlaboratoriet (Ångström Laboratory) of Prof. Daniel Brandell at the Uppsala University, Sweden. This is thoroughly discussed in *Chapter 6*. The main target is to find the most suited liquid electrolyte to exploit the full potential of the material. Such a study is fundamental particularly for organic electrodes, due to their high solubility in liquid electrolyte media, which always leads to rapid decay in electrochemical performances. The use of different (aqueous Na-CMC and non-aqueous PVdF) binders is also investigated, along with the use of mechanical calendering during electrode preparation in order to understand if the cell performances are affected to the composite electrode formulation. The electrochemical study is extended to severe rate capability test at ambient temperature as well as very long-term constant current cycling up to 5C current rate, which confirms the very long-term stability of the newly developed organic electrode as demonstrated by the very stable capacity output in Na metal cells upon prolonged constant current discharge/charge cycling for over 3700 cycles at ambient temperature.

Overall, the efficient implementation of safe and ecofriendly polymer electrolytes in sodium based rechargeable batteries is effectively demonstrated by exploiting UV-induced photopolymerization that, compared to other techniques, is simple, fast, eco friendly and energy saving, thus easily scalable to the industrial level. Moreover, the promising prospects of organic materials are successfully demonstrated as valid alternatives to common inorganic electrodes in NIBs, especially when the severe solubility issues in common liquid electrolytes are

prevented, which can lead to different beneficial effects, not only from the environmental point of view, but also for the realization of flexible, lightweight and low-cost Na-ion battery electrodes.

Contents

Chapter 1

Introduction

1.1 Context

Nowadays, humankind is profoundly dependent from electric energy. Despite the well-known global concerns about the use of fossil fuels, which are finite, non-renewable, and environmentally pollutant as for the huge quantity of CO_2 released every day, we are massively exploiting them in order to satisfy the present energy demand. It is estimated that we need to double our present rate of energy production by 2050, in order to cope not only the actual energy needs, but also to face its forthcoming increase due to the ever increasing global population [1].

Modern lifestyle is focused on the use of portable devices (laptop, mobile phones, smart watches, etc.); actually, without them we would not know how to deal with the most common daily actions. Transportation, public lighting, the continuous need to have electricity suitable for an intensive production, the next smart grid future, are only few examples of the gigantic amount of energy we currently need [2].

The major challenge of this century is to replace the non-renewable resources with sustainable energy supplies. The use of renewable resources, such as wind and solar, is one of the key point in this respect. However, renewable energy technologies are intrinsically intermittent in nature; therefore, they require a very efficient, low cost and eco-friendly storage system to effectively exploit the amount of energy they produce [3-5].

Public/private transportation is another important field where fossil fuels are widely exploited. According to the report from International Energy Agency in 2017, transportation accounts for more than half of the global oil demand, at around 52 million barrels of oil per day (mb d^{-1}). At 1.9 % per year, transport oil demand has grown faster than all other energy demand sectors since 2000 and has contributed at 80 % to the total global oil demand growth between 2000 and 2015. It means that this sector is one of the biggest responsible for climate concerns, with carbon dioxide emissions of 7.8 Gt registered in 2015, the 75 % of which is ascribable to road freight vehicles. Clearly, they play a key role in the global economy, and it is necessary to switch towards clean transportations by developing efficient hybrid electric and electric vehicles (HEVs, EVs), thus drastically reducing CO_2 release and effectively contrasting the rapid global climatic change, [6,7].

In general, it is urgent to proceed with a massive use of renewable resources and the widespread diffusion of electric cars. In all of these technologies, the use of an efficient energy storage system is crucial to their effective application [8]. As a result, in the last years batteries became a fundamental device, particularly rechargeable (secondary) batteries based on lithium electro-chemistry. Indeed, lithium batteries, and their evolution lithium-ion batteries (LIBs), are considered the most powerful choice compared to other technologies. The reason for a battery chemistry based on lithium depends on its number of advantageous characteristics. Li is the lightest of all metals (density = 0.53 g cm^{-3}) with the lowest redox potential ($E°_{(Li^+/Li)}$= −3.04 V vs SHE), which accounts for developing electrochemical cells with high energy density (lithium theoretical specific capacity is 3860 mAh g^{-1}) (Fig. 1.1).

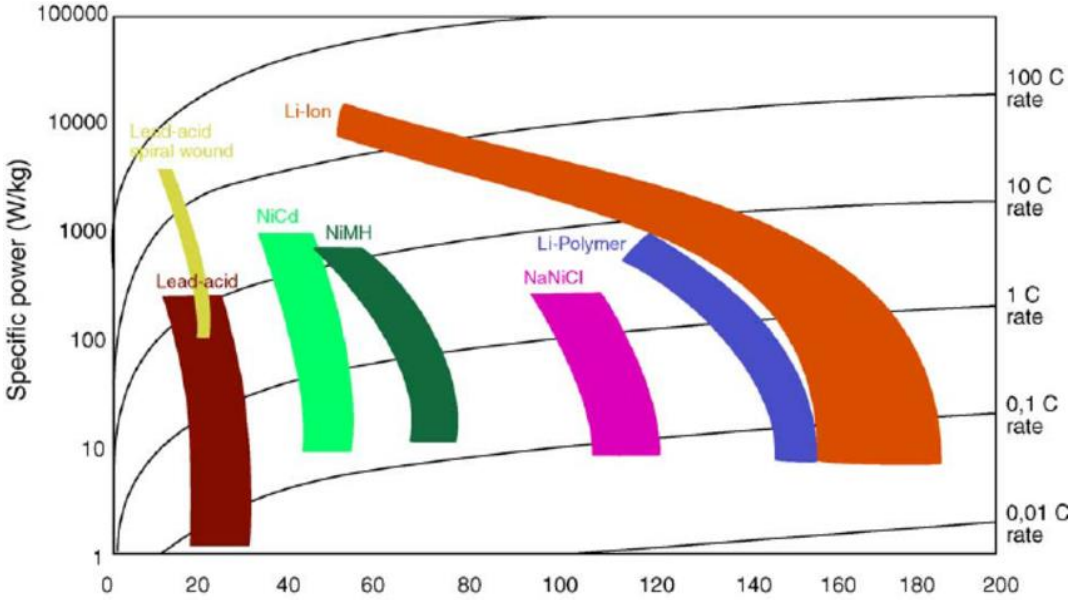

Fig. 1.1 Ragone plot of Specific Energy (Wh Kg^{-1}) vs. Specific Power (W Kg^{-1}). Comparison of different common battery technologies. (Taken from [9])

After the first commercialization in 1991 by Sony, LIBs become the most common energy storage devices for consumer electronics. By far, in the last 30 years electric transportation has grown very fast and, now, we would say that the "electric car" is real and not anymore just a dream in science fiction. Fig. 1.2 describes the actual global EV market and gives a perspective up to 2025, thus enlightening the importance of rechargeable lithium batteries.

As previously discussed, large-scale stationary electrical energy storage is another fundamental energy sector. Energy storage is indeed a global concern [3,9], especially when the implementation of new renewable resources for energy production is envisaged, such as solar and wind power, which are essentially different from the ordinary energy generation, due to their intrinsically discontinuous nature. Indeed, the power output of the Sun is limited by the circadian cycles, and wind is unpredictable both in duration and in intensity. As a result, scientific community, industry backers and policy makers are constantly searching for a fast-acting energy storage. As M. Pasta *et al.* said *"Energy storage systems used for this application must be deployable across the grid, have extraordinarily long cycle life, be capable of high power charge and discharge in minutes, have very high energy efficiency and, above all, have low capital and lifetime costs"* [10]. Batteries, which store energy in the form of (electro-)chemical energy, are the most suitable system, to guarantee high energy density [10]. Actually, the most commonly used batteries are lead acid, LIBs, sodium sulphur (NaS) and

flow batteries; the latter two being promising for low-rate grid storage applications, while LIBs and lead acid batteries are more attractive for transient grid applications, such as short-term smoothing of solar and wind plants [11].

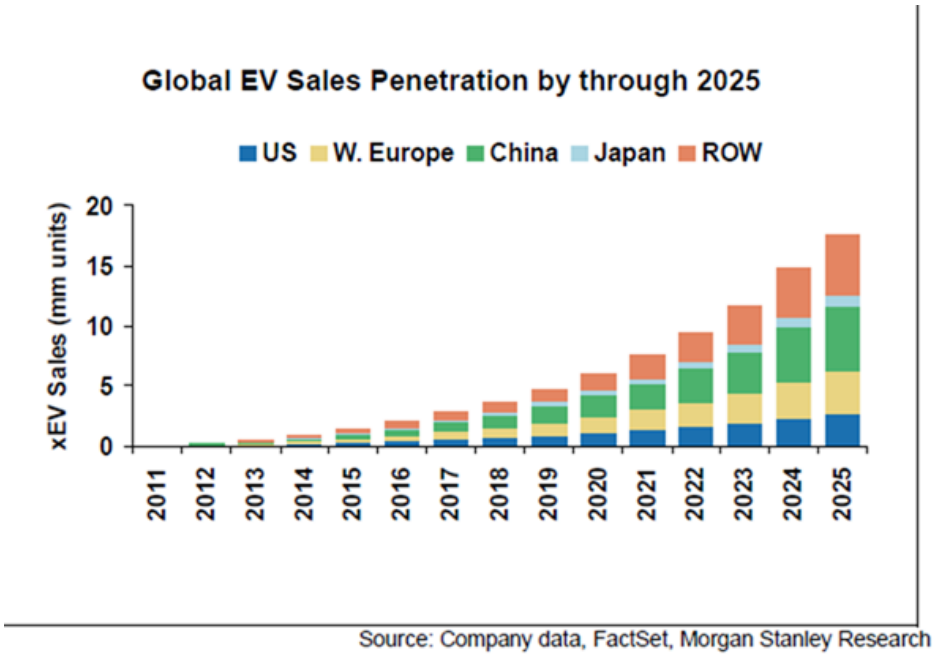

Fig. 1.2 Morgan Stanley projections on electric vehicle (EV) market (ROW = ring of wealth) Taken from: http://www.zdnet.com/article/tesla-will-it-be-americas-fourth-automaker/

Compared to all the other types of batteries, LIBs are the most widespreadly used at present, and are still object of intense study, in order to improve the performances and the characteristics of the existing prototypes, as well as to decrease the current prize of the final product and make it more ecofriendly [12]. Lithium is named after the Greek word “lithos” meaning “stone” and, due to its physico-chemical characteristics of high reactivity and flammability, it never occurs freely in nature but only in the form of ionic compounds, combined with other elements [13]. As an element, Its relative abundancy in the solar system is lower than 25 of the first 32 chemical elements [14]. Very recently, the massive use of lithium-based technology caused an enormous increase in the demand for both the metal and its compounds; moreover, most of the resources are constrained in few economically/politically unstable countries. Fig. 1.3 gives an overview of the global distribution and the averaged resources of Li. Besides China, the 54% of the total amount of lithium compounds (in form of brine and ores) are geolocalised in

South America, in an area called “the triangle of lithium” between Chile, Argentina and Bolivia. All of these factors in the last years contributed to triplicate the prize of lithium, calculated for the lithium carbonate equivalent (LCE), in the global market, from 2,000 \$ t^{-1} in 2000 to 6,000 \$ t^{-1} in 2017 (Fig. 1.4) [15]. In a recent assay, J. M. Tarascon claimed for lithium as “the new gold” [16].

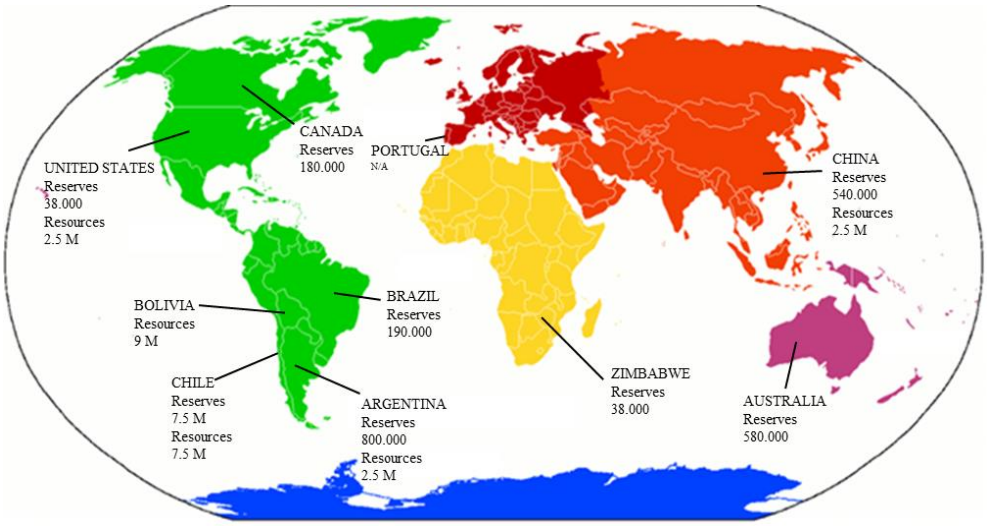

Fig. 1.3 Global overview of lithium reserves and resources. Data taken from ref [15]

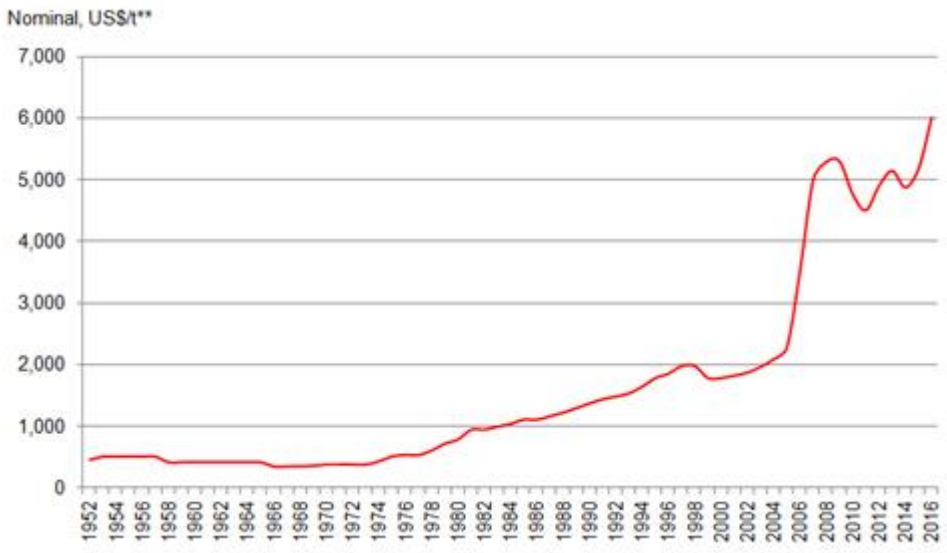

Fig. 1.4 Increment of prize of lithium, from 1952 to 2016 (taken from https://www.wealthdaily.com/articles/lithiums-other-half-the-one-you-dont-hear-about/8386)

In such a scenario, particularly for large-scale stationary electric energy storage systems, is crucial to find a valid alternative to lithium, in order to develop battery prototypes with similar characteristics in terms of energy densities and performances, but cheaper than the existing ones, and with a better look at the sustainability of all the components of the cells [17]. Amongst the post-LIBs technologies under development, sodium ion batteries (NIBs) appears to be the most appealing and ready-to-use system. Indeed, sodium mineral resources are "unlimited", attainable at low cost, and equally geodistributed. Historically, the advancement of NIBs moved on in paralleled with LIBs; indeed, several scientific research articles of the '80 and '90 reported on the development of different Na-based materials and storage systems. Unfortunately, this investigation was deserted immediately after the first commercialization of LIBs, particularly at an industrial level [18]. Nowadays, NIBs started to re-emerge in order to accommodate the necessity to replace the lithium chemistry in the field of batteries, and because it offer the prospect of very similar performances.

Taking into account the above detailed considerations, the research work done in the three years of Ph.D. studies, and here reported and discussed, is focused on the development of novel advanced materials, mainly polymer electrolytes, being high performing, safe and low cost, for the next generation of secondary Na-ion batteries, and the assessment of their physico-chemical characteristics and electrochemical behaviour.

Chapter 2

Fundamentals of a battery

2.1 Introduction on secondary batteries

"A battery is a device that converts the chemical energy contained in its active materials directly into electric energy" is the first sentence of the HANDBOOK OF BATTERIES by D. Linden and T. B. Reddy [19]. It means that the chemical energy stored in the active materials of a cell is spontaneously converted into electricity by means of an electrochemical oxidation-reduction (redox) reaction.

In general, the word "battery" is often used improperly to define any device able to supply an electrical power. On the contrary, one should consider that a battery is the final prototype (complete name: battery pack) composed of sub-units called "modules", each module is then composed of several cells that are connected one to another in series or in parallel.

A cell consists of three main components: a positive and a negative electrode responsible for the chemical reactions, and an electrolyte, which connects the electrodes and allows the ion transfer between them. The electrodes are connected by an external circuit where the electrons generated during the redox reactions flow.

The scheme in Fig. 2.1 shows the basic operation of a cell: at the negative electrode, the anode, the oxidation reaction occurs, the electrons flow into the external circuit toward the positive electrode, the cathode (the positive pole), where the reduction reaction takes place. At the same time, the ions move into the electrolyte solution, typically a solvent with dissolved salt, soaked in a separator, which physically separates the electrodes preventing internal short-circuits.

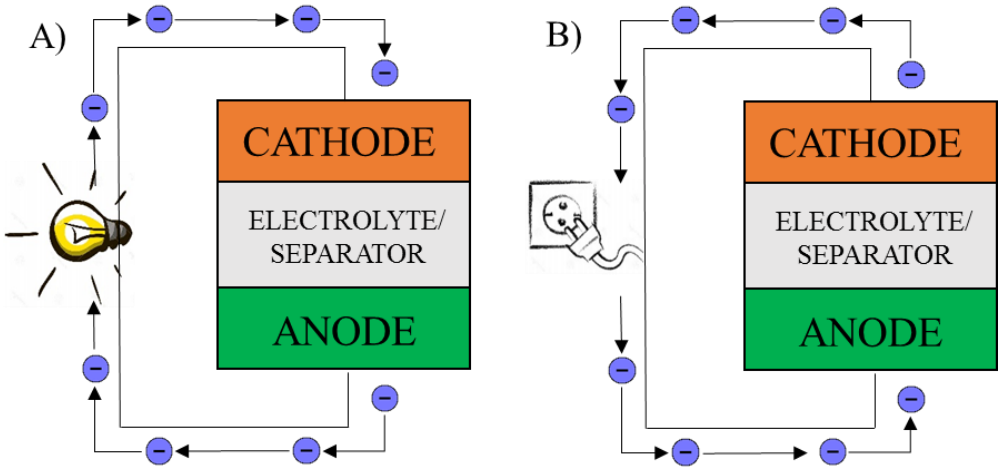

Fig. 2.1 Schematic representation of an electrochemical cell. Discharge process on the left, charge on the right.

Batteries can be classified in primary (disposable), in which the reaction in the cell is not reversible, and secondary or rechargeable, where the redox reactions are reversible. Primary cells can only convert the chemical energy into electric energy, and their operation proceeds until the capacity of the active materials ends. Examples are the alkaline manganese cells, the zinc-silver oxide, or the famous 3 V cells, based on lithium metal combined with different cathodes. One of the most important application for lithium-primary cell technology is in cardiovascular medicine, mainly used in implantable pacemakers (1970, the lithium iodide cell manufactured by Wilson Greatbatch).

Secondary (rechargeable) cells are characterized by their ability to regenerate the electrode materials after the discharge process (spontaneous) by providing electric energy from an external source, which forces the opposite (not spontaneous) redox reaction to take place. The first example of rechargeable battery is the LEAD-ACID CELL (1859 by Gaston Planté) still widely used in the common vehicles based on internal combustion engine (ICE). At the end of the XIX century the Ni-Cd wet-cell was invented , widely used in small electronic devices, but rapidly overcome during 1990s by the advent of nickel-metal hydride (Ni-MH) batteries and LIBs.

As anticipated in the introduction, the work of this thesis is focused on rechargeable batteries, in particular on the use of sodium chemistry as an alternative to lithium. The working principle of the Na-ion battery (NIB) is basically the same of LIB. The sketched picture shown below (Fig. 2.2) illustrates the typical working system of a NIB, where sodium ions are shuttled between the negative and the positive electrodes through an aprotic electrolyte containing a sodium salt

dissolved. The electrolyte is typically soaked in a separator that allows the ions to move back and forth from/to the electrodes, but at the same time avoids the physical contact between them.

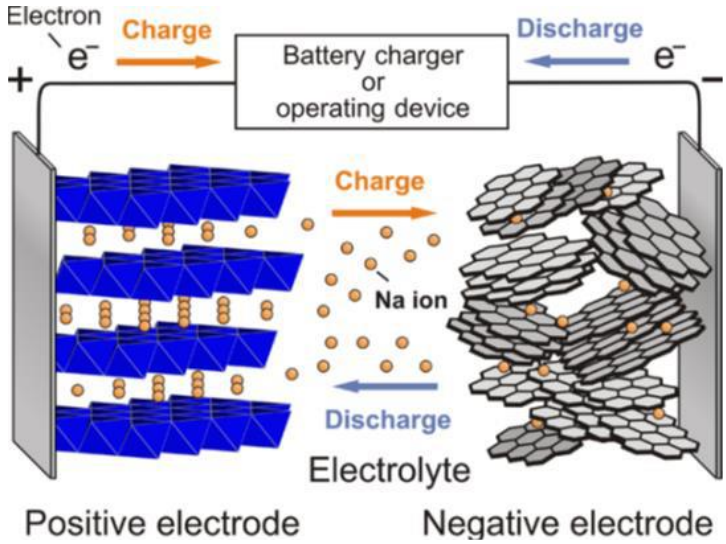

Fig. 2.2 Schematic illustration of the operating principle and components of a sodium-ion battery. (Taken from ref [20])

Typically, both the electrodes have an open structure able to allow and store Na^+ ions. More generally, the anode is the "sodium sink" and the cathode is the "sodium source". During charge (providing electric energy from the external) Na^+ ions are de-inserted from the positive electrode as resulting from the oxidation of the active material:

$$Na_xM_yY_z \rightleftharpoons Na_{(x-n)}M_yY_z + nNa^+ + ne^-$$

The nNa^+ ions move towards the negative electrode across the electrolyte solution and are inserted in the structure of the anode active material, which is reduced:

$$A_mB_w + nNa^+ + ne^- \rightleftharpoons Na_nA_mB_w$$

The complete process can be generalized as follows:

$$Na_xM_yY_z + A_mB_w \rightleftharpoons Na_{(x-n)}M_yY_z + Na_nA_mB_w$$

During discharge the full process is reversed, with the spontaneous oxidation of the anode and the ensuing reduction of the cathode active material.

2.2 Components of a Na-ion battery

Like LIBs, NIBs should have peculiar characteristics in order to meet the specific market demand, particularly in terms of energy density, *viz.* the energy output from a battery per unit mass (Wh Kg^{-1}) or per unit volume (Wh dm^3) (Appendix A). Moreover, paying attention on cost and environmental impact is recently become fundamental to assure a brighter future.

As said before, a secondary battery is composed of three main components: the anode, the cathode and the electrolyte (sometimes, the separator is considered the fourth element). All the components must comply with the requirements set out along the years in this field of research and they should work synergistically when they are contacted together.

In the following sections, the most widely investigated materials, and their main features, for modern Na-ion batteries will be briefly described.

2.2.1 Electrode materials for NIBs

The choice of the electrodes' active materials is crucial to obtain battery prototypes with high performance. Indeed, as summarized in Appendix A, the energy delivered from a battery is given by the product of the capacity (Q) and the OCV (open circuit voltage) of the cell at 100 % of its state of charge.

Actually, in the literature we may find a wide selection of materials for NIBs, most of them being studied by a "lithium like" research approach, which means that the electrode materials are substantially the same of LIBs, but sodium replaces lithium in their structure. However, this kind of attitude does not provide exactly the same performances that are obtained in lithium chemistry. The best example in this respect is graphite. Indeed, graphite is the anode material of choice in LIBs because of its high gravimetric and volumetric capacity, but it cannot be used in NIBs because of its negligible electrochemical activity.

Therefore, is important to define novel active materials, specifically selected for Na chemistry, and follow their extensive investigation and optimisation. Fig. 2.3 shows the diagram of potential (vs. Na^+/Na) versus specific capacity for the different kinds of electrodes currently used in NIBs.

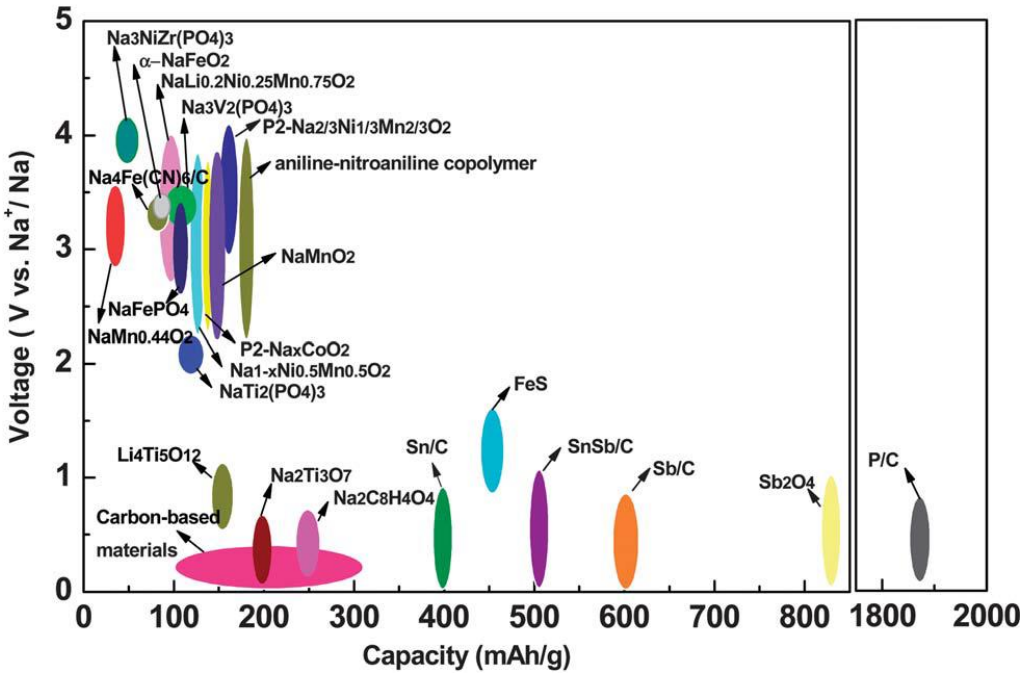

Fig. 2.3 Specific capacity vs. operating potential range of several common active materials for NIBs (taken from [21]).

2.2.1.1 Anode materials

The most attractive anode material would be clearly sodium metal, because of its relatively low redox potential and low atomic weight, which provide the Na anode with a high theoretical specific capacity (1166 mAh g^{-1}, that is competitive with 3860 mAh g^{-1} for Li) in many applications [18]. The Achilles heel of the rechargeable sodium battery is the anode's susceptibility to failure during the charging process. Specifically, during battery charge, sodium ions deposit in rough, low density and uneven patches on the negative electrode, even at current densities below the limiting current where classical instabilities such as electro-convection that drive rough, dendritic deposition are expected to be less important [22,23]. Dendrites on Na (and Li) arise from inhomogeneities in the resistance of the solid–electrolyte interphase (SEI), formed spontaneously on the anode surface when in contact with an electrolyte. The resulting concentration of electric field lines on faster growing regions of the interface drives the morphological instability loosely termed dendrites [24]. At later stages, uncontrolled dendritic deposition leads to metallic structures able to bridge the inter-electrode space, ultimately short-circuiting the cell. Short-circuits lead to two catastrophic failure mechanisms: (i)

Thermal runaway that drives chemical reactions in the electrolyte, ending the cell life by fire, explosion or both [25-27]; and (ii) Melting and breakage of the dendrites, which electrically disconnect the active material particles in the electrode [28,29], causing rapid or gradual reduction in the storage capacity of the anode. Unlike LIBs, where dendrite-induced short circuits are considered the dominant failure mechanism, chemical reactions between the electrolyte and the metal anode are regarded as the most important mechanism of cell failure in NIBs with Na metal anode. Na metal also has a lower melting point than Li, which makes batteries based on Na more prone to failure by thermal runaway [30-32].

The drawbacks described above forced the research community to evaluate different kind of negative electrode active materials. The anode materials for NIBs can be classified in the same categories of LIBs: carbonaceous materials, oxides and sulfides, alloys, and organic compounds. Thus, the use of sodium metal is commonly limited to the laboratory research in order to evaluate the electrochemical behaviour of electrode materials.

As said before, sodium ions cannot intercalate reversibly inside the layered structure of graphite when the common carbonate-based electrolytes are used [33]. However, recent studies proved that graphite might be used in combination with ether-based electrolytes [34-36]. Amongst graphite like materials, hard-carbons (so-called nongraphitizable carbon) are the most studied negative electrodes for NIBs. The first sodium cell with hard-carbons obtained by pyrolysis of sucrose, reported by Doeff et al. [37] in 1993, achieved reversible capacities up to 300 mAh g^{-1}. In such materials the electrochemical potential of Na^+ insertion is close to the one of the sodium metal electrode, likely accounting for a pseudocapacitive mechanism where sodium ions fill the porosity of the material rather than an intercalation process (Fig. 2.4).

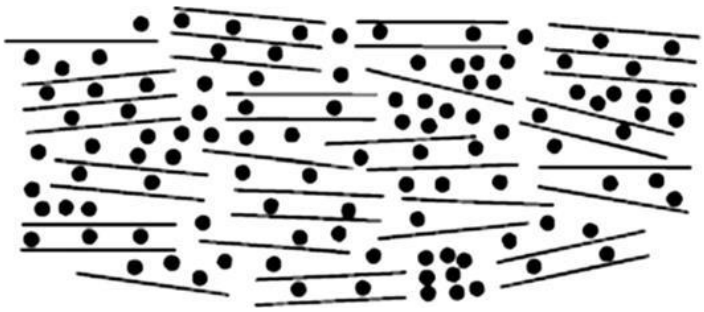

Fig. 2.4 Representation of sodium intercalation into hard carbon, the ‘‘house of cards’’ model. (Taken from [38]).

Many structural models of hard-carbons have been proposed so far and display a wide variety of morphologies such as nanowires, N-doped porous carbon nanosheets and nanosphere [39].

Recently, Komaba et al.[40] demonstrated good performances of hard-carbons in full cell configuration using $NaNi_{0.5}Mn_{0.5}O_2$ as cathode, along with good cycling stability in the potential range of 1-3.5 V vs. Na^+/Na.

Besides carbonaceous materials, oxides are also widely investigated for NIBs. In LIBs, they undergo reversible electrochemical reaction of lithium by means of the so-called conversion reaction and they recently demonstrated promising characteristics also in sodium cells [18,41,39]. In particular, Transition Metal Oxides (TMO, where M = Co, Ni, Cu, Fe, etc.) have been intensively studied, because of their practical reversible specific capacity up to 700 mAh g^{-1}, safety, environmental benignity and low cost. These oxides did not react with Na according to the classical insertion–deinsertion mechanism, but the Na^+ ions can be stored reversibly, upon complete reduction of the metal, according the following reaction:

$$(bc)Na + M_aO_b \rightleftharpoons bNa_cO + aM$$

Among the different TMO studied as anodes for NIBs, TiO_2 polymorphs (amorphous, anatase, bronze and rutile) have attracted great attention due to their extraordinary stability, low toxicity (it is very useful for medical purposes: i.e. sun creams, and other technological application such as Dye Sensitized Solar Cells [42]), relative abundancy of titanium and low cost. TiO_2 has a working potential below 1 V and is able to deliver an acceptable capacity around 140 mAh g^{-1}. The main drawback related to this material in the pristine form is the low electric conductivity (10^{-12} S cm^{-1}) and the poor ion diffusion coefficient that causes the intrinsic low electrochemical activity. Several strategies were adopted to overcome this issue, such as the reduction of particles to the nanoscale, in order to reduce the travelling distances of Na ions and electrons. Other interesting studies are focused on TiO_2 nanotubes (TiO_2-NTs). Huang et al. demonstrated the first TiO_2-NTs based cell, having the following configuration: TiO_2-NTs|1M $NaClO_4$ in EC:DMC 1:2|Na [43]. The cell delivered a specific capacity of 87.1 mAh g^{-1} at a current density of 50 mA g^{-1}. A recent work by Bella *et al* [44]. demonstrated the reversible insertion of Na^+ ions in TiO2-NTs prepared by anodic oxidation without the use of binders and conductive additives; in addition, the mechanism of sodium ions insertion was

modelled by DFT calculation. Besides TiO_2, other kind of metal oxide can reversibly store sodium ions. For instance, the $NiCo_2O_4$ spinel [45] or Sb_2O_4 in the form of thin films [46].

Another category of anode materials for sodium cells are Na alloys. Indeed, also sodium forms binary compounds with the elements belonging to the groups 14 and 15 of the periodic table. These kind of compounds have the peculiarity of interacting with a large amount of sodium atoms, thus in principle allowing very high specific capacity outputs. Noteworthy, unlike lithium, Na does not alloy with Al, and this is a great advantage because is possible to use aluminum as current collector also for the anode, so the total cost of NIB system is reduced. The alloying mechanism can be explained by the following equation:

$$M + xNa^+ + xe^- \rightleftharpoons Na_xM$$

In the case of Si, which provides the highest specific capacity in Li-ion batteries, DFT calculations showed that formation of an alloy with NaSi composition is possible ; however, no reversible cycling was demonstrated so far . Germanium, extensively exploited in the fields of semiconductors, optical, and telecommunication industries, is a rare element (the natural occurrence is approximately 1.6 ppm in the Earth's crust). Therefore, despite its great potential, Ge is not the best choice when low-cost applications are envisaged [47,48]. It is well known that alloying elements undergo drastic volume changes upon (de)lithiation, which prevents their practical use in commercial applications, and similar behavior was found for the corresponding (de)sodiation reactions,[49] as shown in Fig. 2.5.

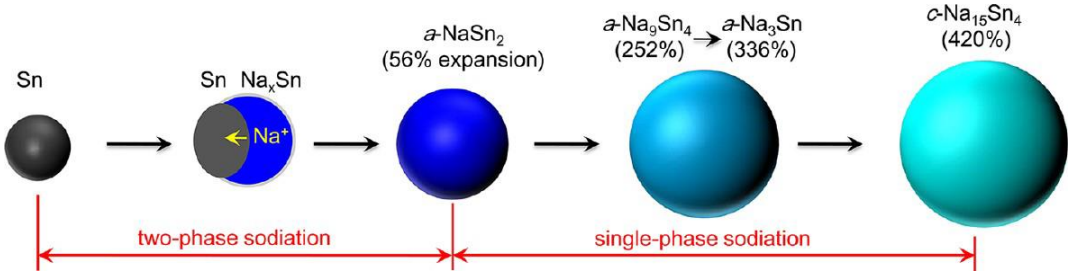

Fig. 2.5 Schematic illustration of the structural evolution and volume expansion of tin nanoparticles during sodiation. (Taken from [50])

The above reported example shows the volume change of a Sn-based electrode during sodiation. Tin anodes are extensively studied by different research groups due to their high theoretical specific capacity (847 mAh g^{-1}). The reversible

sodiation-desodiation processes (4 steps) occur below 0.7 V. During each step, a volume expansion up to 420 % occurs at the end of the alloying process. To alleviate this issue that often causes cracks and pulverization of the active material particles, the formation of intermetallic compounds has been proposed [50].

Another alternative anode material for NIBs is Sb. Antimony is characterized by a theoretical specific capacity value of 660 mAh g^{-1}. Although the theoretical capacity is lower than the Sn one, it undergoes a limited volume expansion, which makes it a good candidate for sodium cells.

As for Li alloy, find a strategy for reduce the volume expansion effect is a crucial point. One of the approach is the reduction of the metal particle size to the nanoscale. Clearly, this does not avoids the volume changes, but the phase transitions during the alloying process are more able to accommodate the large strain that the effect aforementioned causes. Further strategies were used to improve the performances of these electrodes, for example the use of additives in the electrolyte solution, as suggested by Ponrouch et al. [51] in a recent review about electrolytes and additives for negative electrodes in NIBs.

Another class of materials under study as negative electrodes in sodium batteries is represented by organic compounds. In this respect, the last year of my Ph.D. studies has been focused on the development and characterization of organic anodes, thus these materials will be thoroughly discussed in the last chapter of this Ph.D. Thesis.

2.2.1.2 Cathode materials

In general, positive electrodes for Na batteries are materials able to store sodium ions at working potentials exceeding 2 V vs Na^+/Na.

In particular for positive electrodes, many active materials, which are suitable for NIBs, are analogous to the compounds that are employed for lithium-ion batteries. Among them, it is important to mention layered sodium transition-metal oxides, olivines, fluorides, compounds with NASICON framework and, also in this case, organic compounds. Nonetheless, one should point out that, for instance in the case of layered oxides, the tetrahedral coordination is very common in the case of lithium compounds, while it does not occur or is very inconvenient with sodium, which usually occurs in the octahedral or trigonal prismatic coordination. This

difference is principally due to the larger atomic (ionic) radius of sodium if compared to lithium (1.06 vs. 0.76 Å, respectively).

Along the years, major efforts have been devoted to layered system with general formula Na_xMO_2 (M = from Ti to Ni as 3d transition metal). Delmas et al. [52] in 1980 proposed a classification of these materials into two main categories: the O3 type and P2 type, where the Na^+ ions are accommodated at octahedral and prismatic sites, respectively, as shown in Fig. 2.6. Sheets of edge-shared MO_6 octahedra build the layered structure, wherein sodium ions are located between the sheets.

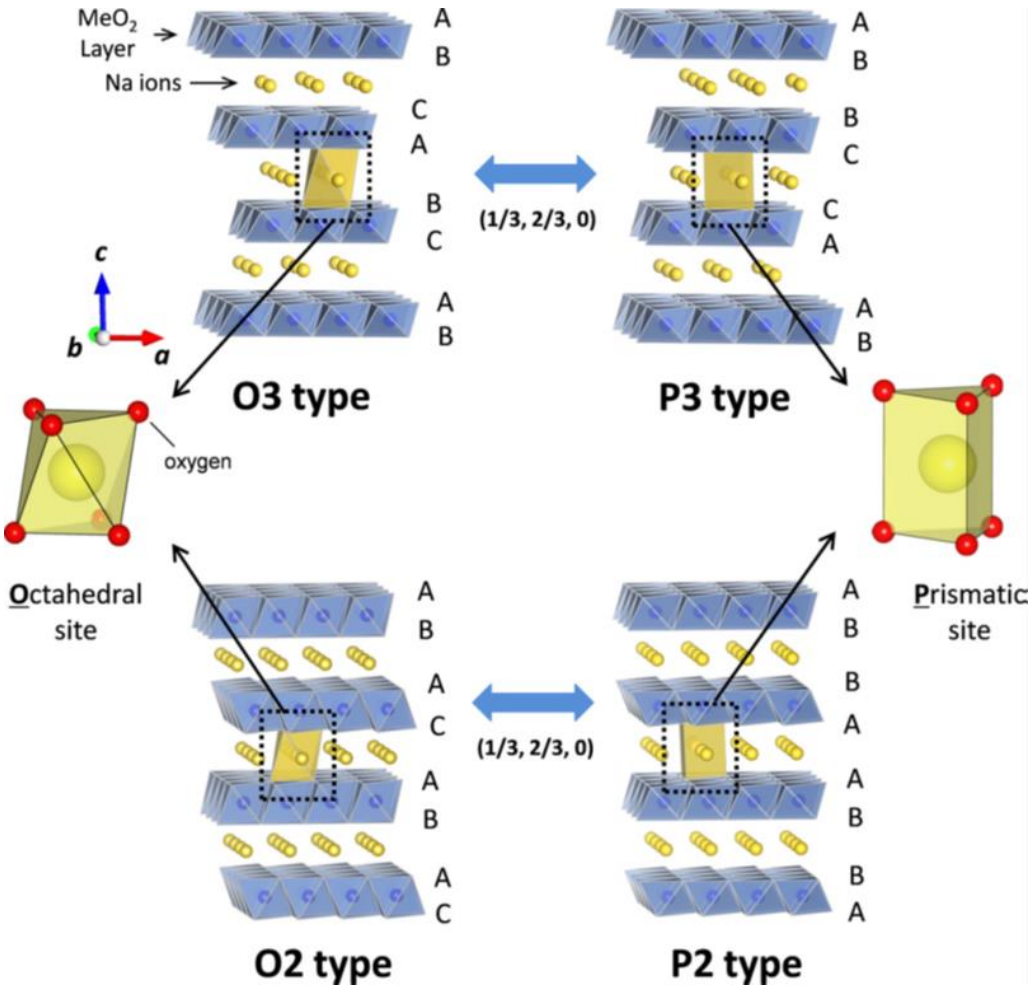

Fig. 2.6 The classification of Na_xMO_2 layered materials with the sheets of edge-sharing MeO_6 octahedra and phase transition processes induced by sodium extraction. (Taken from [53])

Amongst of these active material structures, manganese and cobalt based oxides are the most investigated.

Layered $LiCoO_2$ is one of the most successful cathode used in LIBs technology since the first commercialization by Sony in 1990s. The Na analogue (Na_xCoO_2) exhibits an electrochemical intercalation behavior with more complex phase transitions during the extraction of Na^+ ions. A similar operation is observed in other Na compounds, such as Na_xMnO_2, which might be ascribed to the large ionic radius of Na^+, the longer distances between Na-O bonds and the charge ordering at different Na contents. Based on the Na stoichiometry in the chemical formula, (range $0 \leq x \geq 1$) these materials exhibit a reversible capacity around 100 – 125 mAh g^{-1}. Recently, Ceder research group [54] reported the monoclinic α-$NaMnO_2$ ($C2/m$) which shows a reversible capacity of 185 mAh g^{-1} during the first cycle in the range of potential between 2.0 and 3.8 V vs Na^+/Na, with a rapid capacity decay up to 140 mAh g^{-1}.

Also iron-based oxides can reversibly insert Na ions. Typically, the active compound is $NaFeO_2$, with trivalent iron ions, that crystallizes into two different polymorphs (α and β types). α-$NaFeO_2$ is the low-temperature phase and showed reversible charge and discharge processes in the following cell configuration Na|1M $NaPF_6$ in PC|$NaFeO_2$ [55]. The reversibility of the active compound is influenced remarkably by the cutoff conditions upon sodium extraction. Indeed, beyond 3.5 V the reversible capacity decreases, due to a migration of some Fe^{3+} into the neighboring tetrahedral sites with the formation of vacancies at face-shared tetrahedral sites with FeO_6 octahedra. Fe in the tetrahedral sites perturbs the diffusion of Na^+ ions, often leading to a degradation of the electrode. The best performances were obtained setting a cutoff voltage of 3.4 V with a small polarization, with reversible capacity that reached 80 mAh g^{-1}.

Polyanionic compounds, such as phosphates, pyrophosphates, fluorophosphates, etc. are also worth to be noticed as cathodes in NIBs. In general, these compounds contain Fe(II), Mn (II) or a combination of both. Among phosphates, $LiFePO_4$, widely used in LIBs, is one of the most famous and studied for practical application also in NIBs [56]. The advantages of this material in LIBs are mainly its high specific capacity (170 mAh g^{-1}), the simple production process and the low environmental impact. In general, it is used in the form of carbon coated nanoparticles, because of its poor conductivity. $NaFePO_4$ crystallizes into the thermodynamically stable phase (maricite), but this structure is not very advanyageous for Na extraction/insertion. On the other hand, the metastable

polymorph (triphylite) is electrochemically active and simple to be prepared by ion exchange from $LiFePO_4$ forming the triphylite-phase $NaFePO_4$ [57] [58]. The chemical process starts from the lithium iron phosphate, which is chemically oxidized in acetonitrile by NO_2BF_4 in order to form the $FePO_4$. The oxidized product is used in the lab-scale cell using Na metal as negative electrode and 1 M $NaClO_4$ in EC:PC 1:1 as electrolyte. The cell shows a reversible behavior, but displays also a capacity decay, that is associated to the presence of some lithium residuals in the crystalline structure. Recently, Hassoun et al. [59], presented a refinement of this electrochemical exchange directly in the lab-scale cell configuration by delithiating the $LiFePO_4$ olivine during the first charge and, then, physically moving the active electrode in a fresh cell using the sodium metal anode with a 1 M $NaClO_4$ in PC and FEC (98:2 volumetric fraction) solution as the electrolyte.

Several other positive electrodes are detailed in the literature for NIBs and should be described, but this is out of the purpose of this thesis work; thus, the reader is better referred to the following review articles for more details [60,61].

2.2.2 Electrolyte materials

The third-key component in an electrochemical cell is the electrolyte. In general, the electrolyte of LIBs/NIBs is a solution of salts dissolved in aprotic solvents. Although this cell component often receives less consideration respect to the electrodes, its role is fundamental for the proper operation of a battery system, because its function is to shuttle the charge carrier ions (Li^+, Na^+, K^+, Mg^{2+}, etc.) from the cathode to the anode (charge) and vice versa (discharge). Furthermore, it is greatly responsible for the service life of the cell and its performances in real environment. Therefore, the research on electrolytes is very important, and different parameters must be considered, including the perfect compatibility with the electrode active materials.

For the practical use in an electrochemical system, an electrolyte should respect some requirements, which can summarized as follow:

a) It should be ionically conductive and electronically insulating, in order to facilitate the ion transport (Na^+ in this work) during cell operation and minimize the self-discharge.
b) It should be chemically stable, thus no chemical reactions should occur during cell operation within itself, with the separator and the electrodes in

use, and with the other cell components, like packaging materials and current collectors (Al foils in the case of NIBs).

c) It should be thermally stable, so the melting and boiling points should be higher than the operating temperature of the battery.

d) It should have a wide electrochemical stability window (ESW), which means that no degradation must occur within the range of electrodes working potentials.

e) It must induce morphologically stable protective film (SEI, solid electrolyte interface) on the anode surface and sustain the high operational voltage of the cathode.

Besides these operational requisites, a NIB electrolyte should be selected in order to meet other market criteria:

f) It should be eco-friendly, with low toxicity and limited environmental hazard.

g) It should be based on sustainable chemistries, which means abundant elements and synthesis processes with as low impact as possible.

h) It should be cheap in terms of materials and production, in order not to increase the overall cost of the final prototype.

The above requirements are generally valid for any type of electrolyte, because the specific characteristics must be considered based on the kind of electrode chemistries involved as well as on the final envisaged application.

Electrolytes for a battery system can be categorized in three major categories: organic liquid based electrolytes, ionic liquid based electrolytes and polymer-based electrolytes. In this section, a general overview of the different electrolytes will be reported, focusing the attention on the organic liquid based ones; the next chapter will fully focused on polymer electrolytes, which represent the main subject of the research work done during the three years of Ph.D.

Even if in the last 30 years extensive research was conducted on electrolytes for LIBs and the knowledge on their principal features is rather considerable, the differences between lithium and sodium must be considered (e.g., ionic radius, lower Lewis acidity, etc.). Indeed, to develop the optimum electrolyte system for NIBs, the entire system must be properly optimised, starting (for the electrolyte) from the different constituents, namely solvent(s), Na-salt(s), additive(s), and their respective ratios.

2.2.2.1 Sodium salts

Soluble sodium salts are added to the solvent(s) and they act as charge carries of the current passing in the electrochemical cell during operation (charge and discharge processes). An ideal electrolyte salt should meet the following requisites:

a) High solubility in the solvent(s) used. In particular, the anion should be inert to the solvent(s).
b) Stability vs. oxidation and reduction as for the voltage limits of the ESW. In particular, the anion should be stable against the oxidative decomposition at the cathode.
c) High chemical stability vs. the other cell components.
d) Non-toxicity and other safety related features.

The characteristics just mentioned reduce drastically the number of sodium salt candidates. The role played by the anion is fundamental because it must have a central atom with ligands withdrawing electron density, which delocalize the negative charge and, thereby, weakly coordinating anions (WCAs) [62]. As a result, the most commonly used sodium salts are: $NaClO_4$, $NaBF_4$, $NaPF_6$, NaFSI ($N(SO_2F)_2^-$), NaTf ($CF_3SO_3^-$) and NaTFSI ($[N(CF_3SO_2)_2]^-$).

Table 1 summarizes some examples of these salts with some basic properties. In general, sodium salts have higher melting points than the corresponding lithium salts, so they are more thermally stable, thereby better in terms of overall safety.

Table 1 Sodium salts employed on NIBs and principal characteristics (the data (*) are available only for the corresponding Li-salt)

SALT	**Melting point, T_m [°C]**	**Mw [g mol^{-1}]**	**σ [mS cm^{-1}] in PC**
$NaClO_4$	468	122.4	6.4
$NaBF_4$	384	109.8	(3.4)
$NaPF_6$	300	167.9	7.98
NaTf	248	172.1	(1.7)
NaTFSI	257	303.1	6.2
NaFSI	118	203.3	

Sodium perchlorate salt ($NaClO_4$) is one of the most commonly used, due to its abundance (is the most soluble of the common perchlorate salts), which renders it very cheap. In terms of thermal stability, it outperforms all of others salts (from TGA and DSC analyses, it shows decomposition temperatures of 500 and 474 °C, respectively). However, the use of this salt is restricted to the academic research because even after drying at 80 °C under vacuum for 12 h the water content is relatively high (> 40 ppm); moreover, it is explosive in the dry state. In terms of ionic conductivity, the best results for this salt deliver were obtained in combination with propylene carbonate (PC) solvent. Sodium exafluorophosphate, $NaPF_6$, is also widely implemented; it exhibits the highest ionic conductivity as reported in various studies with different solvent(s) ; as an example, 1M $NaPF_6$ in PC at 25 °C shows 7.98 mS cm^{-1} while $NaClO_4$ provides an ionic conductivity of 6.4 mS cm^{-1}. Although, sodium exafluorophosphate provides the best ionic conductivity compared to the others salt, it must be used carefully because it is very sensitive to moisture and it suddenly reacts in presence of water traces evolving corrosive HF [63].

Imide-based salts (NaFSI, NaTFSI) also show good ionic conductivity, and in some reports they were compared in different solvent media to investigate their anodic stability vs. Al [64]. These salts in a solution with a mixture of ethylene carbonate (EC) and diethyl carbonate (DEC) displayed a hysteresis loop around 3.3 V vs Na^+/Na with an irreversible oxidative current flow at 5.3 V vs Na^+/Na .

Recently, Huang *et al*. [65] synthesized the sodium-difluoro(oxalate)borate ($NaC_2O_4BF_2$, labelled NaDFOB), which is an evolution of the sodium-bis(oxalate)borate (NaBOB) that has limited solubility in conventional carbonate-based solvents. The replacement of an oxalate subunit by fluorides improves the solubility, thanks to the electron withdrawing effect of fluorine. This new salt shows a very high anodic stability over 5.5 V vs Na^+/Na in different solvents, thus it can be used in a cell with high potential cathode .

Further studies were performed in order to find new tailored sodium salt, for example Plewa-Marczewska and coworkers published a work on sodium 4,5-dicyano-2-(trifluoromethyl)imidazolate (NaTDI) and sodium 4,5-dicyano-2-(pentafluoroethyl)imidazolate (NaPDI), but in this case the performance of both the salts are not at the level of the commonly used salts so far [66].

Clearly, the performances of the salts also depend on the solvent(s) in which they are dissolved; thus, a brief overview of the most commonly used solvents is detailed below.

2.2.2.2 Organic solvents

The commonly used solvents in NIBs are almost the same, that have been widely studied and implemented in lithium batteries along the years. The main characteristics for an electrolyte solvent are listed below:

a) High dielectric constant (ε), in order to dissolved sufficient amount of salt(s).
b) Low viscosity, to facilitate the ionic mobility.
c) It should remain in the liquid state in a wide temperature range (typically, from - 20 to + 60 °C), meaning a low melting point and a high boiling point.
d) Non-toxicity, safety (low vapor pressure) and low cost.

All of the above reported features are difficult to be met by just one material; indeed, it is often preferable to use a mixture of 2 or 3 solvents, generally aprotic organic solvents such as carbonates (both linear and cyclic), esters and ethers. The most popular solvents are listed in Table 2 with the relative main physical characteristics.

Table 2 List of solvents commonly used in battery electrolytes. T_m, T_b, T_f, η, and ε stand for melting point, boiling point, flash point, viscosity, and dielectric constant, respectively.

SOLVENT	Melting point T_m [°C]	Boiling point T_b [°C]	Flash point T_f [°C]	η [cP] at 25 °C	ε at 25 °C
Ethylene carbonate (EC)	36.4	248	160	1.9	89.78
Propylene carbonate (PC)	-48.8	242	132	2.53	64.92
Dimethyl carbonate (DMC)	4.6	91	18	0.59	3.107
Diethyl carbonate (DEC)	-74.3	126	31	0.75	2.805
Ethylmethyl carbonate (EMC)	-53	110		0.65	2.958
Triethylene glycol dimethyl ether (TEGDME)	-46	216	111	3.39	7.53

In the case of solvents, *"the Lewis acidity/basicity concept is of primary importance as it will influence the ESW"* as said by P. Johansson and M. R. Palacìn et al.[51].

The ionic conductivity of the Na^+ is proportional to its mobility and the number of mobile ions. As said before, mixture of solvents are generally much more suited. Indeed, EC and PC that have high ε and wide ESW, exhibit a relative high viscosity, consequently the ion mobility is reduced. On the other hand, others solvents, such as diethyl carbonate (DEC) and dimethyl carbonate (DMC) have lower viscosity, limited salt dissociation is related, infact, to low solvent dielectric contants. Therefore, is common to combine solvents with different characteristics in order to obtain a solution with suitable properties for high performing batteries.

The selection of solvent(s) is very important and depends not only from its intrinsic features, but also from its compatibility with the other cell components. When a battery is designed, one should first consider its field of application. Based on this assessment, electrodes are selected that better meet the requirements of specific energy, power density, working temperature, etc. Once the electrodes are established, the choice of the solvent is crucial, because the performances of the active materials strongly depend upon the electrolytes. In this respect, the use of graphite in NIBs can explain this concept very well; indeed, graphite-based electrodes were discarded because of the co-intercalation in the layered structure of solvating molecules of PC together with Na^+, which causes the exfoliation of the graphene layers and the consequent fast degradation of the electrodes. Nevertheless, if the solvent is ether-based, like TEGDME, the graphite structure is preserved and it can be eventually used [36,34].

In general, polar aprotic solvents and the sodium salts during the first oxidation/reduction process in the cell are reduced to form insoluble Na compounds, which precipitate onto the surface of the electrodes, thus resulting in the formation of a passivating layer, typically called Solid Electrolyte Interface (SEI). This thin film, which acts as a protective membrane between the electrode and the electrolyte solution, is permeable to the metal ions that can cross it and avoid the electrons passage. The formation of the SEI is fundamental to set different parameters, such as safety, shelf life, cycle life, power capability. Furthermore, it is very important when using native Na metal because of its very high reactivity. However, there are few studies on Na metal batteries and often the weak point is their failure during charge because the solid electrolyte interface that is formed on the surface of the metallic Na is rather wrinkled. From this roughness, the dendrites

are generated spontaneously with detrimental effects on the cell behavior [67]. Actually, that are some studies for prevent the dendrites growth, designing an artificial passive layer on the metallic electrode [68].

Although liquid organic solvents are the most useful in batteries, their volatile nature is one of the great issue associated to the somewhat limited safety of rechargeable batteries. The most recent event on wretched failure in terms of explosion is the Samsung Note 7, in which an entire batch of mobile phones had problems of overheat and even catched fire. For this reason, the famous brand was forced to withdraw the products from the market. To guarantee a safe device is fundamental to solve these issues, in particular for portable technologies, but also for the large-scale electrical energy storage where explosion hazards must be absolutely avoided.

In terms of safety, room temperature ionic liquids (RTILs) have attracted a lot of attention in the last years. RTILs, thanks to their unique physico-chemical properties, are considered practically non-flammable, so very safe. A room temperature ionic liquid is a molten salt at room temperature, in practice are salts with melting point below 100 °C. These compounds have several attractive features, such as wide ESW, high thermal and chemical stability, and fascinating ionic conductivity. The characteristics of a RTIL match very well the sufficient requirements for the use as electrolyte. In sodium rechargeable batteries different studies have been conductive particularly on NaTFSI-Pyr_{14}TFSI ionic liquid based electrolytes. Often the performances of a cell with this electrolyte are compared with those of a conventional organic carbonate-based liquid electrolyte, like L.G. Chagas et al. [69], which investigated the behavior of a layered $Na_{0.45}Ni_{0.22}Co_{0.11}Mn_{0.66}O_2$ in two electrolytic solutions, with organic carbonate (0.5 M $NaPF_6$ in PC) and a RTIL-based NaTFSI-Pyr_{14}TFSI. The study revealed that the electrochemical performance with the RTIL is definitely improved with respect to the PC-based electrolyte. The explanation of the better response of the cell with the RTIL is due to the fact that in general layered electrodes with manganese suffer from Jahn-Teller distortion, and the result is a partial dissolution of the material in the carbonate-based liquid electrolyte, with consequent strong capacity fading [69]. Another study on NaTFSI-Pyr_{14}TFSI is the work of I. Hasa et al., where the authors investigated the RTIL in both half and full sodium and sodium-ion configurations. The results obtained seem promising for an eventual application in NIBs [70]. Passerini and coworkers recently published a study on different RTILs that are prepared with the same cation (Pyr_{14}^+), by varying the anion with $TFSI^-$, FSI^-, and $FTFSI^-$. The comparative investigation was focused on the stability towards

corrosion of the Al current collector, which typically occur with organic carbonate-based electrolytes [71]. They found an improvement in RTIL-based electrolytes, where the corrosion is suppressed, thanks to the formation of a passivation layer. In general, between the different RTIL-based electrolytes investigated, the best performances are obtained when using the $TFSI^-$ anion [64].

2.2.2.3 Additives

Additives are often encompassed in the electrolyte solutions to improve the battery performances (in both LIBs and NIBs). They are added in little amount, usually not exceeding 5% by weight or by volume of electrolyte solution [72]. Their principal use is to improve the characteristics of the electrode-electrolyte interface, mainly modifying the SEI by increasing the wetting of the electrode surface, and protecting it towards overcharging (e.g., by redox shuttles that store the extra charge). Additives are also employed, occasionally, as flame-retardants, or to enhance the physico-chemical properties of the electrolyte (e.g., decrease the viscosity, radical scavengers, etc.).

The most famous additive in NIBs electrolytes (widely used also in LIBs) is fluoroethylene carbonate (FEC). It is the most common SEI layer enhancer, in particular during fast rate charging. FEC improves the capacity retention of anodes, and mitigates the irreversible reactions at the interface of the Na metal electrode [73]. However, the addition of FEC in the electrolyte solution often causes anomalies in the potential vs. time profile, which have been recently explained. In 2016, Dugas et al. demonstrated the beneficial effect of FEC on the minimization of the irreversible capacity of a Na-half cell, but found a continuous release of small quantities of gases, clearly detrimental to the cell performances upon long term cycling [74].

Komada et al., in a paper published in 2011, investigated several additives including not only FEC but also vinyl carbonate (VC), ethylene sulphite (ES) and the doubly fluorinated EC (DFEC). In this research work, FEC was found to be the additive that gave the best response. In the same study, VC, widely employed in LIBs, was demonstrated to have very low performance in NIBs [73].

2.2.3 Additional battery components

2.2.3.1 Binders

The realization of a good electrode (both anode and cathode) requires the use of additional components: an electronic conductivity enhancer (typically, carbon black – CB in various forms), that enhances the electronic conductivity, and a binder that efficiently holds together the active material particles and the conducting additive. The most common procedure for the preparation of an electrode is to mix the active material particles, the CB and the binder in a proper solvent. The mixture is then casted in the form of a film onto a current collector and, after evaporation of the solvent by mild heating, the electrode is ready to be assembled in the cell.

The binder must be electrochemically stable in the electrode/electrolyte environment, and must support the dimensional changes during electrode operation. The role of the binder becomes increasingly fundamental as the size of the active particles decreases.

Ideally, the best binder must be able to form a polymeric network that efficiently enwraps the particles even if used in as little amount as possible, thus not reducing significantly the overall energy density because it is an inactive component.

Despite their positive influence on the electrodes' performance (particularly NIBs anodes), studies on binders are not very popular, compared to the other components in secondary batteries. Fig. 2.7 shows the most recent statistics on the number of publications on binders applied in NIBs. Most of the electrodes commercially available and/or prepared for scientific studies are made with poly(vinylidene fluoride) (PVdF) as binder, due to its good chemical and electrochemical stabilities. However, some problems remain, such as the relatively high production cost and the need of using volatile and toxic organic solvents to dissolve it, such as N-methyl pyrrolidone (teratogenic) [75,76]. Recently, in both LIBs and NIBs, alternative water-soluble binders have been introduced that guarantee cross-linked 3D interconnection, such as sodium carboxymethyl cellulose (Na-CMC), poly(acrylic acid) (PAA) and sodium alginate (Na-Alg) [77-80] . These binders were introduced to enhance the cycling performance of alloying reaction materials that undergo large volume change upon sodiation–desodiation. In particular, Na-CMC is an environmentally friendly and inexpensive binder, derived from cellulose. During the electrochemical reaction process, Na-CMC plays an important role in improving the SEI characteristics on the electrode

surface, which reduces the irreversible capacity and in some way enhances the service life of the cell. Na-Alg is a high-modulus natural polysaccharide extracted from brown algae [78]. In a work of Kovalenko *et al.* [78] they compared the performances of a composite nano-silicon electrode for LIBs, prepared with three different binders (Na-Alg, Na-CMC and PVdF). The composite electrode containing the sodium alginate yields a remarkably stable battery anode. Compared to Na-CMC, it ensures an enhanced interfacial interaction between the polymer binder and the active material particles, as well as stronger adhesion between the electrode layer and the current collector substrate. Compared to PVdF, PAA has carboxylic groups, which play an important role in achieving better uniformity and stronger binding ability in the composite electrode [79]. This is due to their amorphous and cross-linking nature via the hydrogen bonds between carboxylic groups. PAA also allows the formation of a stable and adaptable SEI layer on the elastic binder-coated electrode surface, in which the elasticity of the polymer matrix may prevent cracks in the SEI when the volume changes occur [79,80]. The polymeric cross-linking network can regulate the mechanical/chemical stresses resulting from the large volume expansion in many composite electrodes [81]. In addition, the decomposition reaction of the electrolyte was reduced compared to the use of PVdF, due to the stable SEI layer formation.

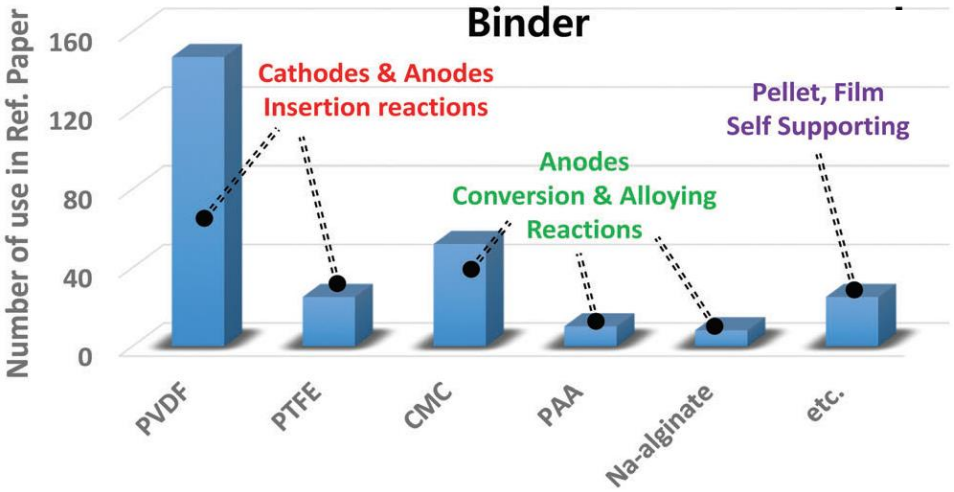

Fig. 2.7 Research progress on binders for NIBs (Taken from [82])

Notwithstanding the binder is generally not considered among the main components of modern secondary batteries, its role is fundamental to obtain high

performing electrodes that can also properly operate for thousands of cycles thus guaranteeing sufficient service life of the device.

2.2.3.2 Separators

As previously described in the section "Fundamental of a battery", in all batteries based on liquid electrolytes, the electrolyte solution is normally soaked in a proper separator, that is *"A porous membrane placed between electrodes of opposite polarity, permeable to ionic flow but preventing electric contact of the electrodes"* [83].

A good separator has to meet some minimal requirements:

a) It must be electronically insulating (the electrons flow occurs in the external circuit).

b) It must be chemically and electrochemically stable vs. the electrolyte and the electrode components.

c) It must be mechanically robust, in order to withstand the solicitations occurring during battery assembly and operation.

d) It must be effective in preventing migration of particles or colloidal or soluble species between the two electrodes.

e) It should have a high porosity for soaking as much as possible electrolyte solution, thus assuring high ionic conductivity.

f) It should be uniform in thickness and, at the same time, lightweight. Quantitatively speaking, the McMullin number should be near 1. [84]

g) It must be thermally stable: less than 5% shrinkage after 60 min at 90 ° under vacuum. [83] Moreover, it should be able to close the pores when the internal temperature in the battery increases dramatically. This phenomena is call *Shutdown*.

h) It should be low cost. In general, the prize of a separator counts for about the 20 % of the total battery cost (mostly because of the expensive fabrication process).

Essentially, a separator should be thin and highly porous, while preserving excellent mechanical robustness. It may be considered as a fundamental safety factor in a battery.

Separators actually used in batteries can be grouped in three categories: micro-porous polymeric membrane, nonwoven materials and composite inorganic membranes.

Micro-porous polymeric membranes are semi-crystalline materials based on polyolefins, such as polyethylene (PE), polypropylene (PP), and their blends. Sometimes these materials are assembled layer by layer (2 or 3), like the commercial Celgard® 2325.

The nonwoven materials are made of fibers, either oriented or randomly arranged, bonded together by chemical, or physical methods. These kind of materials can be natural (e.g., cellulose), or synthetic, such as polyamide (PA) or PVdF.

Inorganic composites, also called “ceramic separators” are polymers with added as filler, very often ceramic nanoparticles such as γ-$LiAlO_2$, Al_2O_3, TiO_2, SiO_2, etc., in order to enhance mechanical robustness or ionic conductivity or other fundamental physico-chemical characteristics.

Chapter 3

Polymer electrolytes

3.1 General features

Liquid electrolytes, because of their high performance, simple availability and simple preparation are most commonly used in NIBs, but they suffer from a series of drawbacks.

Indeed, they are generally based on organic solvents, which are toxic and volatile, thus sometimes leading to unwanted safety hazards (the recent problems of Samsung Note 7 are a clear example). Moreover, with high potential cathode materials, liquid electrolytes need the support of additives to increase their ESW, generally lower than 4.5 V. The use of a liquid electrolyte restricts the use of the battery in a limited range of temperatures, depending on the thermal stability of the solvent used. Moreover, the use of these electrolytes does not allow to design batteries having different shapes, thus also limiting their use in the actual smart electronic technologies. The utilization of all solid state devices can bypass the problems related to the liquid counterparts, and now is very important not only in the battery field, but also in a wide variety of energy related applications such as solar cells, electrochromic displays and smart windows technology, etc. [85-88].

Generally speaking, polymer electrolytes consist of a polymer matrix solvating a salt. More precisely, polymer electrolytes can be divided in three main categories, based on few differences in the matrix that contains the salt:

a) Solid polymer electrolytes (SPE): the polymer acts as the solvent to dissolve the alkali metal salt and, at the same time, gives mechanical strength to support processability.
b) Gel polymer electrolytes (GPE): are polymers encompassing a liquid electrolyte solution. The polymer acts similarly to a separator in which the electrolyte is soaked and confined.

c) Composite polymer electrolytes (CPE): are polymer electrolytes such as SPEs or GPEs in which fillers (most likely ceramic fillers, such as TiO_2, Al_2O_3, ZrO_2) are added.

The first evidence of ion conduction in solid electrolytes dates back to 1800s by Faraday, when studying PbF_2 as solid electrolyte . Successively, the interest on solid state ionic conductors was addressed to silver halides and β-aluminas, in particular the latter which had surprisingly good sodium ion transport properties [89] β-alumina is historically the first fast Na ion conductor. β-alumina and its crystal structures were extensively studied without success in practical use, because of the fracturing of the β-alumina ceramic structure upon operation, that leads to cell failure[90]. About solid electrolytes, either ceramics or glasses, as Baril *et al.* [90] said: *"the relative paucity of true solid electrolytes, ..., is to be compared with the infinite choice offered by molten salts, solutions of salts in water or polar solvents. An intermediate situation is offered by polymers."* However, the real interest on this materials started during the seventies when A. F. Diaz *et al.* [91] developed macromolecules with electronic conductivity and, after the discovery of insertion electrode materials, Fenton and co-workers [92] demonstrated the capability of ether-based polymers (poly(ethylene oxide) – PEO) to dissolve inorganic salts, and exhibit ionic conductivity at room temperature [92]. During the same years, M. Armand poses PEO at the center of his research on polymer electrolytes [93].

Since a polymer can be used as matrix in which ions can move, it must be able to form complexes with the salt. There are four main factors governing the formation of these complexes:

a) High concentration of sequential polar solvating groups (-O-, -NH-, -CN, etc.).
b) Low lattice energy of the salt.
c) Low lattice energy of the polymer.
d) Donor number and polarizability of the solvating groups.

A salt is composed of the cation and the anion, and both of these charged species are shuttled back and forth between the electrodes in the cell once the salt is dissociated. In particular, the cation assures proper cell operation, so when selecting the salt, it is necessary that the anion has a delocalized negative charge (WCAs) in order the cation to have more chemical interactions with the polymer

matrix. These interactions are very important during the charge transfer, because the solvating groups in the polymer, that should have a high dielectric constant (ε), must facilitate the salt dissociation, and the resulting ionic conductivity improves when large anions are used [62]. When the polymer host has a low ε, the cation-anion interaction becomes more significant, with a considerable contribution from the anions.

Until 2001, the transport mechanism was ascribed to the amorphous phase region in the polymer, based on NMR studies conducted above the glass transition temperature (T_g). This theory was proposed in 1983 by Berthier et al. [94], who claimed that the ionic conductivity was facilitated by the local segmental motion of the polymer chains, as if the amorphous region was a liquid. In this state of the elastomeric region, the polymer chains have fast internal modes in which bond rotations cause segmental motion. Although at macroscopic level the viscosity is very high, at the microscopic level the local relaxation processes can be seen as liquid-like, where the degrees of freedom are comparable to the molecular liquid situation [94].

The solvation ability of the polymer chains depends upon the number of the repetitive units. For example, in $CH_3O(CH_2CH_2O)_nCH_3$ the cation solvation improves if "n" is 3, compared to n = 2.

For all the reasons described above, PEO with different molecular weights was one of the most studied polymer matrix in the battery field. In this respect, Souquet suggested an elegant model for poly(ethylene oxide) in which the ion transport occurs along the ordered coils that this polymer forms upon complexation of the salt (Fig. 3.1).

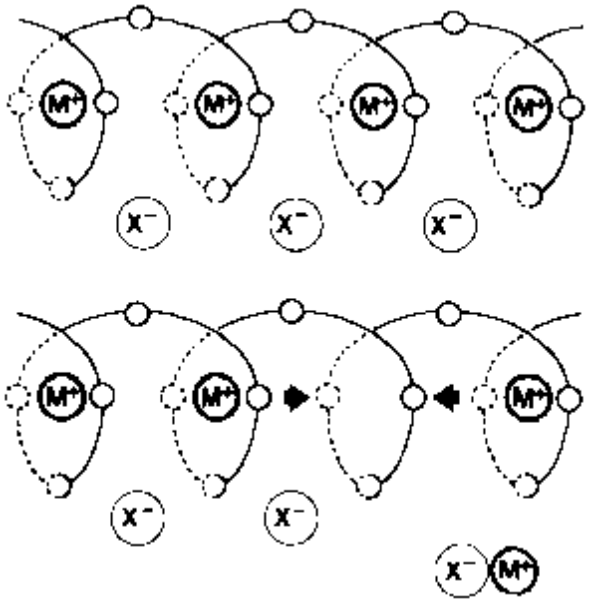

Fig. 3.1 Structure of polyethylene oxide (PEO) complex with an MX salt [95].

As ion transport was considered to occur only in the amorphous region, the research community investigated only polymers having a low T_g, so that at the standard cell operating temperature, the material is in the rubbery state and the ion conductivity is similar to the "liquid-like" conductivity.

In order to improve the ionic conductivity of SPEs, different paths have been explored in the last 50 years. In 2001 Bruce *et al*. [96] demonstrated the ionic conductivity in a crystalline polymer, PEO_6:$LiXF_6$ (where X = As, P, Sb), revealing that the ion transport can occur differently than the classic "liquid-like" mechanism. Indeed, above the T_g, ion hopping takes place along fixed pathways in the crystal lattice (Fig.13A-B) [97]. Recently, the same behavior has been demonstrated for other alkali metal, such as Na and K [96]. In the research work, they showed the temperature-dependent conductivities of the crystalline polymer electrolytes PEO_8:$NaAsF_6$, PEO_8:$NaPF_6$, PEO_8:$KAsF_6$ and PEO_8:$RbAsF_6$, all prepared using -OCH_3- terminated PEO with an average molar mass of 1,000 Da. The samples prepared with sodium alkali ion show an ionic conductivity around 0.5 10^{-5} S cm^{-1} at 25 °C, in particular the sample PEO_8:$NaAsF_6$ is 1.5 orders of magnitude higher compared to PEO_6:$LiAsF_6$. This results, not only confirms the hoping mechanism occurring in the polymer crystalline phase, but also suggests that by modifying the chain ends the ionic conductivity of the 8:1 complexes overcomes the values of pure crystalline phase.

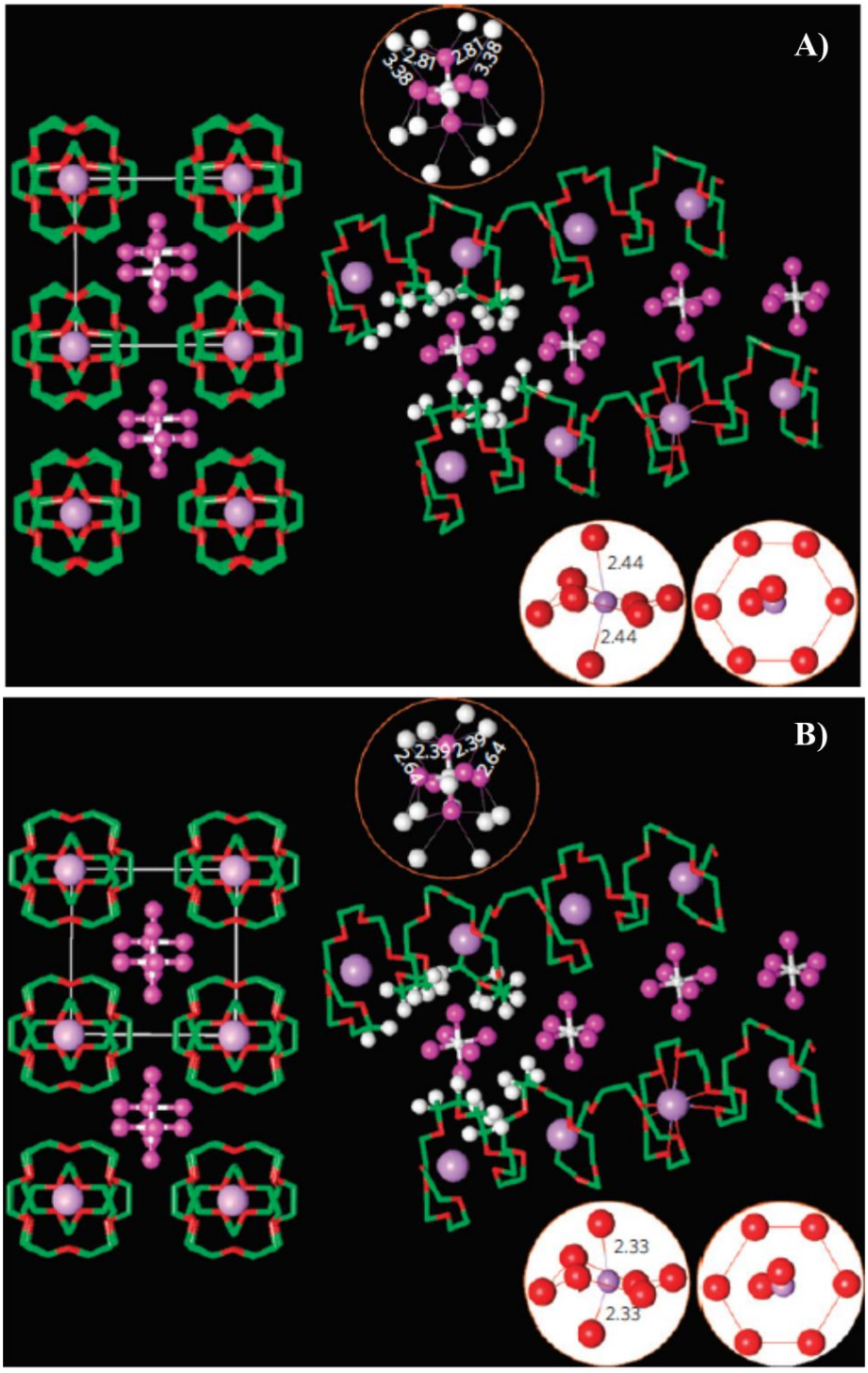

Fig. 3.2 The structure of PEO_8:$NaAsF_6$. From the single-crystal data collected at 25 °C (A) and -180 °C (B). (Adapted from [96]).

Although these materials are very appealing for battery application, because they can offer different advantages compared to non-aqueous liquid electrolytes, they also show some drawbacks: indeed, a polymer electrolyte shows lower ionic conductivity compared to a liquid electrolyte (around 10^{-5} S cm^{-1} order of magnitude lower). This is still the main inconvenience that restricts the real massive industrial production of polymer batteries. Actually, GPEs are among the best candidates, due to their characteristics (physical and electrochemical) close to non-aqueous electrolytes.

Clearly, most of the studies in the last 50 years were focused on lithium ion conducting polymer electrolytes. However, in the last years, also the research on polymer electrolytes for NIBs became increasingly important. In the next section, the state of the art of polymer based electrolytes for NIBs will be illustrated along with the next future perspectives in this field.

3.1.1 Solid Polymer Electrolytes - SPEs

Poly (ethylene oxide) can be considered the "father" of polymer electrolytes. In general, PEO can be considered a polymer derivative of the ethylene oxide (C_2H_4O) with high molecular weight, typically more than 20000 g mol^{-1}. Another polymer derivative of the ethylene oxide is the poly (ethylene glycol) (PEG) with molecular mass below 20000 g mol^{-1}. Both PEO and PEG where extensively employed in different fields, from medical/pharmaceutical applications to industrial uses. After the discovery of the ionic conductivity in alkali metal salt complexes of PEO, the study of these polymer electrolytes in rechargeable batteries became one of the most important challenge in this field. The principal goal for polymer electrolytes was, and still is, to reach the electrochemical properties of a liquid electrolyte, coupling the positive features of a polymer, such as the thermal stability, and the possible use with a metal anode (it may eventually suppress the dendritic growth often leading to short circuit, thus cell failure) with the ionic conducting characteristics of a liquid.

The first applications in sodium ion battery dates back to the '80s, when West *et al.* studied an all solid-state cell with Na|PEO-NaI (10:1)|MoS_3 configuration. The performances of the cell was not really appreciable, with a Coulombic efficiency during cycling far lower than unity[98]. Few years later, the same authors published a research article on the study of a cell having Na|PEO-$NaClO_4$|α–V_2O_5 configuration. The polymer film was prepared by solvent casting from acetonitrile (ACN) using PEO with $M_w = 4\ 10^6$ g mol^{-1} mixed with $NaClO_4$ sodium salt. In the

article, they showed also the evaluation of the ionic conductivity of polymer films prepared with the same method, but containing different amounts of $NaClO_4$, expressed as molar ratio of monomer units to sodium salt: x = [EO]/[Na]. The best ionic conductivity (6.5 10^{-4} S cm^{-1} at 80 °C) was obtained for x = 12. This sample was used to study the evolution of the surface resistance at different deep cycles (15, 69 and 128), and also showed a reasonably high cycling stability [99]

A further study on PEO based polymer electrolyte was conducted by Doeff *et al.* [37], in which they applied a $P(EO)_8NaCF_3SO_3$ electrolyte (prepared by solvent casting from acetonitrile) in a sodium metal battery using different carbon derivatives as anode, and also demonstrated cycling in full cell configuration of $Na_{0.6}CoO_2|P(EO)_8NaCF_3SO_3|C$. The cell displayed a reversibility electrochemical insertion of sodium ions. The same electrolyte media was investigated by this research group in half cell configuration with Na_xCoO_2 as cathode and in full configuration using $Na_{15}Pb_4$ as anode. In the case of the half configuration, the cell was cycled at 90 °C at a current density of 0.5 mA cm^{-2} for 200 cycles. In this work, they also compared the evolution of the surface resistance in the cell with Na metal electrode with the results obtained few years before, from West [99]. They found stable evolution of the sodium/PEO interface resistance, a very different behavior with respect to the system with the sodium perchlorate salt, because in that case corrosions processes at the Na/electrolyte interface occurred, which contributed to increase the cell resistance upon cycling.

In 1995, Hashmi and Chandra reported a PEO based SPE with $NaPF_6$ salt. The membranes were prepared by solvent casting from methanol using a 600000 g mol^{-1} PEO [100]. The formation of complexes was evaluated by optical microscopy, IR and XRD studies. They displayed how the crystalline phase of pure PEO changed upon salt addition: in fact, the spherulites (attributed to the crystalline phase) decreased, and the formation of smaller spherulites occured. Indeed, as the salt content was increased, the number and the size of spherulites decreased. The formation of the complexes was confirmed by the appearance of new peaks in the XRD profiles when comparing the XRD spectra of pure PEO, pure $NaPF_6$ and the membrane PEO + $NaPF_6$. Also the IR spectra on the same samples gave the evidence of the formation of polymer-salt complexes. They reported the ionic conductivity of different samples with different [EO]/Na, reaching the highest value of 5 μS cm^{-1} at room temperature for the sample with [Na]/[EO] = 0.065. The profile of conductivity (σ) vs 1/T showed an Arrhenius behavior within the experimental temperature range. They also calculated the total ionic transport number (t_{ion}) and

the Na^+ transport number for the sample [Na]/[EO] = 0.065 at 75 °C. They found t_{Na} = 0.45 and t_{ion} = 0.98 which indicates a higher contribution from the anion.

More recently, other sodium salts were investigated for PEO-based SPEs. S. Moreno *et al.* [101], studied a PEO based polymer electrolyte with sodium bis(trifluoromethanesulfonate) imide (NaTFSI), prepared by solvent free approach. They prepared a mixture of PEO_{20}:NaTFSI varying the salt content and then hot pressing the polymer-salt mixtures. They investigated different EO:Na ratios, *viz.* 6:1, 8:1, 10:1, 12:1, 20:1 and 30:1. They explored extensively the thermal properties, the ionic conductivity and the sodium transference number of the membranes. The PEO-based electrolytes showed increasing ionic conductivity as the PEO:NaTFSI ratio decreased, while the polymer electrolyte with the highest salt content dropped to the lower value. The sample 20:1 reached a remarkable conductivity value of 1.1 mS cm^{-1} at 80 °C. In the same work, they also tried to enhance the mechanical properties of the sample 20:1 by adding silica particles, and they investigated the time evolution of the Na/polymer electrolyte/Na interface at 75 °C for 30 days on the pristine sample as well as on the samples with 5 and 10% of SiO_2. For all the samples, they found an unstable behavior, which was attributed to the sodium metal used for the impedance measurement. In particular, the variation of the resistance values was attributed to a continuous formation-deterioration process of the SEI layer upon storage. They also calculated the transference number for these membranes: 0.39, 0.51 and 0.48 for the samples 20:1 with 5 and 10 wt.% of SiO_2, respectively. The t_{Na^+} clearly increased upon the addition of 5 wt.% of SiO_2 and, then, slightly decreased at higher filler concentration. The SiO_2-Na^+ interactions likely played a favorable role in this respect.

A. Boschin, and P. Johansson [102] investigated for the first time PEO-based SPEs using sodium bis(fluorosulfonyl) imide (NaFSI) salt with different ether oxygen to sodium (EO:Na) molar ratios, and compared the obtained results with the corresponding NaTFSI$(PEO)_n$ sample in terms of thermal properties, ionic conductivity, and nature of charge carriers. All the membranes were prepared by solvent casting using acetonitrile as solvent. They prepared samples with EO:Na molar ratios of 6, 9 and 20, respectively, with both NaFSI and NaTFSI. The authors focused the attention on the thermal properties observed for all the NaFSI based SPEs that were much prone to crystallization compared to the NaTFSI-based analogous. This, as always happens in polymer-based electrolytes, clearly affected the ionic conductivity. The highest conductivity was 4.5 10^{-6} S cm^{-1} at 20 °C for the sample EO:Na 9:1 with NaTFSI; all the other samples showed lower values. The

authors also observed a stronger interaction of FSI^- with Na^+ for more concentrated SPEs, the lower conductivity can be attributed to strong ion interactions, compared to $TFSI^-$ [102]. The best performances in terms of ionic conductivity was provided by NaTFSI$(PEO)_9$, and this SPE was used recently for a further work from this group, where they evaluated the feasibility of sodium metal as pseudo-reference electrode in solid state electrochemical cells. At first, they evaluated by visual inspection the changes on the sodium metal in contact with the SPE, stored the sample in coffee bags for 90 hours, in order to simulate the sealed conditions of NIB cells. They observed changes for the sample with the polymer electrolyte, while the pristine Na metal remained unchanged. They also followed the time evolution of the resistance at the Na/SPE interface, showing a continuous increase upon time, which likely indicated that the sodium metal electrode is not stable upon time, because of its high surface reactivity [103].

Recently Hu *et al.* [104] studied in detail a NaFSI/PEO based SPE. In this work, they presented a self-standing polymer membrane with EO:Na^+ ratio of 20. From electrochemical stability window measures, they obtained a good value around 4.66 V vs Na^+/Na, excellent for practical application in NIBs. The conductivity of the polymer electrolyte reached 4.1 10^{-4} S cm^{-1} at 80 °C, not so far to the values of Boschin et al. previously described. The remarkable results obtained from the characterizations where confirmed by cell performance studies, obtaining stable cycling behavior with $Na_{0.67}Ni_{0.33}Mn_{0.67}O_2$ and NASICON $Na_3V_2(PO_4)_3$@C cathode materials.

A very interesting recent paper was published by Ma *et al.* [69] where they studied a Na[(FSO_2)(n-$C_4F_9SO_2$)N] (NaFNFSI) PEO-based polymer electrolyte. It was prepared by solvent casting with a EO:Na^+ molar ratio of 15. The results obtained in this work are very interesting because, despite the rather low ionic conductivity of 3.36 10^{-4} S cm^{-1} at 80 °C (almost the same that can be obtained with PEO-based SPE), the polymer displayed a very high decomposition temperature (up to 300 °C), and the highest ESW showed so far for a PEO-based SPE, that is 4.87 V vs Na^+/Na. Furthermore, they tested the membrane in half-cell configuration in terms of galvanostatic cycling with $NaCu_{1/9}Ni_{2/9}Fe_{1/3}Mn_{1/3}O_2$ as cathode. The cycling performances were found to be excellent, with a capacity retention of 70 % after 150 cycles at 1C.

In the field of SPEs for NIBs, in our research group we investigated a PEO-based polymer electrolyte blended with sodium carboxymethylcellulose (Na-CMC). We also published two research articles on photopolymer electrolytes for

application in sodium rechargeable batteries. The details of these research works will be presented in the experimental section.

In the last years, several research groups investigated alternative polymers to PEO, in particular for LIBs, after the suggestion of several authors of some limitations on the cell performances of PEO and other polyether-based polymer electrolytes. In fact, although PEO and its analogous represent a good alternative to liquid electrolytes due to their highly improved safety, they slightly react with lithium metal and are oxidized at relatively low potential values (~ 4.5 V), thereby restricting the choice of positive electrode materials to low working potential cathodes. The ionic conductivity of the polymer electrolytes remains below 10^{-4} S cm^{-1} at room temperature, and transference numbers also remain low. Furthermore, ionic conductivity are strictly related to the glass transition temperature, which implies poorer mechanical properties as the ionic conductivity improves [105]. The same drawbacks, obviously, are reflected on NIBs.

In this respect, Mindemark *et al.* developed different polycarbonate-based SPEs, such as poly trimethylene carbonate (PTMC), and also copolymers of trimethylene carbonate (TMC) and ε-caprolactone (CL) as polymer electrolytes for LIBs [106-108]. Subsequently, in this group they studied polycarbonates for sodium batteries. The aliphatic polycarbonate PTMC, previously successfully applied to lithium polymer batteries, is the first example of non-polyether host matrix used in solid-state sodium batteries. Compared to PEO, it has a higher glass transition temperature, which negatively affects the cell performances for high-power application. However, by proper combination of plasticizing and crosslinkable moieties, the ionic conductivity can be greatly enhanced, because of the decrease of the T_g. The same research group showed the first application of PTMC based SPE in NIBs, using two different sodium salt (NaTFSI and $NaClO_4$) with PTMC as polymer host. The membranes were prepared by solvent casting. Ionic conductivity similar to the analogous Li salt electrolytes (10^{-6} S cm^{-1} at 60 °C and 10^{-8} S cm^{-1} at room temperature) were obtained. Since the best ionic conductivity was found for the sample $PTMC_3$-NaTFSI, this sample was assembled in Na metal cells with Prussian blue working electrode, which displayed high specific capacities upon discharge and limited polarization at C/10 and 60 °C [109].

Despite the amount of research efforts in NIBs, SPEs are still at the early stage of development, and only few examples are reported in the literature so far of practical cell application.

3.1.2 Gel Polymer Electrolytes - GPEs

Compared to SPEs, GPEs show higher ionic conductivity, due to the enhanced ionic mobility guaranteed by the liquid electrolyte solution trapped in the polymer matrix. The salt and organic solvent can be picked from the list of common Na salts and solvents used in liquid electrolytes. The solvent acts as plasticizer and its addition results in the swelling of the polymer matrix, the physical aspect of which changes from a solid to a gel. The gelification of the membrane facilitates the interfacial contact with the electrodes in comparison to SPEs. The most common polymers used to prepare GPEs are polyacrylonitrile (PAN) [110-112], polymethylmethacrylate (PMMA) [113-115], polyvinylchloride (PVC) [116], and polyvinylidene fluoride (PVDF). The room temperature ionic conductivity of GPEs generally stands in the range of 10^{-4} to 10^{-3} S cm^{-1}. While polymers with an amorphous character like PMMA provide higher ionic conductivities, their mechanical properties are usually lower due to the lack of rigidity in their matrix. PAN and PVDF provide higher mechanical properties due to a higher degree of crystallinity but it also implies a loss in ionic mobility. Copolymers, such as poly(vinylidene fluoride–hexafluoropropylene) (PVDF–HFP) [117,118] can help in overcoming the loss of mechanical properties while keeping a promising [119-121] ionic conductivity. The presence of CF_3 groups on the HFP monomer increases the amorphocity of the copolymer in comparison to PVDF, which is more prone to crystallization. The higher ratio of amorphous phase enhances the ionic conductivity of the pure PDVF-based GPE up to 7.5 10^{-3} S cm^{-1}, while the crystallinity provided by PVDF eases the cohesion of the film and its processability [122].

Recently, Goodenough and co-workers, presented an hybrid GPE prepared by the integration of PVDF-HFP with glass fiber paper, which acts as reinforcement [123]. The use of this glass fiber tunes the mechanical and surface properties of the PVDF-HFP. The hybrid polymer matrix so conceived, exhibits good mechanical strength and a thermal stability up to 200 °C. They tested the GPE in a sodium half-cell using $Na_2MnFe(CN)_6$ as cathode, obtaining an improvement of the rate capability, cycling performance, and Coulombic efficiency compared with a conventional glass fiber soaked in a liquid electrolyte. This kind of strategy using of some sort of reinforcement on the classical PVDF-HFP copolymer, was also used by Zhu *et al.* [124], which employed polypropylene nonwoven (NW) as reinforcement. The NW/P(VDF-HFP) GPE gelified with $NaClO_4$ organic liquid electrolyte shows very interesting Na^+ ionic conductivity at room temperature was

found to be four times higher compared to the conductivity of the commercial separator saturated with the same electrolyte. Electrochemical tests performed using coin cell configuration with $Na_4Mn_9O_{18}$ as cathode, Na as counter and reference electrodes and NW/P(VDF-HFP) GPE as electrolyte, give promising insights on the use of this GPE in NIBs [115].

Despite the strong interest on GPEs, actually there are a limited number of works on GPEs for NIBs application [123,116-127,121], but the works in this field will most likely increase in the upcoming years, following the increasing research interesting on Na-based technology.

3.1.3 Composite Polymer Electrolytes – CPEs

Due to the low ionic conductivity of PEO-based polymer electrolytes, another strategy proposed to improve the performances of such materials is the addition of inorganic fillers, particularly ceramic fillers. They act in two ways: they suppress the local crystallization of the polymer chains, therefore increasing the ionic mobility and providing more ionic conducting pathways at the filler/polymer interface; in addition, the incorporation of fillers is supposed to improve the stability at the interface between the electrolyte and the electrodes [118].

Ceramic fillers can be divided in two main categories: inactive, such as TiO_2, Al_2O_3, etc. or active fillers (also called fast ion conductors), for example $Li_{0,33}La_{0,557}TiO_3$, $Li_7La_3Zr_2O_{12}$, $Li_{1,3}Al_{0,3}Ti_{1,7}(PO_4)_3$ [118]. The main difference between these two ceramic classes is the capacity of the active fillers to get higher conductivity and higher ion transference number since the active fillers participate in the conduction process of mobile ions.

Weston and Steele in 1982 [62] first reported on the use of inorganic fillers in polymer electrolytes to improve the mechanical properties of SPEs for lithium batteries. In the case of NIBs there are few examples on such materials.

As was previously discussed, in the section of SPEs, Moreno *et al.* [101] used silica in order to improve the mechanical properties of their SPE, and they obtained two positive effects: the mechanical features were enhanced and the ionic conductivity was increased.

Another example recently reported is on a composite polymer electrolyte prepared using nano-sized TiO_2 as filler. In this work, the authors prepared by solvent casting a CPE with EO:Na ratio of 20 adding 5 % w/w of TiO_2. The

composite polymer electrolyte exhibited an ionic conductivity of 2.62 10^{-4} S cm^{-1} at 60 °C, slightly better compared to the analogue SPE without the inorganic filler (1.35 10^{-4} S cm^{-1}). This material was galvanostatically tested in a Na|CPE|$Na_{2/3}Co_{2/3}Mn_{1/3}O_2$ half cell configuration, and the results were compared with the performances given by the same electrode using a liquid electrolyte. The CPE displayed good cycling stability, with capacity values around 50 mAh g^{-1}, approximately the half obtained with the liquid electrolyte. The lower amount of the capacity obtained with the CPE is due to the large polarization mainly ascribed to the thickness of the polymer electrolyte (~18 mm) [119].

Among these electrolytes, there are several studies on CPEs for Na-Sulfur batteries, which are virtually applicable in high temperature energy storage devices [120].

Chapter 4

Cellulose-based hybrid polymer electrolytes for green and efficient Na-ion cells

This chapter is an extract of the first scientific research article delivered during this three years PhD program [121].

4.1 Introduction

In the present work, the incorporation of a pyranose ring based was ionic backbone (sodium carboxymethyl cellulose, Na-CMC) into a PEO-based polymer matrix containing a suitable sodium salt proposed. Carboxymethyl cellulose (CMC), an important ionic ether derivative of cellulose, which is prepared from alkaline cellulose and chloroacetic acid by etherification and usually used in the form of its sodium salt (Na-CMC), is widely applied in industrial applications. Na-CMC has been selected as it can improve the mechanical integrity of the final film without affecting the ionic mobility and the electrode/electrolyte interfacial characteristics. Moreover, it shows good solubility in water, low cost, biodegradability, biocompatibility and lack of toxicity. This is the first ever report where the useful characteristics of Na-CMC as additive in a Na^+-ion conducting polymer electrolyte were explored. The same Na-CMC was also used as binder for the electrode active material particles, which enabled the overall process including the electrodes and electrolyte preparation to be carried out through very simple, cheap and absolutely eco-friendly water based procedures. The preliminary results of lab scale cell testing in terms of galvanostatic charge/discharge cycling strongly recommends the use of such hybrid SPE for the development of safe and sustainable Na-ion polymer cells.

4.2 Experimental

4.2.1 Preparation of the solid polymer electrolyte

Polyethylene oxide (PEO, average Mw: 400,000), sodium carboxymethylcellulose (Na-CMC, average Mw: 250,000) and sodium perchlorate ($NaClO_4$, battery grade) were purchased from Sigma-Aldrich. PEO, $NaClO_4$ and Na-CMC (in the 82:9:9 ratio, respectively) were thoroughly mixed in water under mild heating. The mixture was stirred at 80 °C, until a clear homogeneous liquid solution was obtained. The film formation was carried out by casting the aqueous liquid electrolyte precursor in a Petri dish, followed by drying overnight under ambient condition. Final SPE films (thickness ~90±2 μm, see Fig. 4.1) were obtained by hot-pressing (80 °C, 25 bar) the dried precursor for 15 min. A reference membrane having a PEO to $NaClO_4$ 9:1 w/w ratio was also prepared. This procedure yielded homogeneous and mechanically robust membranes (namely, PEO-Na for the pristine and PEO-CMC-Na for the CMC-laden SPE), which were dried under vacuum at 50 °C for 24 h for further characterization.

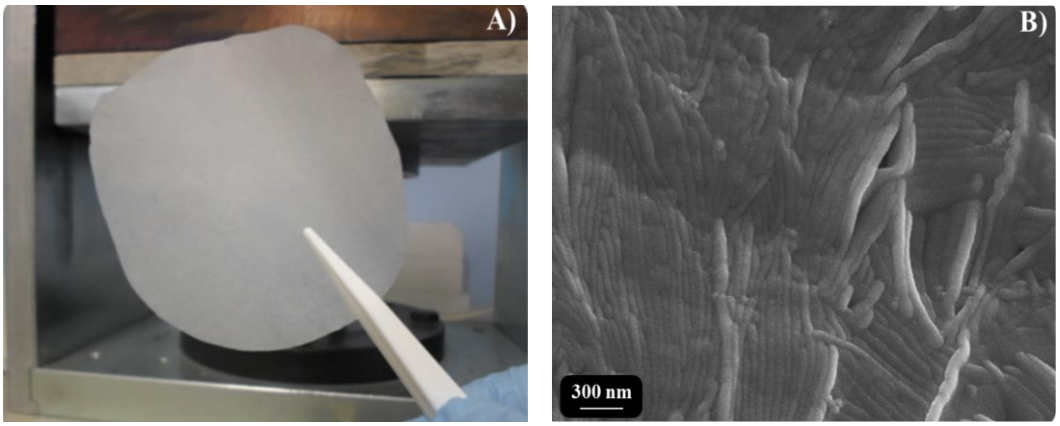

Fig. 4.1 A) Aspect and B) FESEM analysis of the PEO-NaCMC membrane (adapted from [131])

4.2.2 Characterization techniques, lithium/sodium cell assembly and testing

Thermo-gravimetric analysis, by TG 209 F1 Libra1 instrument from Netzsch, was performed up to 800 °C (10 °C min^{-1}) under nitrogen to assess the thermal

stability of the samples. Dynamic mechanical thermal analysis (DMTA) was performed by a TTDMA instrument (Triton Technology Ltd), at 1 Hz frequency and 2 °C min^{-1} in the tensile configuration, over a temperature range of –110/+60 °C. The characterization methods are the same as already described elsewhere [122]. The surface morphology of the solid polymer electrolyte was imaged by Field Emission Scanning Electron Microscopy (FESEM) analysis on a ZEISS Supra 40, equipped with an energy dispersive X-ray spectrometer (EDX). For analysis, the samples were subjected to metallization by sputtering a very thin Cr layer (around 10 nm maximum) to minimize the effect of the electron beam irradiation that may possibly lead to charging and "burning" of the polymer network.

The ionic conductivity of the polymer electrolytes (SPEs) was determined by electrochemical impedance spectroscopy (EIS) between frequency range 100 kHz and 1 Hz at open circuit potential using a PARSTAT-2273 potentiostat instrument. For testing, discs of 2.54 cm^2 (ECC-Std test cells, EL-CELL GmbH, http://el-cell.com/ products/test-cells/ecc-std) were cut from the SPE film and sandwiched between two stainless steel (SS-316) blocking electrodes. The assembled cells were kept in a climatic chamber purchased from BINDER GmbH and tested between 20 and 90 °C. The resistance of the electrolyte was given by the high frequency intercept determined by analysing the impedance response using a fitting program provided by Princeton Applied Research.

The sodium ion transference number (t_{Na^+}) was measured at 60 °C by combined AC impedance and DC polarization measure- ments of a symmetric Na/SPE/Na cell (ECC-Std), as explained by Bruce and Watanabe for Li-ion battery systems [133-[124]. The surface of Na metal was refreshed using a scalpel before test cell assembly [125] in the dry box. Before testing, the cell was kept at the testing temperature overnight to achieve an intimate contact and a stable interface between the electrolyte and the electrodes.

The interfacial properties of the prepared SPE films with the Na metal electrode, and the corresponding variation in resistance with the contact time, were measured by monitoring the time evolution of the impedance (EIS) response of Na/SPE/Na symmetrical cells (ECC-Std test cells, EL-CELL GmbH, http://el-cell.com/ products/test-cells/ecc-std, Fig. 4.2). The cells were stored at 60 °C under open circuit conditions in the climatic chamber.

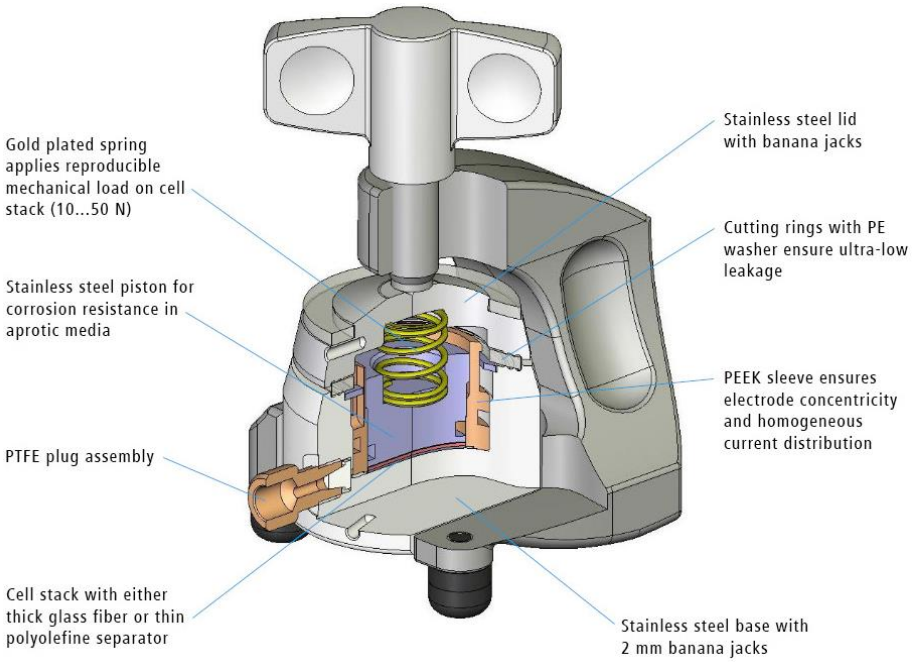

Fig. 4.2 Schematic representation of ECC-Std test cell (taken from http://el-cell.com/products/test-cells/ecc-std).

The electrochemical stability window (ESW) of the SPE was evaluated at ambient temperature by linear sweep voltammetry (LSV) in two electrodes cells (ECC-Std) using a CHI-660 electro- chemical workstation. Separate LSV tests were carried out on each polymer electrolyte sample to determine the cathodic and anodic stability limits. The measurements were performed by scanning the cell potential from the OCV towards more negative (cathodic limit) or positive (anodic limit) potential values. Cell configuration adopted for anodic scan (potential scan range from the OCV to 6 V vs. Na/Na^+): SS-316 piston as the working electrode [125] and Na metal disc as both the counter and the reference electrodes, SPE as the electrolyte (active area equal to 2.54 cm^2). Cell configuration adopted for cathodic scan (from the OCV to –0.2 V vs Na/Na^+): Cu disc as the working electrode, Na metal disc as both the counter and the reference electrodes, SPE as the electrolyte. In both cases, the potential was scanned at a rate of 0.100 mV s^{-1}. The current onset of the cell was associated with the decomposition potential of the electrolyte.

Galvanostatic charge (Na^+ deinsertion)/discharge (Na^+ insertion) cycling was conducted at 60 °C) in ECC-std cells, purchased from EL-Cell, Germany. The PEO-CMC-Na membrane was sand-wiched between a TiO_2-based working electrode or a $NaFePO_4$-based electrode, respectively, and a Na metal (99.8 %, Sigma Aldrich)

counter electrode. Thus, all potential values given in this manuscript refer to the Na/Na^+ reference couple. The exact composition of the electrode was 87:8:5 wt.% in active material (commercial Hombikat anatase TiO_2 or $NaFePO_4$, respectively), conductive carbon (Shawinigan Black AB50, Chevron Corp., USA) and Na-CMC binder [126]. Initially, CMC was dissolved in deionized water followed by the addition of conductive carbon and active material nanoparticles under continuous stirring (~3 h). The obtained slurry was then spray coated on a copper (or aluminium) current collector, dried under a fume hood at ambient conditions and later vacuum dried overnight at 120 °C. Later, electrodes (area 2.54 cm^2) were cut from the foils and assembled in the cells. $NaFePO_4$ was electrochemically prepared following the procedure reported in the reference [127] starting from a hydrothermally synthesised $LiFePO_4$ [128]. To confirm the obtained results, tests were performed at least three times on different clean electrodes and fresh samples. Procedures of cell assembly and related activities were performed in the inert atmosphere of a dry glove box (MBraun Labstar, O_2 and H_2O content <1 ppm) filled with extra pure Ar 6.0.

4.2.3 Results and discussion

An optimal PEO:$NaClO_4$:Na-CMC composition was selected for the preparation of the polymer electrolytes, that is 82:9:9 in weight ratio. Before arriving to the reported formulation, several tests were performed to understand the fundamental aspects of polymer electrolytes, to decide the quantity and type of cellulosic additive, as well as the suitable molecular weight of PEO depending on the easiness in processing, solubility of salt, ionic mobility in terms of [EO]/[Na] ratio and mechanical integrity. Na-CMC was selected in the 5% w/w ratio with respect to the PEO content because of optimal solubility and mechanical properties. Moreover, it was found out that a higher amount of Na-CMC reduces the ion transport properties, thus here the results are presented pertaining only to lower content that was found to be sufficient to improve the mechanical property and dimensional stability at higher temperatures, as shown in the following paragraphs. The polymer electrolyte films produced by the easy and sustainable water-based technique were opaque, flexible and easy to handle as shown in Fig. 4.1A. FESEM analysis (see Fig. 4.1B) reveals the homogeneity of the Na-CMC laden polymer electrolyte prepared; only the typical aligned PEO bundles obtained by the water-based procedure employed are clearly visible, without noticeable signs of CMC agglomerates.

Thermal history studies of the final membranes involved Thermo-Gravimetric Analysis (TGA) and Dynamic Mechanical Thermal Analysis (DMTA). The thermogravimetric profiles, shown in Fig. 4.3A, reveal that PEO-Na SPE was stable up to around 350 °C, exhibiting a single degradation process, whereas the presence of CMC in the sample PEO-Na-CMC led to a two-step degradation process. The first dip before 100 °C indicates the loss of humidity that may absorbed during the handling of the sample for testing. The following weight loss of <5% at around 290 °C for the sample PEO-Na-CMC was ascribed to the degradation of some of the moieties (e.g., CO_2, acetic acid, etc., denoted as '*' in Fig. 4.3A.) present in the pyranose chain, which was followed by an irreversible degradation of the composite material above 350 °C leaving behind some inert residues at 800 °C. A support from these values helped us to finalise the formulation by appropriately adding the minimal quantity of additive.

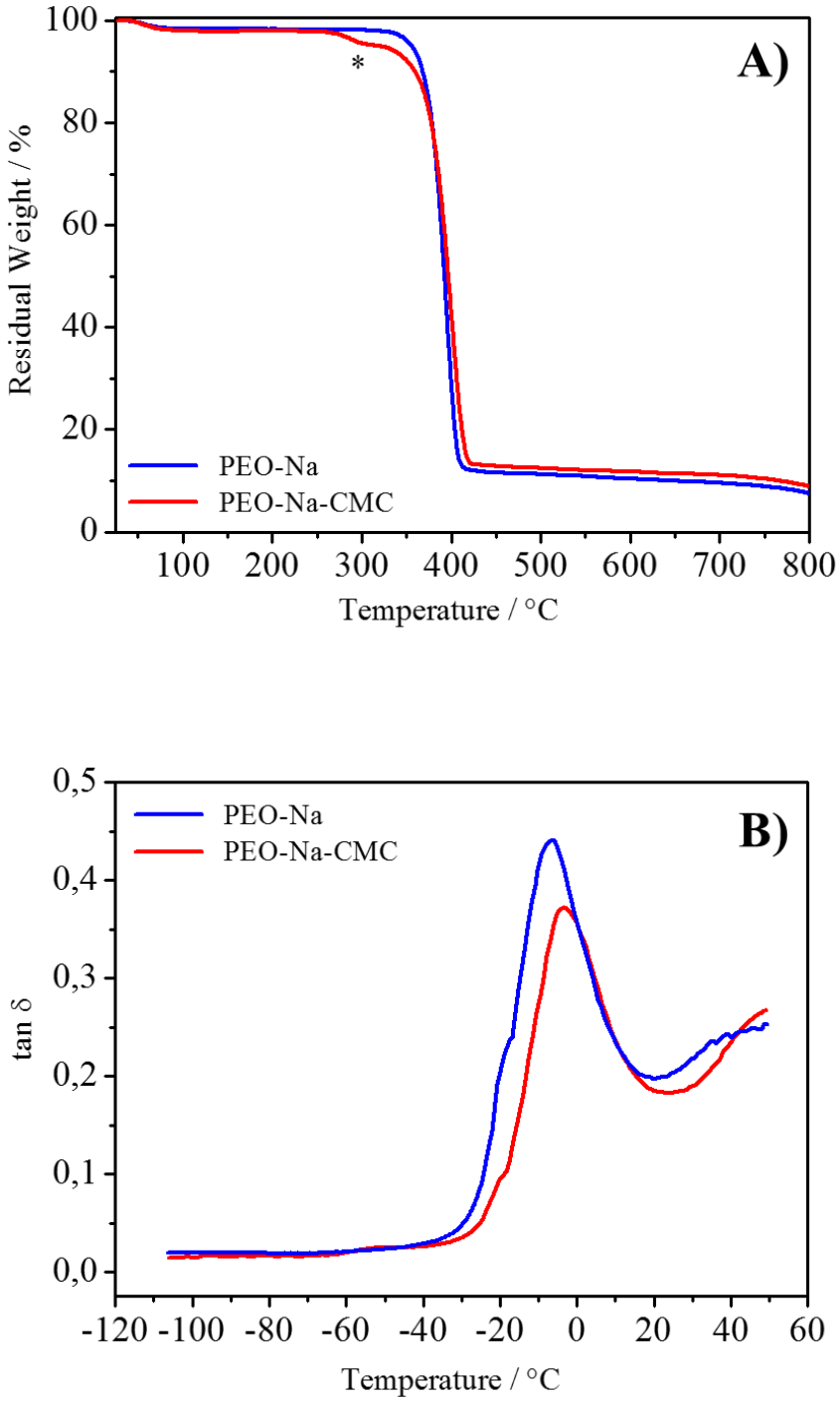

Fig. 4.3 A) TGA and B) DMTA profiles of PEO-Na (blue) and PEO-Na-CMC (red) SPEs.

Viscoelastic characterization of the polymer membranes was carried out by means of DMTA analysis, which consists of measuring storage (E') and loss (E") modulus, and evaluating the damping factor tan δ as E"/E' ratio [129]. The curves of tan δ as a function of temperature are shown in Fig. 4.3 B. Glass transition temperature (T_g, obtained as the tip of the tan δ peak) of PEO-Na membrane was found to be –12 °C; an increase at around –5 °C was observed due to the presence of Na-CMC. A small increase in T_g upon addition of Na-CMC may be associated with the Na-CMC/PEO interactions, particularly the hydrogen bonding between the acidic hydrogen of the oxidrilic groups of the CMC and the oxygen of the ethylene oxide (–EO–) repeating units, which in turn reduces the segmental mobility of the amorphous PEO chains. Noteworthy, the T_g of PEO-Na sample was unexpectedly high, based on the typical low T_g of PEO-based polymers supporting lithium salts [141,142] that lies between -55 and -25 °C. As already reported in the literature for similar systems [132], it was attributed to the presence of sodium salt which drastically improves the transition temperature of PEO-based systems. At similar compositions, T_g of PEO–$NaClO_4$ is larger than that of typical $LiClO_4$ doped system, which may account for an increased T_g. Nevertheless, the reason for such a behaviour is not yet clear, further studies are needed to understand the reason behind this huge jump in glass transition behaviour.

The Arrhenius plots for the temperature dependence of the ionic conductivity are shown in Fig. 4.4. Clearly, the presence of Na-CMC did not influence the experimental trends. Both the curves show a slow and continuous change in the slope up to -55 °C, beyond which a noticeable change in slope was observed. It may be ascribed to the well-known transition of PEO from crystalline to amorphous phase. Ionic conductivity values around 10^{-3} S cm^{-1} are obtained at higher temperatures, definitely sufficient for an appropriate functioning in NIBs conceived for moderate temperature application.

A deep understanding of the interfacial properties between the sodium metal electrode and the polymer electrolyte is mandatory in order to provide more insight into the factors controlling the rechargeability of sodium-based solid polymer batteries.

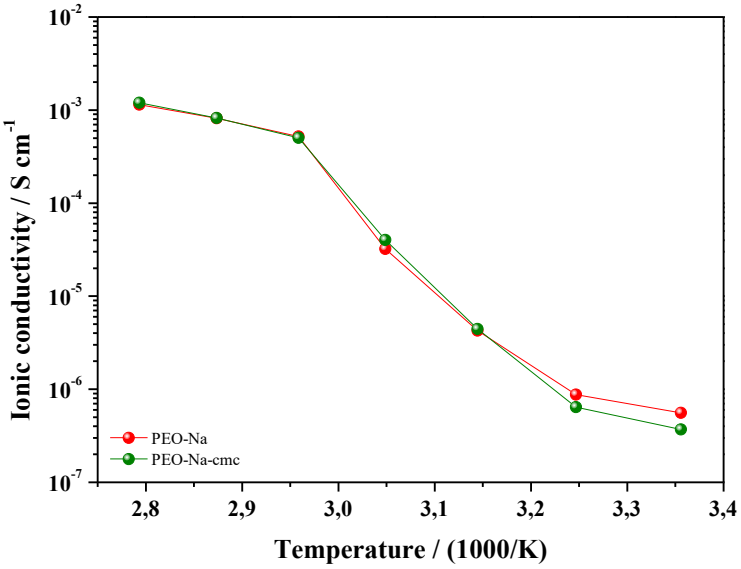

Fig. 4.4 Arrhenius plot for the temperature dependence of the ionic conductivity for the PEO-Na and PEO-NaCMC SPEs.

Thus, the SPEs were examined in terms of compatibility (interfacial stability) with the sodium metal electrode. The EIS measurements carried out on a Na/SPE/Na symmetrical cell stored under open circuit potential (OCV) at 60 °C are shown in Fig. 4.5A. In general, the resistance of a cell is composed of bulk resistance of the electrolyte medium and interfacial resistance, which reflects the compatibility between the electrodes and the electrolyte [19]. Clearly, the value of charge transfer resistance slightly increased during the first day of storage for sample PEO-Na-CMC, which indicates the formation of a passivating layer on the surface of the sodium metal due to the reactivity with the polymer electrolyte. It decreased and, then, stabilised after about 6 days of storage at about 65 kV. After these days, the charge transfer resistance was found to be steady, only slightly fluctuating within ± 3 % of the latter value. Such stabilisation of the interface may be explained by assuming that the morphology of the passivation film changes slightly during the initial time to finally acquire a thin, non-compact, possibly porous structure [113]. The increase in bulk resistance was almost negligible. On the contrary, the symmetric cell assembled with the PEO-Na electrolyte did not stabilise upon storage (see plot of Fig. 4.5 B), with a continuous increase of the interfacial resistance, thus indicating a worse compatibility with the sodium metal electrode.

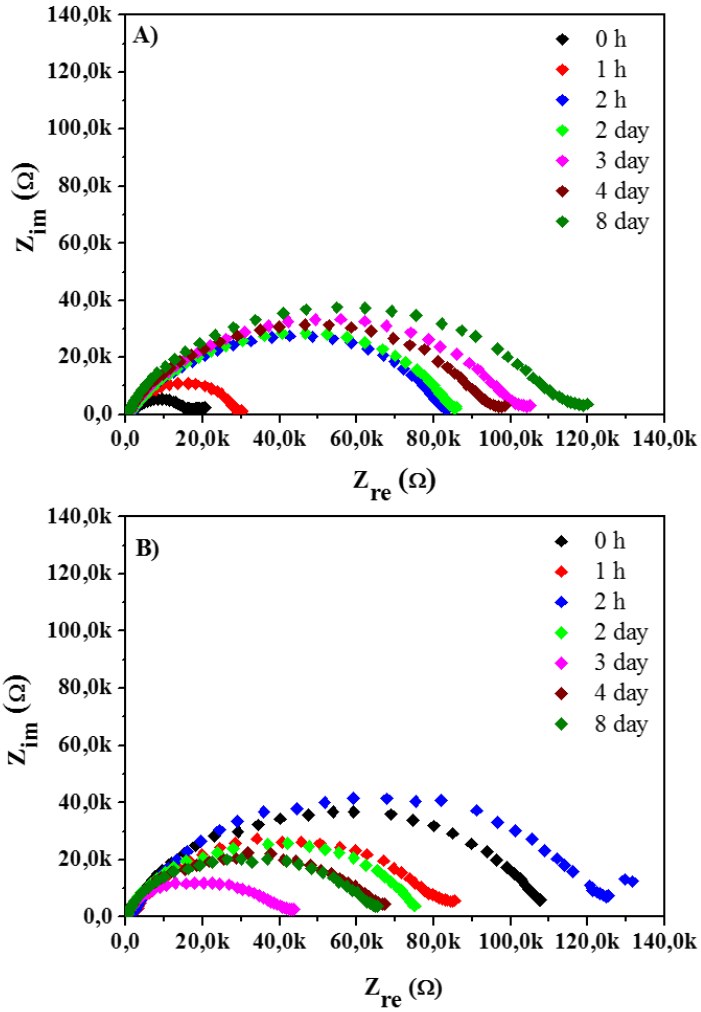

Fig. 4.5 Interfacial stability studies: time evolution of the impedance spectra of the Na/SPE/Na test cells, stored under open-circuit conditions at 60 °C of PEO-Na-CMC (A) and PEO-Na (B) SPEs.

The ion transference number (t+) is a key factor in the optimization of battery electrolytes. Indeed, high t^+ guarantees high enough power density [8]. In our novel pyranose ring laden polymer electrolyte, the sodium transport number t_{Na^+} is 0.15 ± 0.03 (see Fig. 4.6), reasonably high at a moderate temperature of 60 °C, which is realistic for the envisaged application. EIS was also used as an indirect method to evaluate the compatibility between CMC-binded TiO_2 electrodes and the solid polymer electrolytes, either with or without incorporation of NaCMC, at 60 °C. A Na/SPE/TiO_2CMC configuration was adopted. In general, lower charge transfer

resistance was obtained for the NaCMC-laden SPE, which was also definitely more stable upon prolonged storage at 60 °C, as already obtained in interfacial stability studies. Noteworthy, the slope of the Warburg diffusion coefficient was exactly at 45° indicating an almost ideal ion diffusion in the PEO-Na-CMC based cell, which was not the case for the PEO-Na based cell.

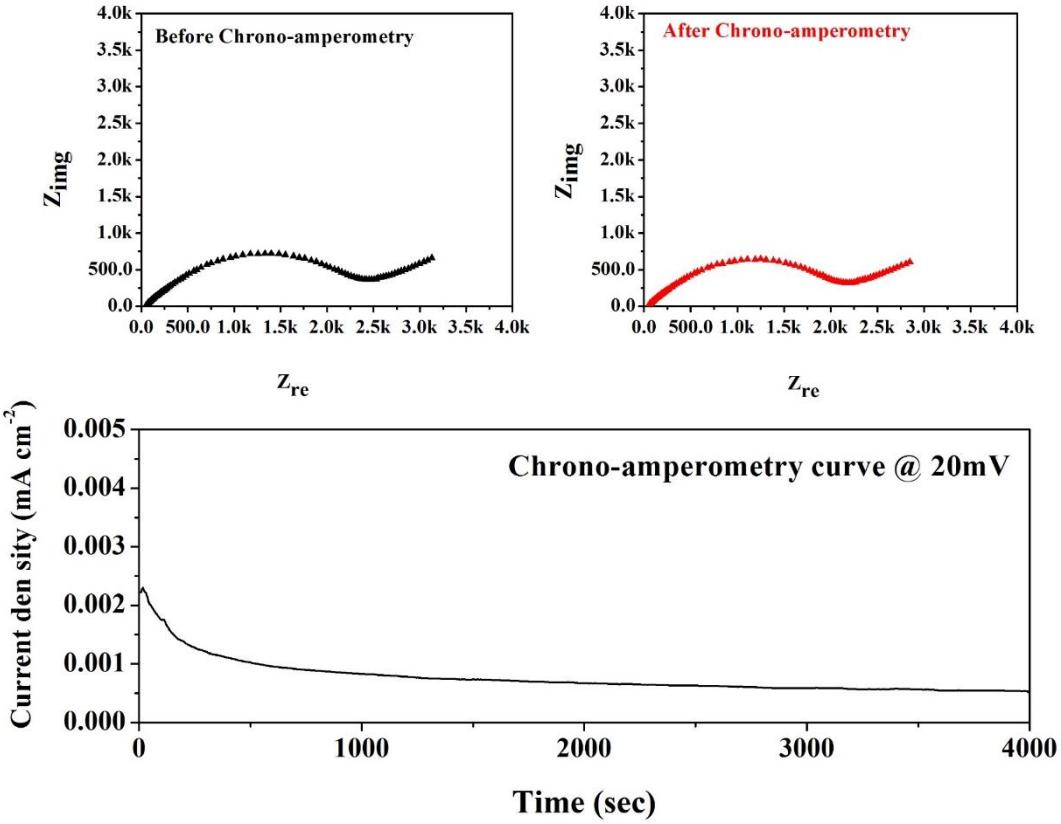

Fig. 4.6 Transference number measurements of the Na/PEO-Na-CMC/Na test cell at 60 °C.

Electrical Stability Window measurements with respect to Na/Na^+ reference were performed at 60 °C. Fig. 4.7 shows the stability of the polymer electrolyte membrane towards anodic oxidation and cathodic reduction reactions, in particular for the CMC-laden SPE. From the cathodic curves (1^{st} and 5^{th} cycles are shown) it is noticeable the stripping and plating process of Na centred at around 0.0 V. The resulting stability window is very wide between 0 and 4.5 V. Such a wide stability window bodes well with electrolytes application in NIBs. Noticeably, even if the offset of the current flow in the first cycle is set at a lower potential, already after few cycles its trend consistently evolves, showing a sort of "passivation" phenomenon, which extends the anodic stability up to 5 V. This behavior has

already been observed in previous studies concerning lithium-based polymer electrolytes reinforced by cellulose [133].

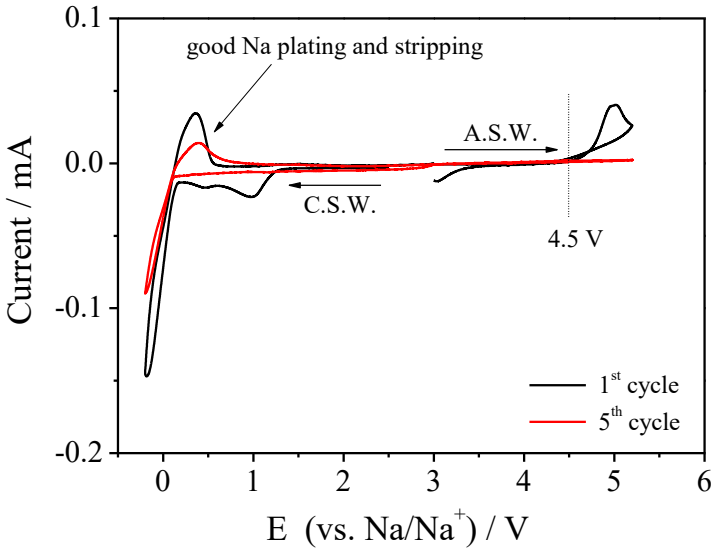

Fig. 4.7 Anodic (A.S.W.) and cathodic (C.S.W.) electrochemical stability window for PEO-Na-CMC (1st and 5th cycles are shown) at 60 °C.

Such a high decomposition potential suggests promising prospects for these newly elaborated electrolytes in sodium batteries focused at high safety and high voltage. The satisfactory results obtained from physical and electro-chemical characterization of the Na-CMC incorporated SPE encouraged the investigation of their performances as separating electrolyte in lab-scale sodium metal cells, using TiO_2 and, also, $NaFePO_4$ as working electrodes. The electrochemical behaviour was investigated by means of galvanostatic charge/discharge cycling at 60 °C. Note that the $NaFePO_4$-based cell was electro- chemically cycled in solid state configuration after five formation charge/discharge cycles using a 1.0 M $NaClO_4$ in PC liquid electrolyte solution in order to exchange lithium with sodium following the procedure reported by Hassoun and co-workers [16], starting from a hydrothermally synthesised $LiFePO_4$ [128]. The results are shown in Fig. 4.8. In particular, plots (A, B) show the typical charge/discharge potential versus time profiles of the two lab-scale cells.

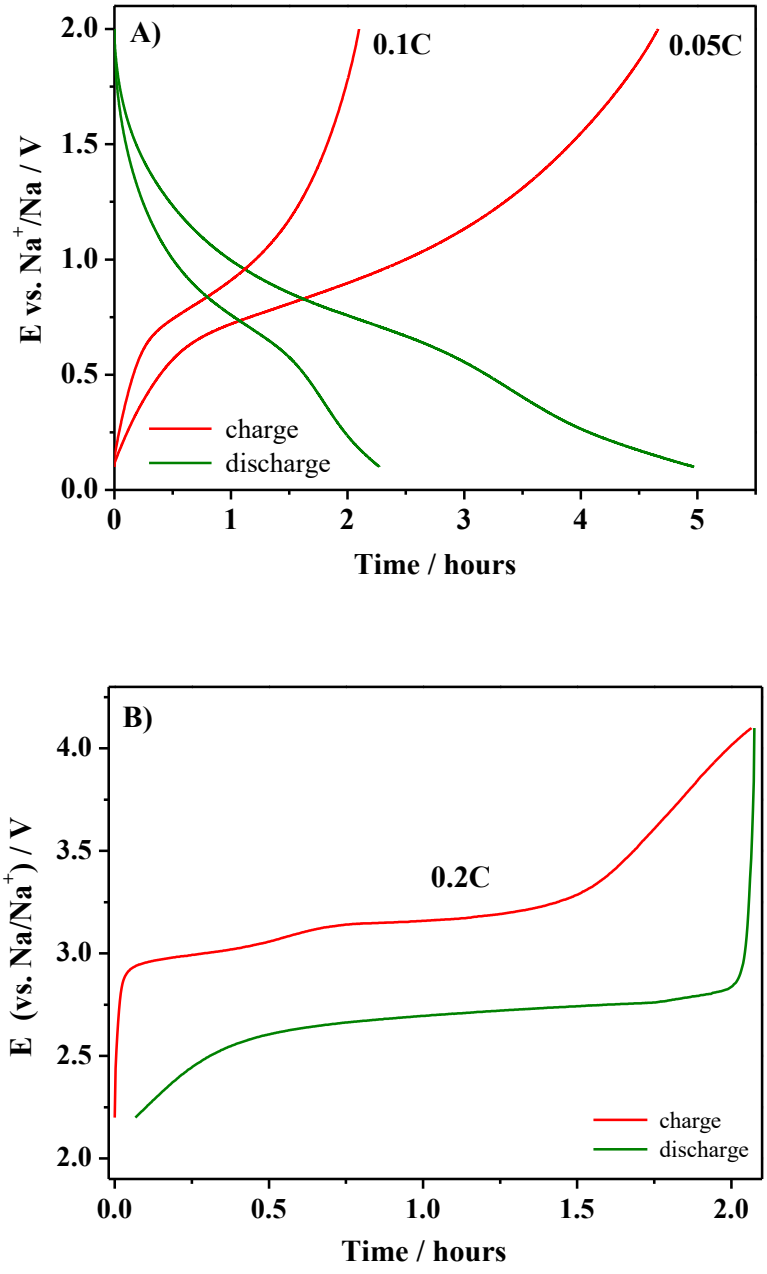

Fig. 4.8 Potential vs. time charge/discharge profiles of A) Na/SPE/TiO_2 cell (5^{th} cycle at 0.05 C and 10^{th} cycle at 0.1 C) and B) Na/SPE/$NaFePO_4$ cell (10^{th} cycle at 0.2 C), both the measurements were conducted @ 60 °C.

The behaviour of the cells was found to be clearly in agreement with the literature data for both TiO_2 and $NaFePO_4$ materials [138,[134], showing highly reproducible and reasonably well defined plateaus. Good performance at higher current rate may be ascribed to the efficient ionic conduction in the polymer separator and the favourable interfacial charge transport between electrodes and electrolyte in the cell. The cells demonstrated stable behaviour at each of the tested currents. The drop in potential while passing from charge to discharge was found to be rather limited for an all-solid Na polymer cell, which means low resistance of the cell. The Coulombic efficiency approached the unity and the specific capacity vs. cycle number data (Fig. 4.9 A and B), being preliminary results, were considered encouraging.

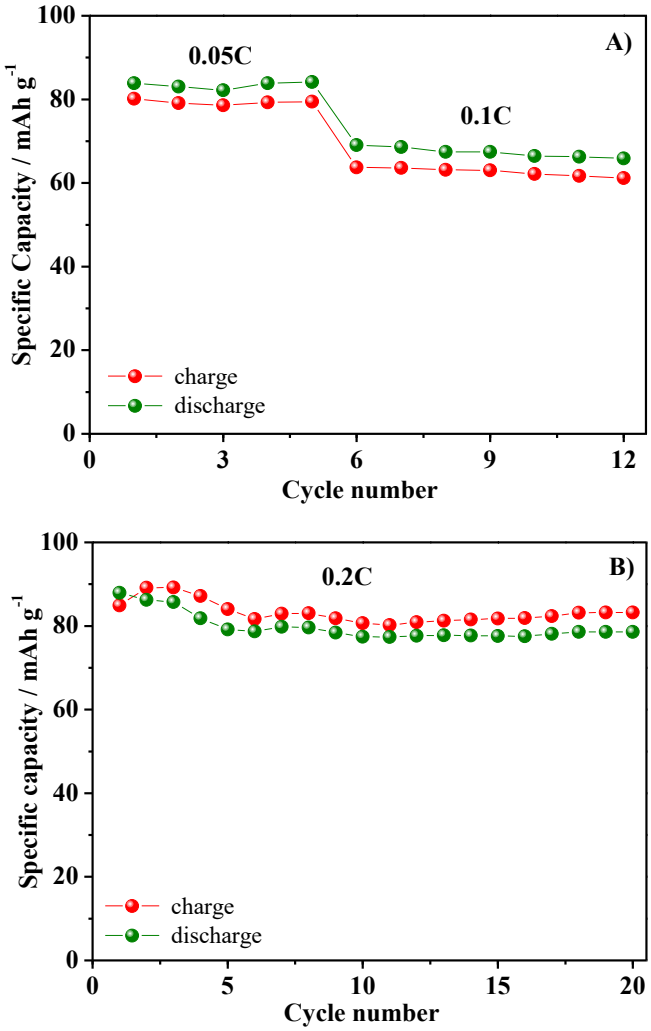

Fig. 4.9 Charge/discharge cycling behavior for the A) Na/SPE/TiO_2 cell @ 0.05 C and 0.1 C current rate, and B) Na/SPE/$NaFePO_4$ cell @ 0.2 C current rate

Overall, the latter indicate good mechanical stability of the electrodes during the Na^+ ion insertion/deinsertion process, good interfacial contact and charge transport between the electrodes and the polymer electrolyte, and excellent reversible cycling after the initial surface reactions are complete.

4.2.4 Conclusions

Overall, optimisation in terms of specific energy output and long-term performance must be targeted; however, these new series of materials could facilitate the beginning of a path for energy storage devices towards safer, biosourced and reliable options. Results reported in the present chapter, that resumes the initial work of my PhD Thesis, firstly demonstrate the possibility of using Na-CMC as an additive in improving the mechanical properties without hampering the ionic conductivity and thermal stability of solid polymer electrolyte for Na-ion cells. The adopted preparation method is simple, cheap and eco-friendly, being water-based. The overall electrochemical performance in separate Na-metal cells with TiO_2 or $NaFePO_4$ working electrodes was demonstrated to be stable, which can be further elaborated for truly solid Na-ion polymer cells conceived for moderate temperature application. There is a large scope for improvement before such systems may become a practical reality, and work is under progress in this direction, nonetheless surely these preliminary results represent a positive indication towards accomplishing such reality.

Chapter 5

Crosslinked polymer electrolytes for safe and sustainable Na-ion cells

Introduction

The most facile way for preparing polymer membranes is the simple solvent casting, where the salt is mixed with the polymer matrix in a solvent. Often this method require the use of organic solvents (toxic) and furthermore the entire process time is largely dependent from the evaporation time of the solvent. Although being easy to perform, solvent casting is tedious and does not allow an effective modification of the polymer structure, in particular in terms of crystallinity. This negatively affect the polymer electrolyte performances, because does not allow proper amorphisation of the polymer network and the amorphous phase is fundamental for guaranteeing high ionic motion.

In order to increase the amorphization of the polymer, different approaches were applied. Particularly in the last years, photopolymerization became increasingly popular, thanks to its easiness, ecocompatibility, low-cost, and reproducibilityIt is already commercially utilized in a wide variety of applications (e.g. coatings, adhesives, microelectronic resists, etc.). The photopolymerization exploits the absorption of light by molecules (photo-initiators), which in responselead to an excited state. If the energy of the excited state is enough to activate some molecular bond of chemical species (the polymer) present in the reactive mixture, new molecular bonds are created. Typically, the radiation source is UV-light (100-400 nm), and this is the reason why the process is also called UV-curing.

In this section, which resumes the experimental work carried out in the first two years of my PhD, two different kind of UV-cured photopolymer electrolytes will be presented and thoroughly discussed.

The work led to two scientific research articles, which are the results of collaborative work by myself and my colleagues in the research group [135] [136].

5.1 Methacrylic based photopolymer electrolyte operating at ambient temperature

In this work, the first example of photopolymer electrolyte for NIBs was proposed, which demonstrated the potential of the UV-induced photopolymerization as a feasible and scalable preparation technique for large-scale grid storage systems. High thermal stability and a low glass-transition temperature (T_g) along with outstanding ionic-conductivity values and a wide electrochemical stability window were obtained. Moreover, TiO_2-based lab-scale sodium polymer cells were assembled, which operated with very stable cycling and specific capacity values at the level of similar liquid-based systems for 250 cycles at current densities as high as 1 mA cm^{-2}. The possibility of in situ design to form an electrode/polymer electrolyte composite with intimate interfacial characteristics and promising performance in NIBs was finally demonstrated as a proof of concept.

5.1.1 Experimental

5.1.1.1 Preparation of the photopolymer electrolyte

Bisphenol A ethoxylate dimethacrylate (BEMA, average Mn ~ 1700), poly(ethylene glycol) methyl ether methacrylate (PEGMA, average Mn ~ 700), chloroform, sodium perchlorate (battery grade), sodium (99.8 %), sodium carboxymethyl cellulose (Na-CMC, average Mw 250000), and propylene carbonate (PC, battery grade) were purchased from Sigma–Aldrich. 2-Hydroxy-2-methyl-1-phenyl-1-propanone (Irgacure 1173) was purchased from BASF.

UV-cured polymer membranes were prepared from the oligomers BEMA (difunctional) and PEGMA (monofunctional) in a 35:65 weight ratio; Irgacure 1173 (2 wt %) was added as a free-radical photoinitiator. The resulting reactive mixture was sandwiched between two UV-transparent glass plates, separated by a 200 μm thick tape. Self-standing membranes were obtained by UV irradiation of the mixtures for 2 min with a medium-vapor-pressure Hg lamp (Helios Italquartz, Italy) with an irradiation intensity on the surface of 30 mW cm^{-2}, as measured with a Power puck II radiometer (EIT).

5.1.1.2 Thermal and structural characterization

The reaction kinetics of the photopolymerization was determined by RT-FTIR spectroscopy with a Thermo-Nicolet 5700 instrument. The reactive mixture was deposited as thin layer over silicon wafers and exposed simultaneously to a UV beam (to induce the polymerization) and an IR beam (to analyze in situ the extent of the reaction). The conversion of methacrylate double bonds at a given time was calculated by monitoring the peak area under the band at ν = 1634 cm^{-1} (methacrylate C=C signal), normalized to a stable signal in the spectra (C=O peak at ν = 1726 cm^{-1}). The real-time monitoring was performed in air; therefore, it is expected that a certain oxygen inhibition could reduce the final conversion of the methacrylate double bonds. For this reason, the same materials were also prepared under an inert atmosphere, and the completeness of the UV curing process was assessed by FTIR spectroscopy before and after 2 min of irradiation.

The gel content (insoluble cross-linked fraction) of the UV-cured polymer membranes was determined by measuring the weight loss after 24 h of extraction in chloroform at ambient temperature (standard test method ASTM-D2765-11). The final sample thickness was measured with a Mitutoyo Series 547 thickness gauge equipped with an Absolute Digimatic indicator (model IDC112XBS) with a resolution of ± 1 μm and a maximum measuring force of 1.5 N.

The membranes were activated by swelling in 1 M $NaClO_4$ in PC for 2 h. The duration of this process was fixed after five swelling kinetics experiments, the results of which are shown in Fig. 5.1.

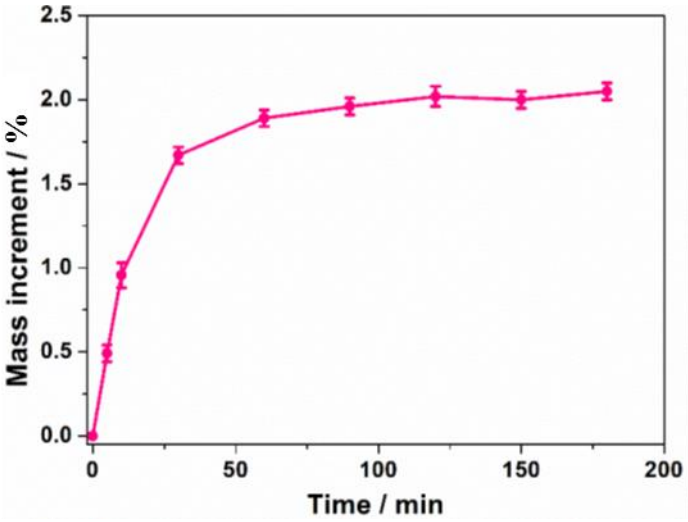

Fig. 5.1 Swelling kinetics of a UV-cured BEMA:PEGMA membrane in $NaClO_4$ 1.0 M in PC.

The glass-transition temperature (T_g) was evaluated by DSC with a DSC 204 F1 Phoenix (Netzsch) instrument between the temperature range -70 to +70 °C at a heating rate of 10 °C min^{-1} under N_2 flux. The reported thermal traces were recorded after a heating/cooling cycle, which is useful to cancel the thermal history of the polymer. The thermal stabilities of the samples were tested by TGA with a TG 209 F1 Libra instrument from Netzsch over a temperature range of 25–600 °C under N_2 flux at a heating rate of 10 °C min^{-1}.

5.1.1.3 Electrochemical characterization

The ionic conductivities of the activated UV-cured polymer electrolytes were determined by EIS in the frequency range between 100 kHz and 1 Hz at the open-circuit potential (amplitude: 10 mV) with a PARSTAT-2273 frequency-response analyzer (Princeton Applied Research). For testing, discs of 2.54 cm^2 were cut from the polymer membranes and sandwiched between two stainless-steel (SS-316) blocking electrodes in ECC-Std test cells (EL-CELL GmbH, http://el-cell.com/products/test-cells/ecc-std). The assembled cells were kept in a climatic chamber purchased from BINDER GmbH and tested between -10 and 80 °C. The resistance of the electrolyte was given by the high-frequency intercept determined by analysis of the impedance response with a fitting program provided by Princeton Applied Research.

The ionic conductivity values obtained at various temperature were used to calculate the activation energy, and the resulting values were fitted with the VTF equation. This is generally used to describe the relationship between viscosity and temperature near the T_g of the polymer matrix. Equation (1) was used to fit the conductivity:

$$\ln \sigma = \ln \sigma_0 - \frac{E_a}{R} \cdot \frac{1}{T - T_0} \qquad \text{(Eq. 1)}$$

The interfacial properties with the sodium metal electrode and their changes with increasing contact time with the electrolyte were measured by monitoring the time evolution of the impedance response of a symmetrical cell, formed by sandwiching the given photopolymer electrolyte between two sodium metal electrodes (configuration Na|polymer electrolyte|Na). The resulting cell was stored

at ambient temperature under open-circuit conditions and tested daily by EIS analysis using a PARSTAT-2273 instrument.

The sodium-ion transference number (t_{Na^+}) was measured at 20 °C by combined alternating current (AC) impedance and direct current (DC) polarization measurements of a symmetric Na|polymer electrolyte|Na cell [137]. A DC potential (DV=20 mV) was applied until a steady current was obtained (generally 3–5 h), and the initial (I_0) and steady (I_{ss}) currents through the cell were measured. Before and after the DC polarization, the impedance spectra of the cell was recorded between 100 kHz and 0.1 Hz with an oscillating potential of 10 mV. Later, the initial ($R_{b\text{-}0}$) and final ($R_{b\text{-}ss}$) bulk resistances of the electrolyte and the initial ($R_{ct\text{-}0}$) and final ($R_{ct\text{-}ss}$) charge-transfer resistances of the interfacial layers of the Na metal electrode/electrolyte were derived, and t_{Na^+} was calculated with Equation (2):

$$t_{Na^+} = \frac{I_{ss} \cdot R_{b-ss} \cdot (\Delta V - I_0 \cdot R_{ct-0})}{I_0 \cdot R_{b-0} \cdot (\Delta V - I_{ss} \cdot R_{ct-ss})} \quad \text{(Eq. 2)}$$

The ion diffusion coefficient of the photopolymer electrolyte ed as a function of salt concentration by using the method proposed by Ma *et al.* [138] The cell was polarized at 50 mV before the potential was interrupted. Once the potential was interrupted, the cell was kept for sufficient time at OCV until a stable state was achieved. Later, the curves were plotted as the natural logarithm of potential versus time. The D_{Na^+} values were calculated from the slopes of the linear curves.

The ESW was determined by linear sweep voltammetry (LSV) with an Arbin instrument (model BT2000 battery testing system). For the anodic stability window (ASW), the photopolymer electrolyte was sandwiched between aluminum foil and sodium metal as the working and counter electrodes, respectively, in the ECC-Std cell. For the cathodic stability window (CSW), the same setup was used, but a copper current collector coated with acetylene black replaced the aluminum foil. A potential scan rate of 0.100 mV s^{-1} was used from the OCV to 5.2 V vs Na^+/Na for the anodic scan and from the OCV to -0.2 V vs Na^+/Na for the cathodic scan.

Galvanostatic discharge/charge (Na^+ insertion/deinsertion) cycling was conducted at ambient temperature in ECC-Std test cells by using an Arbin Instrument testing system. In a typical experiment, a disc of the activated photopolymerized electrolyte membrane was sandwiched between a Na metal counter electrode and a TiO_2-based working electrode, the latter of which was composed of a 74:8:18 ratio between commercial anatase (Hombikat), Na-CMC,

and conductive carbon, prepared as previously described for the laden-CMC SPE [121]. As reported by the Passerini group, considering the reversible uptake of one sodium ion per formula unit of TiO_2, the theoretical specific capacity of the TiO_2 electrode is 335 mAh g^{-1} [139]. The discharge/charge cycles were set at the same rate from 0.05 to 1 mA cm^{-2} (cut-off potentials: 0.2–2.5 V vs. Na^+/Na). To confirm the obtained results, tests were performed at least three times with different clean electrodes and fresh samples. The cell assembly procedures were performed in the inert atmosphere of a dry glovebox (MBraun Labstar, O_2 and H_2O content < 0.1 ppm) filled with extrapure Ar 6.0. All samples were prepared and stored in an environmentally controlled dry-room (10 m^2, relative humidity <(2 ± 1)% at 20 °C) produced by the Soimar Group.

5.1.1.4 Results and discussion

Sodium-ion-conducting polymer electrolytes were prepared for the first time using a UV-induced polymerization process. The process is economical and eco-friendly as it does not use any harmful solvents, costly catalysts, and lengthy heating, cooling, or purification procedures. Indeed, the preparation of the photopolymer electrolyte involved the mixing of a dimethacrylate oligomer (i.e., bisphenol A ethoxylate dimethacrylate, BEMA) with a reactive diluent with dangling ethoxy groups [poly(ethylene glycol) methyl ether methacrylate, PEGMA] and a photoinitiator (Irgacure 1173, 2 wt %). From preliminary scanning and results evaluation, the combination of BEMA and PEGMA in a ratio of 35:65 was found to ensure the best physicochemical, thermal, and electrochemical properties. BEMA is a dimethacrylate oligomer that cross-links readily under UV irradiation to form a self-standing three-dimensional network. The PEGMA co-monomer is a monomethacrylate oligomer (reactive diluent). Its addition allows the modification of the characteristics of the final polymer membrane by reducing the cross-linking density, diminishing the T_g, and increasing the mobility of the sodium ions by coordinating with the -O- units of pendant ethoxy groups [42]. The mixing of the methacrylate-based oligomers (the molecular structures are shown in Fig. 5.2) and the photoinitiator is instantaneous, and the completion of the subsequent UV irradiation process takes 2 min.

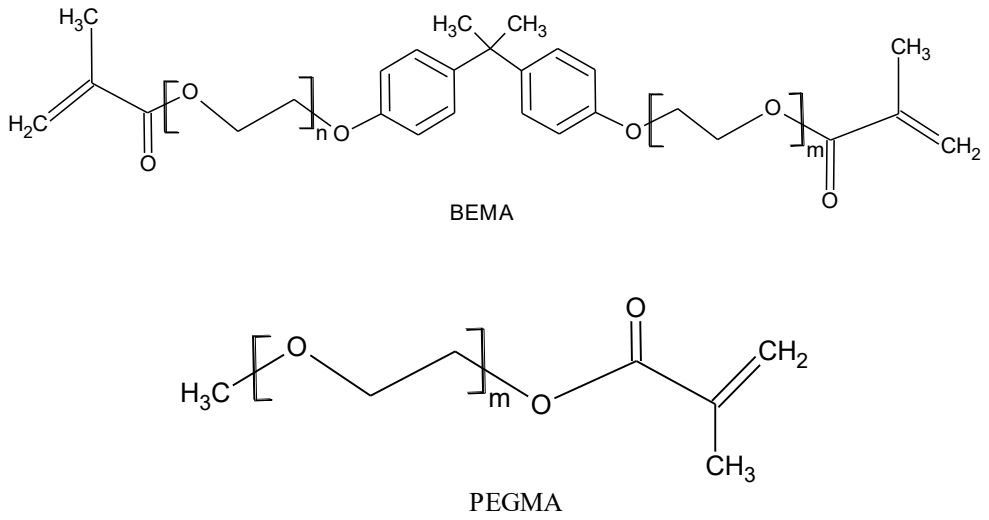

Fig. 5.2 Structure of BEMA and PEGMA oligomers, involved in the photopolymerization process.

The kinetics of the photopolymerization process was followed by real-time Fourier transform infrared (RT-FTIR) spectroscopy, and the resulting response of the conversion is shown in Fig. 5.3.

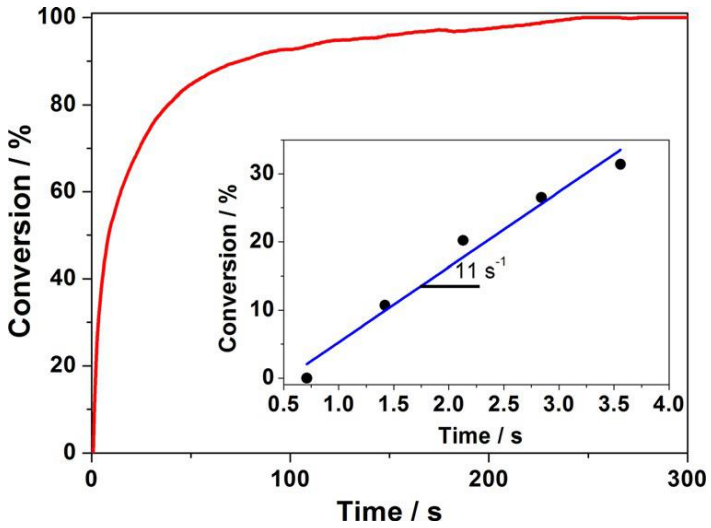

Fig. 5.3 RT-FTIR photopolymerization kinetic curve of a reaction mixture containing BEMA and PEGMA in a 35:65 ratio along with 2 wt % of photoinitiator. Inset: initial stages of the UV curing process used to calculate the initial polymerization rate. (taken from [136])

The achievement of 100% final conversion in less than 5 min demonstrates the rapidity of the photoinduced polymerization reaction, especially in comparison to the traditional time-consuming solvent-based polymer membrane formation processes (e.g., solvent casting, melt flow) [140],[141]. The initial polymerization rate, calculated by fitting the RT-FTIR data in the initial stages of the process, demonstrates the very fast conversion rate (approaching 11 s^{-1} in the initial stages). The gel content, which represents the percentage of the polymeric matrix that is insoluble in chloroform, exceeded 98 %; thus, the final UV-cured sample is a highly cross-linked thermoset material. The value is also in good agreement with the monomer-to-polymer conversion results obtained by the RT-FTIR studies.

Soon after the photopolymerization process, the resulting pristine cross-linked polymer membrane was soaked in a liquid-electrolyte solution 1M $NaClO_4$ in propylene carbonate (PC) to activate before testing in NIBs. The activated polymer electrolyte was still self-standing, nontacky, transparent, flexible, and easy to handle. Furthermore, a bending test was performed after the activation process: the photopolymer electrolyte can be reversibly bent and rolled easily and withstands a bending radius of up to 2.5 mm without deterioration of the overall integrity and elasticity. Digital photographs of the pristine (A) and swollen (B) photopolymer electrolyte in bend mode are shown in Fig. 5.4, which indicate that the samples are easy to manage even after swelling. These results account for the truly solid and self-standing characteristics of the newly elaborated photopolymer electrolyte system, which is definitely different in terms of mechanical robustness from the typical gel-polymer electrolytes [102, [153-155].

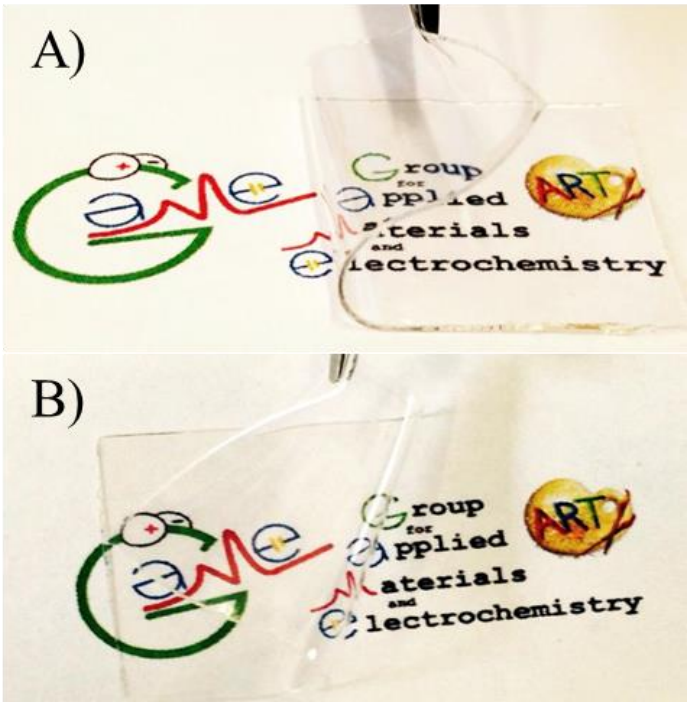

Fig. 5.4 Digital photographs of the UV-cured BEMA/PEGMA membranes before (A) and after (B) the activation process in $NaClO_4$/PC. The pictures were taken after 50 bending cycles around a cylinder with a radius 2.5 mm. (adapted from [147]).

The T_g values of the pristine and activated samples were evaluated by differential scanning calorimetry (DSC), and the resulting curves and values are shown in Figure 5.5. In general, the T_g is defined as the midpoint of the heat-capacity deflection in the DSC trace during the transition from the glassy to rubbery state. The pristine polymer showed a T_g of -49.9 °C, which is already low. After activation, the T_g decreased further to -55.8 °C. The presence of $NaClO_4$ and PC influenced the T_g value slightly, maybe because the volume expansion that occurred during the swelling process allowed the free dangling chains to move locally with less energy. Moreover, the plasticization effect induced by the PC solvent cannot be neglected. However, in summary, the shift in the T_g value was not drastic, and a polymer electrolyte in the rubbery state at room temperature (necessary for efficient functioning of NIBs) was obtained readily.

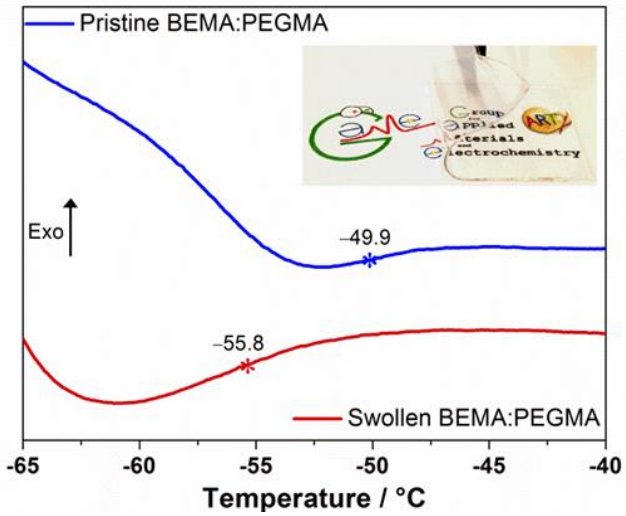

Fig. 5.5 DSC traces of UV-cured BEMA/PEGMA membranes before and after the activation process (adapted from [147]).

The thermal stability of the polymer electrolyte was evaluated by thermogravimetric analysis (TGA) under flowing nitrogen, and the results are shown in Fig. 5.6. The activated photopolymer electrolyte showed a three-step degradation process, which corresponds to the stabilities of the materials used for the sample preparation. The first degradation step occurred slightly above 100 °C and is in line with the evaporation of the PC solvent. The second step (350 °C) was caused by the degradation of the polymeric matrix and was in agreement with that of the pristine polymer sample. Finally, a third step due to $NaClO_4$ degradation occurred well above 400 °C. Overall, the test results indicate that BEMA/PEGMA-based photopolymer electrolytes could be implemented safely in sodium-based battery systems that are envisaged for large-scale grid storage in the temperature range between -40 and 100 °C.

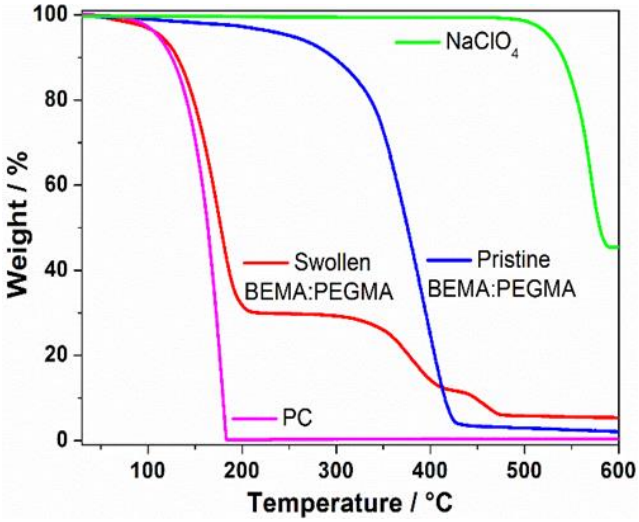

Fig. 5.6 TGA profiles of the UV-cured BEMA/PEGMA samples before and after the activation process in $NaClO_4$/PC; the thermograms of PC and $NaClO_4$ are also shown for comparison. (taken from [147])

The ionic conductivity of the polymer electrolyte was tested by electrochemical impedance spectroscopy (EIS). For testing, a disk of the activated photopolymer electrolyte was sandwiched between two stainless-steel blocking electrodes, and the behavior of the samples was monitored in the temperature range between -10 and 80 °C. The results are shown in Fig. 5.7. The photopolymer electrolyte achieved an ionic conductivity of (5.08 ± 0.05) mS cm^{-1} at 20 °C and even exceeded 13 mS cm^{-1} at 80 °C [(13.4 ± 0.03) mS cm^{-1}].

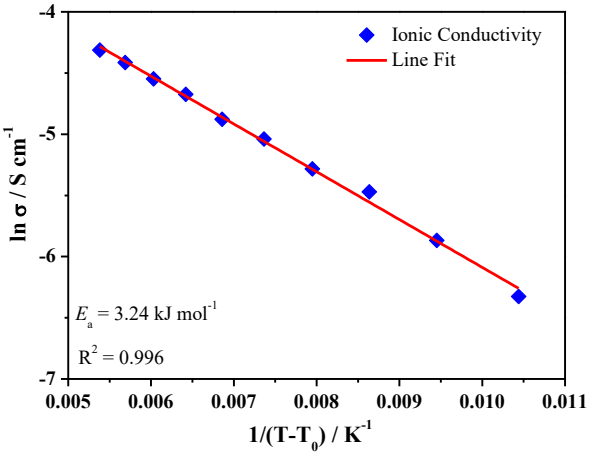

Fig. 5.7 Arrhenius plot showing the ionic conductivity in the temperature range of -10 to 80 °C of the BEMA/PEGMA photopolymer electrolyte.

To the best of my knowledge [156,157] these remarkable values are the highest achieved for a polymer electrolyte as a separator for NIB applications, especially if operation under ambient conditions is envisaged. The calculations of the activation energy (E_a) and related values are useful for the elucidation of the mechanism of ionic conductivity in polymer electrolytes. In the present case, E_a was calculated by fitting the conductivity values to the Vogel–Tamman–Fulcher (VTF) eq. 1, [158] which describes the conduction behavior of highly concentrated liquid electrolytes and molten salts. As shown in Fig. 5.7, the VTF fit gave a fitting efficiency (R^2 value) of 0.996, and an Ea of 3.24 kJ mol^{-1} was obtained. This value is very low and, thus, indicates that the conduction mainly occurs through the PC medium.

The activated polymer electrolyte was sandwiched between thin sodium metal discs in a symmetric cell (Na|polymer electrolyte|Na) to test further its compatibility towards Na metal. The resulting curves are shown in Fig. 5.8, in which the evolution of the interfacial resistance over 21 days is shown. The resistance of a cell is composed of the bulk resistance (R_b) of the electrolyte, which is the one corresponding to the higher frequency response, whereas the interfacial resistance (R_i) is the reflection of the interfacial (charge transport) characteristics of the electrolyte at lower frequency [159,106]. The R_b was observed to be rather stable with time and well in agreement with the ionic-conductivity studies discussed previously; therefore, the solvated sodium ions embedded in the UV-cross-linked polymeric network did not leak out of the system along with the PC solvent even after a prolonged period of storage. Moreover, the results also indicated that no vigorous undesired side reactions occurred, which in turn confirmed that the polymer electrolyte was in intimate interfacial contact with the Na metal electrode. On the other hand, the rapid increase of R_i during the first six days indicates the formation of a passivation layer at the surface of the sodium electrode. The R_i value subsequently decayed and, finally, remained stable at a value of approximately 6 kΩ. Such stabilization of the resistance can be related to the quality of the chosen PC solvent, the polymeric material, and its architecture, which modify the electrode surface to form a thin and stable protective coating. The solid–electrolyte interface (SEI) layer may further prevent the contact of the electrolyte components with the sodium metal and, thus, suppresses the reactivity at the Na metal/polymer interface.

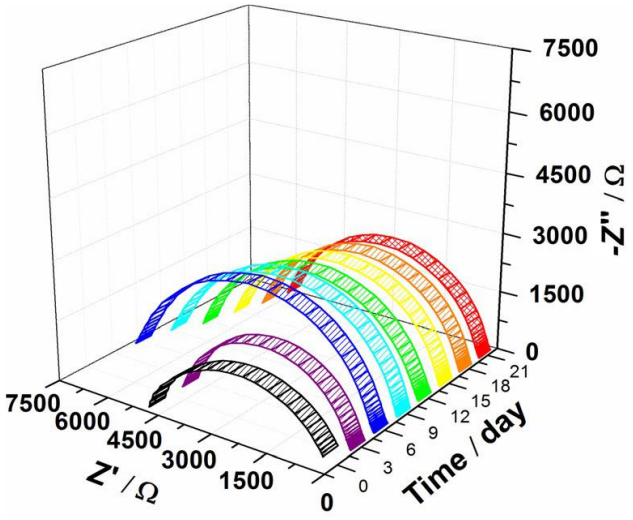

Fig. 5.8 Interfacial stability studies: evolution of the impedance spectra versus time for a Na/polymer electrolyte/Na symmetric cell, stored at the OCV under ambient conditions.

Such a good interfacial stability, the excellent ionic conductivity discussed above, the optimum mechanical robustness, the electrolyte retention capability, and the thermal properties are key factors for the practical application of this easy-to-prepare photopolymer electrolyte in advanced sodium batteries envisaged for long-lasting or aging-resistant cycle-life operation under ambient conditions.

Ionic conduction in a polymer electrolyte and its influence on the electrochemical behavior can be derived from transport-number studies. Thus, the sodium-ion transference number (t_{Na^+}) was calculated for the activated photopolymer electrolyte under study by using the method proposed by Abraham et al. and reported in the Experimental part of this chapter [135].

This method also considers the resistance variation that occurs if the photopolymer electrolyte is kept in prolonged contact with the reactive metal. An optimum t_{Na^+} is necessary for the proper function of the electrolyte in a sodium cell; indeed, poor transport behavior may induce dendrite growth inside the cell, which may result in safety hazards, a major obstacle for entry to the global battery market. The proposed photopolymer electrolyte showed a very high transference number (0.53 ± 0.05) at 20 °C, and the relative curves are shown in Fig. 5.9.

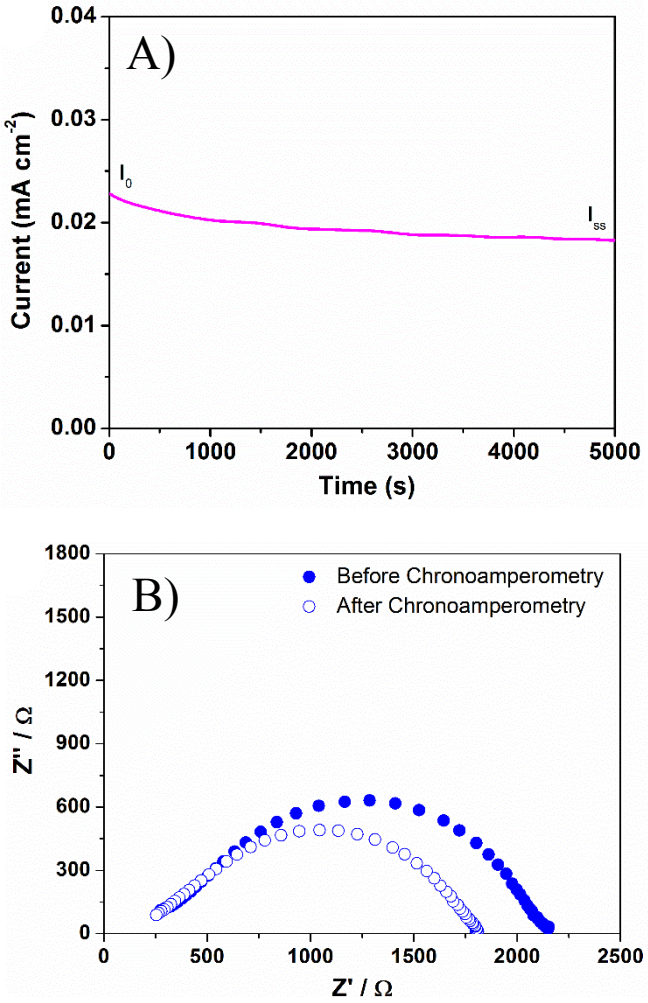

Fig. 5.9 A) Chronoamperometry measurement obtained by 25 mV of polarization from OCV to steady state current. B) Nyquist plot of the photopolymer electrolyte before and after chronoamperometry.

If one considers that these numbers were obtained at 20 °C for a photopolymer electrolyte, the results are extremely encouraging. The diffusion coefficient (D_{Na^+}) was evaluated by the method reported by Ma *et al.* [160] and was in good accordance with the results obtained from the ionic-conductivity and transference number investigations. In general, these results correlate, and the summary of all of these studies may give a clear idea of the effective functioning of the thermoset photopolymer electrolyte under study. It is worth noting that the value achieved for D_{Na^+} (i.e., 2.52 10^{-7} cm^2 s^{-1}) is remarkably high; indeed, it is the highest reported so far for a sodium-ion-conducting polymer electrolyte system.

To demonstrate the possible application of the proposed electrolyte as a separator in NIBs, its fundamental electrochemical response was investigated. For a rechargeable sodium battery, the electrochemical stability window (ESW) is a fundamental parameter that determines the overall functioning of a polymer electrolyte, particularly its cycling stability and reversibility. In addition to the outstanding conductivity behavior discussed previously, the UV-cross-linked polymer electrolyte demonstrated a reasonably wide ESW. The current–potential response measured at ambient temperature by linear sweep voltammetry is depicted in Fig. 5.10. The data were obtained in the potential range between the open-circuit voltage (OCV) and 5.2 V versus Na^+/Na for the anodic scan and between the OCV and -0.2 V versus Na^+/Na for the cathodic scan and then collected in a single plot. No noticeable electrochemical reactions occurred at positive potentials from the sodium reversible plating/stripping process (below 0.2 V) to above 4.6 V vs Na^+/Na, at which the start of current flow indicated the anodic breakdown potential. A polymer electrolyte with such an extended anodic stability would represent a very important result in view of a possible practical application in NIBs with high working potentials. The reversible plating and stripping reaction peaks in the cathodic scan (with the exception of a very small signal before Na plating that is under investigation) confirm that the photopolymer electrolyte can transport sodium ions effectively under ambient conditions.

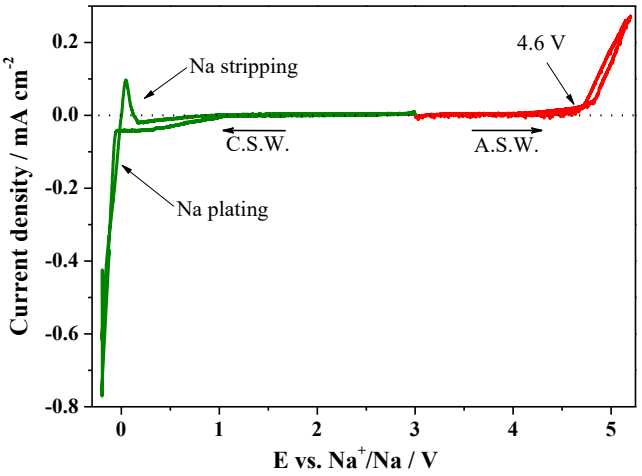

Fig. 5.10 Electrochemical Stability Window of the photopolymer membrane. In the cathodic branch (green, C.S.W.) the Na plating/stripping is clearly evidenced; the red profile shows the anodic stability window (A.S.W.)

Constant-current galvanostatic discharge/charge cycling tests were performed at ambient temperature and at different current rates from 0.05 to 1 mA cm^{-2} to demonstrate the feasibility of the proposed photopolymer electrolyte for sodium-based cells. A plot of the specific capacity versus cycle number for a cell assembled with a TiO_2-based working electrode and a metallic Na counter electrode is shown in Fig. 5.11 A (the potential vs. specific capacity profiles are shown in Fig. 5.11 B). The polymer cell provided an average specific capacity of approximately 335 mAh g^{-1} upon discharge in the first cycle. As already reported for different studies on TiO_2-based sodium cells [161-163] the initial ten cycles at low current evidence the rapid decrease of the discharge capacity, whereas the charge capacity remains almost stable. The cycling behavior stabilized progressively after the initial induction period, and the cell also demonstrated a sufficient rate capability of >130 mAh g^{-1} at an increased current density of 0.1 mA cm^{-2}. The ambient-temperature cycling stability was remarkable, and the stable capacity exceeded 50 mAh g^{-1} for 250 cycles at 1 mA cm^{-2}.

Thus, the TiO_2-based lab-scale polymeric cell demonstrated long-term durability and specific capacity values at the level of those of similar liquid-based systems [164,165].

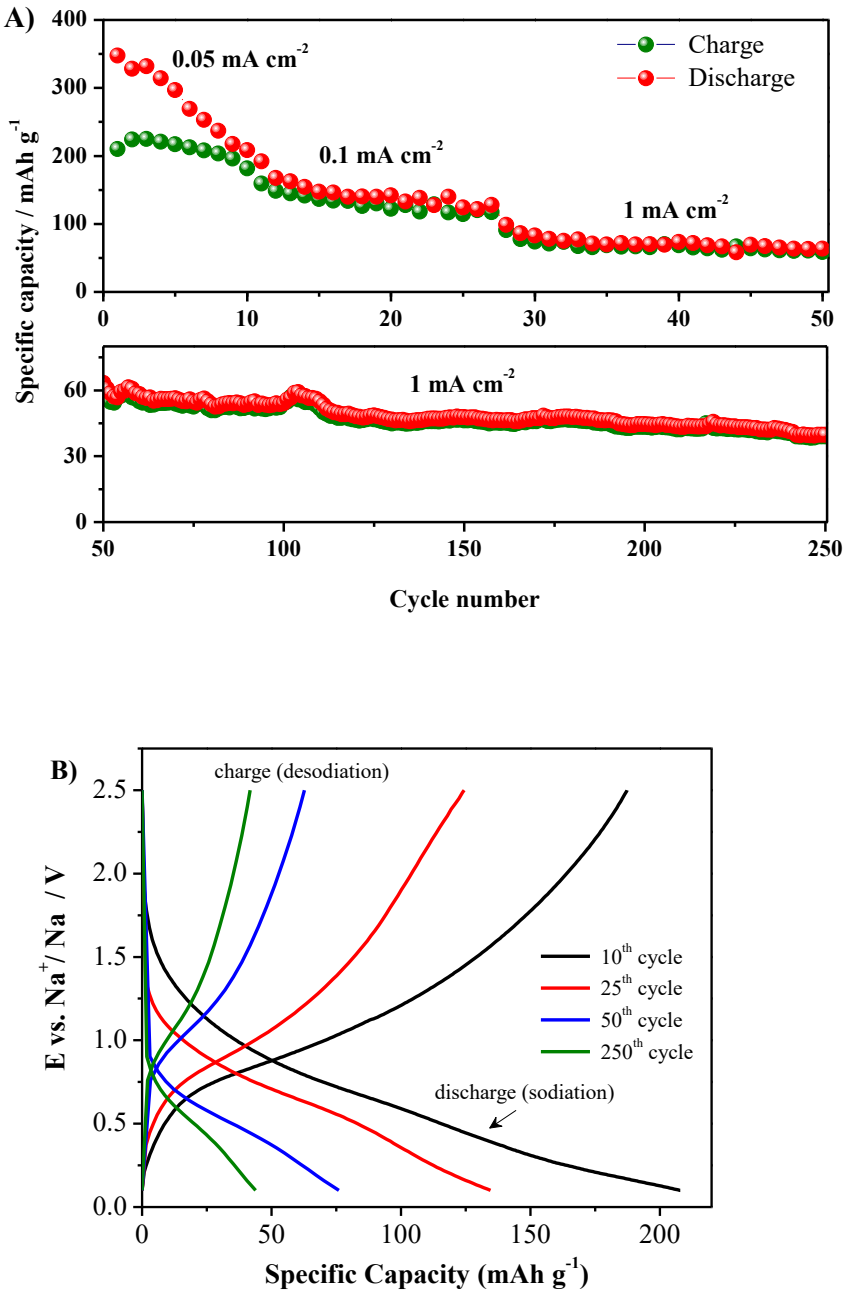

Fig. 5.11 Constant current discharge/charge cycling capability test of the sodium cells at ambient temperature and at different current regimes: a) specific discharge/charge capacities vs. cycles, b) potential vs. specific capacity profiles extracted from different cycles.

Polymer electrolyte membranes are truly valid systems for energy-storage devices, as they manage to provide excellent performance in terms of ionic conductivity, thermal stability, and mechanical robustness (they also act as separators). However, a major drawback of electrolytic membranes is represented by their ex situ fabrication; they are subsequently activated and put in contact with the electrodes. Such a two-step preparation process is definitely a limit to the large-scale industrial implementation of polymer electrolyte systems in NIBs. A onestep process would definitely be preferable. To this purpose, a 50:50 w/w reactive mixture based on BEMA/PEGMA (1:1 ratio) and $NaClO_4$ (10 wt%) in PC along with 3 wt% photoinitiator was drop-cast onto the surface of a TiO_2 electrode to intimately wet the pores of the electrode and guarantee an adequate interfacial contact. Then, UV light was focused on the anode/electrolyte assembly, and the photo-cross-linking reaction occurred. In this way, the polymer electrolyte was insitu generated directly on the electrode in a single step [166,167].

The resulting photopolymerized multiphase electrode/electrolyte was subjected to a proof-of-concept cycling in an all solid-state TiO_2/Na sodium cell. The constant-current charge/discharge cycling test and representative profiles extracted from the 5^{th} and 50^{th} cycles are shown in Fig. 5.12, obtained at cut-off potentials of 0.2–2.5V versus Na^+/Na and a current density of 1 mA cm^{-2}. The good electrochemical performance may be ascribed to the efficient ionic conduction in the polymer separator and the favorable interfacial charge transport between the electrodes and electrolyte in the cell. The potential drop from charge to discharge was rather small, which means that the resistance of the cell is low.

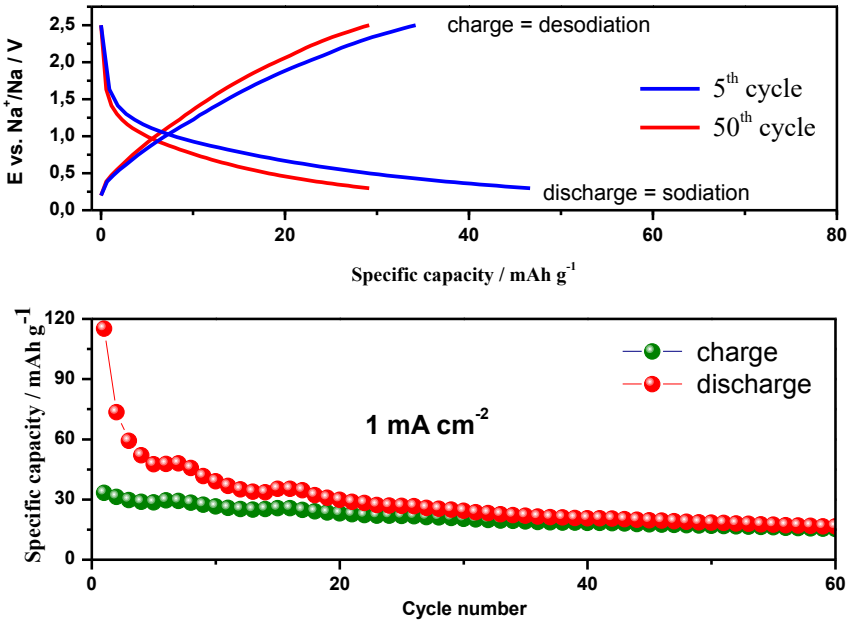

Fig. 5.12 Constant-current charge/discharge cycling test of the sodium polymer cell assembled by contacting a TiO_2-based multiphase electrode/electrolyte and a Na metal anode at ambient temperature and at 1 mA cm^{-2} current density.

A few improvements should be made, especially in the preparation of the multiphase electrode/electrolyte; in particular, the thickness of the reactive liquid film drop-cast onto the TiO_2 electrode must be controlled carefully to obtain a solid polymeric film as uniform as possible after UV irradiation. Overall, this first example of an NIB prepared in a single step through an in situ light-curing process shows promising prospects and could be a good starting point for the scientific community dealing with sodium-based storage systems.

5.1.1.5 Conclusions

A methacrylate-based polymer membrane was fabricated by a UV-induced photopolymerization technique and converted successfully to a sodium-ion-conducting electrolyte separator by an activation step in a liquid electrolyte. The obtained photopolymer electrolytes exhibit thermal stability above 100 °C, very high ambient-temperature ionic conductivity, and excellent sodium-ion transport, along with stable interfacial characteristics and a very high electrochemical stability window. In tests against TiO_2-based working electrodes, the newly elaborated electrolyte system showed remarkable performance that was clearly at the level of

similar liquid-based systems, namely, a reasonably high specific capacity and rate capability as well as excellent stability upon prolonged cycling (250 cycles).

These results are highly encouraging for the implementation of these membranes in ambient-temperature large-scale energy storage. Notably, the light-cured polymeric networks were also used successfully for the fast in situ fabrication of electrode/electrolyte composites with excellent interfacial properties, which are ideal for all-solid-state, safe, and easily upscalable device assemblies. The overall characteristics of these materials such as their intrinsic safety, eco-compatibility, low production time, and easy industrialization features make them strong contenders in the field of sodium-ion rechargeable batteries for large-scale grid storage applications.

5.2 PEO-based photopolymer electrolyte

The methacrylic-based photopolymer electrolyte demonstrated a series of peculiar characteristics and interesting properties when tested in lab-scale Na cells. However, these results were obtained by using a swelling step after membrane preparation, which results in a sizeable amount of volatile liquid in the electrolyte system. This is not highly advantageous in view of the practical application of the photopolymer electrolytes. With this in mind, I proceeded further with the optimization of the electrolyte towards a truly quasi-solid system.

Is reported a PEO-based crosslinked polymer electrolyte (XPE) for NIBs prepared via light-induced free-radical polymerization (UV curing) process. It is based on the transformation of a starting liquid reactive mixture into a crosslinked solid film upon irradiation within few seconds to few minutes. It is rapid, energy saving and environmentally friendly, being volatile organic compounds emission-, solvents- and catalysts-free, thus particularly suitable for a large-scale production of NIBs. In the present case, the starting PEO-based reactive mixture included $NaClO_4$ as sodium salt dissolved in propylene carbonate (PC). When assembled in labscale cells, this quasi-solid state sodium-ion conductor demonstrated electrochemical performances close to those of its liquid counterpart, which accounts for the promising prospects of PEO-based XPEs to successfully fabricate safe and stable NIBs.

5.2.1 Experimental

5.2.1.1 Materials

Poly(ethylene oxide) (PEO, average Mw: 100 000), sodium perchlorate ($NaClO_4$, battery grade), sodium metal (99.8 %, ingots), carboxymethylcellulose sodium salt (Na-CMC, average Mw: 250 000) and 4-methoxybenzophenone (photoinitiator) were purchased from Sigma-Aldrich. Propylene carbonate (PC, battery grade) was provided by Solvionic. Anatase TiO_2 (UV100) electrode nanoparticles was provided by Hombikat. Acetylene black (Shawinigan Black® AB50%, Chevron Corporation) was used as conductive carbon additive.

5.2.1.2 Preparation of PEO-based electrolyte

PEO-based XPE was prepared inside an environmentally controlled dry-room (10 m^2, R.H. <2% ± 1 at 20 _°C, Soimar Group) as described below. A reactive mixture was obtained by mixing $NaClO_4$, PC, PEO (5:50:45 weight ratio, respectively) and 4 wt% of photoinitiator. After the formation of a homogeneous viscous gel, it was casted between two transparent polypropylene (PP) sheets. The latter were separated by a plastic thin spacer in order to obtain a polymer film with a thickness of 90 μm when the sample was hot-pressed at 90 °C for 15 min. Then, it was transferred into a UV curing set-up equipped with a Hg medium-pressure UV lamp (Helios Italquartz) and irradiated at an intensity of 30 mW cm^{-2} for 3 min on both the sides. The curing was carried out at ambient temperature under inert N_2 atmosphere to avoid oxygen inhibition, and a self-standing film was easily peeled off from the PP sheets. Thus, by UV curing we obtained a ready-to-use crosslinked polymer electrolyte membrane was obtained, and no further steps are necessary before its characterization and/or use.

5.2.1.3 Thermal and structural characterization

To check the efficacy of the UV-curing process, the polymer electrolyte insoluble fraction (gel content) was determined by measuring the weight loss of the sample that was clamped inside a metallic net after having been immersed for 24 h in acetonitrile at ambient temperature. The crosslinked fraction was calculated dividing the weight of the dried specimen after its permanence in acetonitrile and the weight of the original sample.

The thermal stability was evaluated by thermo-gravimetrical analysis (TGA) with a TG 209 F1 Libra® instrument from Netzsch; the measurement was performed between 25 and 800 °C under N_2 flux at a heating rate of 10 °C min^{-1}. The glass transition temperature (Tg) was evaluated by dynamic-mechanical thermal analysis (DMTA) with a TTDMA instrument (Triton Technology Ltd) in the temperature range of -120 °C to ambient temperature at a heating rate of 10 °C min^{-1} under N_2 flux.

The surface morphology of the polymer electrolyte was studied by field emission scanning electron microscopy (FESEM) analysis using a ZEISS Supra® 40VP instrument, equipped with an energy dispersive X-ray (EDX) spectrometer. Before carrying out the analysis, the specimen was subjected to metallization by sputtering a very thin Cr layer (~10 nm) to minimize the effect of electron beam irradiation towards charging and burning of the polymer matrix.

5.2.1.4 Electrochemical characterization

The ionic conductivity of the XPE was determined by electrochemical impedance spectroscopy (EIS) analysis between 100 kHz and 1 Hz at the open circuit potential (OCV) using a PARSTAT® 2273 potentiostat. A 2.54 cm^2 disc of XPE was cut and placed between two stainless steel (SS 316) blocking electrodes of an ECC-Std test cell (EL-CELL® GmbH). The cell was placed inside an environmental simulation chamber (BINDER model MK-53, with a temperature control of ± 1 °C) and tested in the temperature range from -40 to + 90 °C; the EIS measurement was performed every 10 °C on a thermally equilibrated cell.

The electrochemical stability window (ESW) of the XPE was evaluated at ambient temperature by linear sweep voltammetry (LSV) using a CHI-660 electrochemical workstation by CH Instruments, Inc. Separate LSV measurements were performed on the XPE in order to evaluate the cathodic and the anodic potential limits. As for the cathodic part, the XPE was sandwiched between a copper working electrode foil and sodium metal (counter and reference electrodes), and tested from the OCV down to -0.5 V vs. Na^+/Na. The anodic stability was determined using an aluminum foil as working electrode and sodium metal as both counter and reference electrodes. The potential was scanned from the OCV up to 5.2 V vs. Na^+/Na. Both the experiments were carried out at a scan rate of 0.100 mV s^{-1}.

The Na^+ transference number (t_{Na^+}) was determined combining alternating current (AC) impedance and direct current (DC) polarization as described in the previous section of this chapter (see 5.1.1.3) for the BEMA-PEGMA membrane. The method is based on the application of a DC pulse to a symmetrical cell (Na|XPE|Na), measuring both the initial and steady state current values (I_0 and I_{ss}) that pass through the cell. EIS analysis is performed before and after the application of the DC potential (ΔV = 20 mV) in order to obtain the initial ($R_{b\text{-}0}$) and final ($R_{b\text{-}ss}$) bulk resistances of the electrolyte, and the initial ($R_{ct\text{-}0}$) and final ($R_{ct\text{-}ss}$) charge-transfer resistances of the interfacial layers of the Na metal electrode/electrolyte. t_{Na^+} was calculated using the Equation 2 showed in the previous chapter.

The interfacial properties of the UV-cured XPE against sodium metal electrode and the variation of the resistance as a function of contact time were measured using a symmetrical cell (Na|XPE|Na). The cell was stored at ambient temperature at the OCV and the evolution of the contact resistance was evaluated every day for several days, recording the EIS response using a PARSTAT® 2273 potentiostat. The surface of the sodium metal electrodes was refreshed using a scalpel before test cell assembly.

The lab-scale polymer sodium cell was assembled using the XPE as separating electrolyte and tested in terms of constant current (galvanostatic) discharge/charge cycling at different current rates using the battery testing system BT2000 by Arbin Instruments [168,171]. To this purpose, a TiO_2-based composite working electrode was prepared with 8 wt % Na-CMC, 18 wt % of conductive carbon and 74 wt % of TiO_2 active material nanoparticles. The configuration of the cell for the evaluation of the galvanostatic behavior of the XPE was TiO_2|XPE|Na.

Cell assembly for several electrochemical characterizations was performed in the inert and controlled atmosphere of a GP Dry-Glove Box Workstation (O_2 and H_2O content < 0.1 ppm) by Jacomex, filled with extra pure Ar 6.0.

5.2.2 Results and discussion

In this study, truly quasi-solid crosslinked polymer electrolyte membranes for sodium-based batteries were prepared by UV-curing process and thoroughly characterized in terms of their physic-chemical and electrochemical properties [147]. Inspired from polymer electrolytes for LIBs, PEO was selected as the polymeric matrix for preparing the XPE, which was studied extensively so far [172,173].

Upon mixing PC with different ratios of $NaClO_4$ and PEO, a rather thin (~90 ± 2 μm), self-standing and flexible membrane was obtained, as shown in Fig. 5.13. In this picture, one may appreciate that once an applied tensile force was released after stretching, the XPE can easily return to its previous shape without any visible damage, thus evidencing its highly elastic characteristics. In addition, the XPE was truly transparent, which accounts for proper amorphisation of the polyethylene oxide matrix.

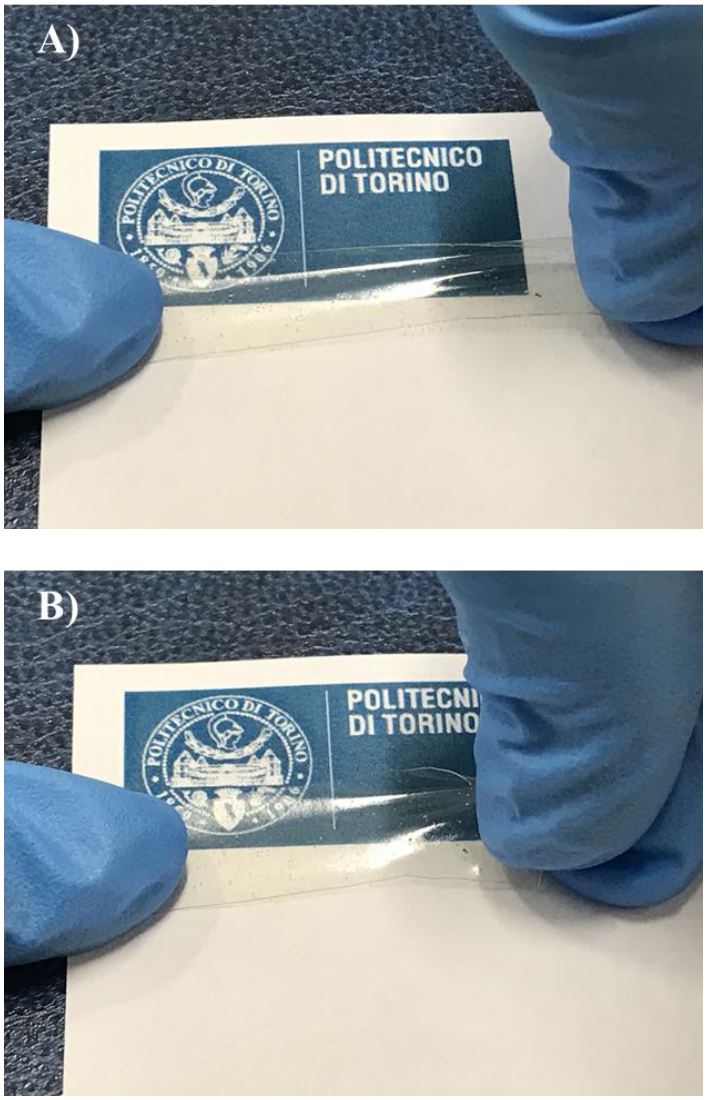

Fig. 5.13 Digital photographs of the crosslinked polymer electrolyte. A) under stretch and B) in relaxation mode.

The expected reaction mechanism of light-induced crosslinking upon XPE preparation along with the chemical formula of the photoinitiator and different

ingredients are shown in Fig. 5.14. In summary, under UV exposure, the photoinitiator is excited into higher energy state and abstracts a proton from a methylene group; it generates a free radical on the PEO chain [174], which may combine with another free radical from the same chain or a neighbour chain, thus promoting the crosslinking between the thermoplastic PEO chains transforming it into a thermoset material.

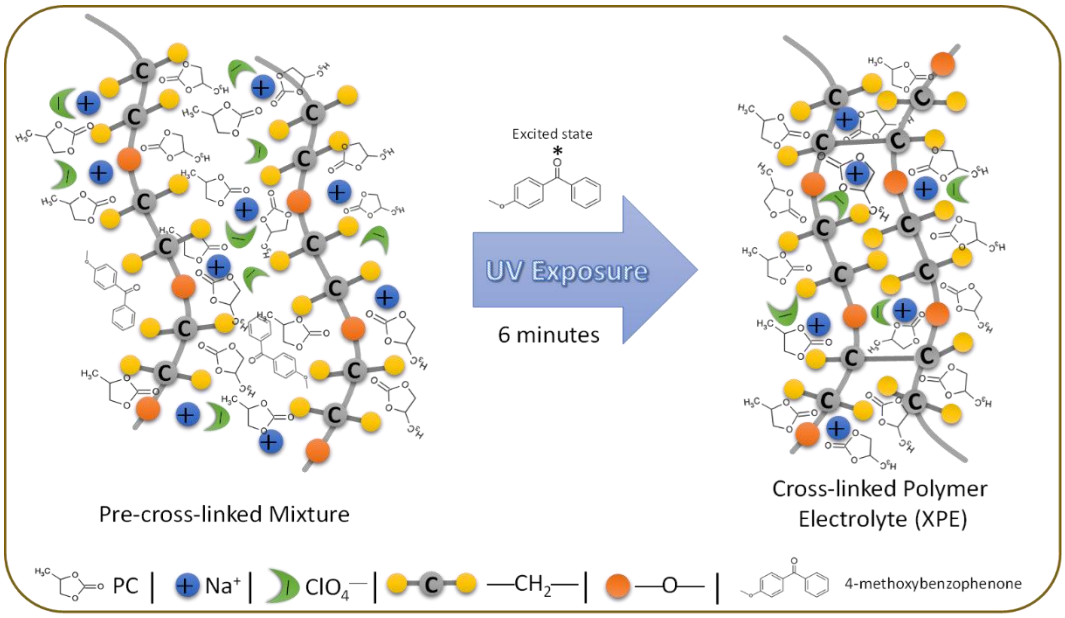

Fig. 5.14 Schematic representation of the expected reaction mechanism of light-induced crosslinking upon XPE preparation.

Fig. 5.15 shows the ATR-FTIR spectrum of the obtained XPE. The bands observed at 2872, 1451, 1351-1388, 948 and 847 cm^{-1} are assigned to stretching, scissoring, wagging doublet, symmetric rocking and asymmetric rocking, respectively, of $-CH_2$ moieties in PEO chain. The triplet observed between 1000 and 1200 cm^{-1} is assigned to C-O-C stretching of PEO. The band at 616 cm^{-1} is assigned to the stretching of ClO_4^- anion [129]. The band at 1789 cm^{-1} indicates the symmetrical C=O stretching of PC, while its ring stretching is visible at 777 cm^{-1} (red arrow) [175]. These latter signals confirm the successful co-presence of PEO, $NaClO_4$ and PC in the homogeneous XPE.

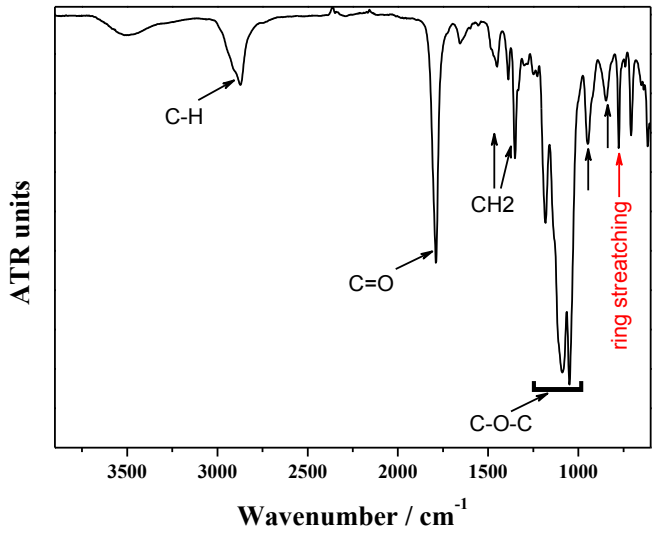

Fig. 5.15 ATR-FTIR pattern of the XPE under study. The red arrow indicates the ring stretching of the PC.

The thermal properties were investigated by TGA and DMTA. The thermograms of pristine PC, PEO, $NaClO_4$ and the XPE are shown in Fig. 5.16. In the same graph, the first derivative of the thermal response of the XPE is also shown, which clearly indicates the evaporation of PC above 120 °C, and the second weight loss above 350 °C corresponding to the PEO matrix degradation. $NaClO_4$ decomposition is not clearly visible in the XPE thermograph due to its very high thermal stability exceeding 550 °C.

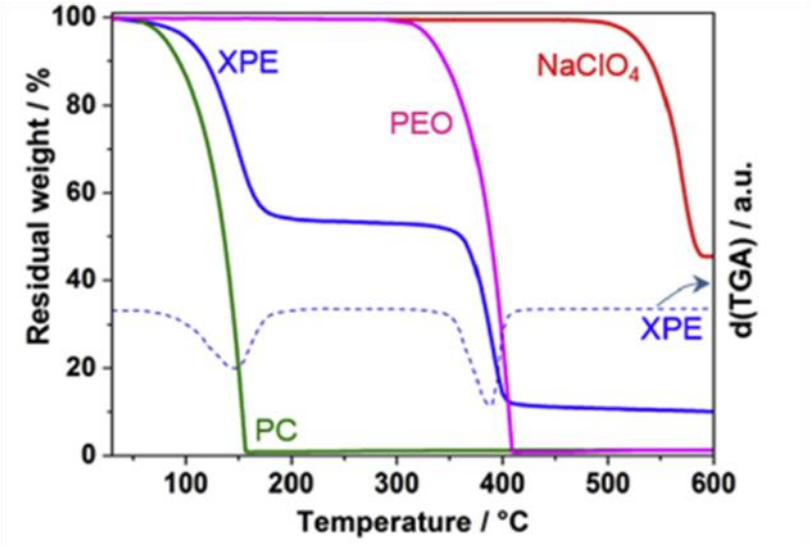

Fig. 5.16 TGA of the XPE membrane and termograms of the pristine materials which composed the crosslinked polymer electrolyte. The first derivative of the thermal response is shown (dashed line).

It is interesting to note that pristine PC evaporates at much higher rate and at lower temperature than the PC encompassed in the XPE, which clearly indicates that the crosslinked PEO matrix becomes highly viscous and more capable to retain the PC molecules, thus delaying their escape from the electrolyte system. Indeed, PC in the XPE is at least 25 °C more stable than the pure PC under the same testing condition. This confirms that the crosslinking process is useful in retaining both the dimensional and thermal stabilities. As a further confirmation, when the test was performed on a non-crosslinked PEO-PC sample (Fig. 5.17), clear evidence of solvent leakage from the polymer matrix was observed. The decomposition steps of the XPE thermogram are well in accordance with the proportion of materials used for its preparation.

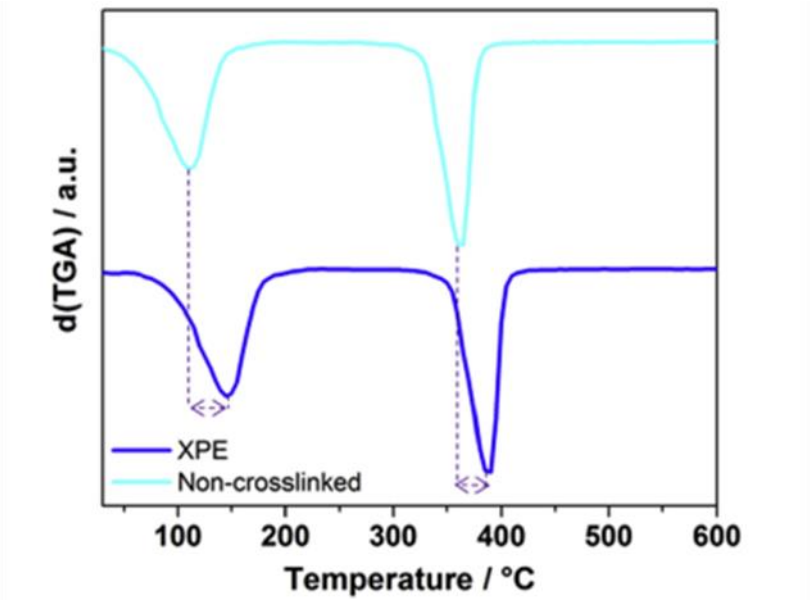

Fig. 5.17 Comparison between TGA traces of cross-linked (XPE) and non-crosslinked samples.

The glass transition temperature (T_g) was assessed by DMTA, and the obtained value for the XPE was around -63 °C (for pure PEO it is around -58 °C [131]) (Fig. 5.18).

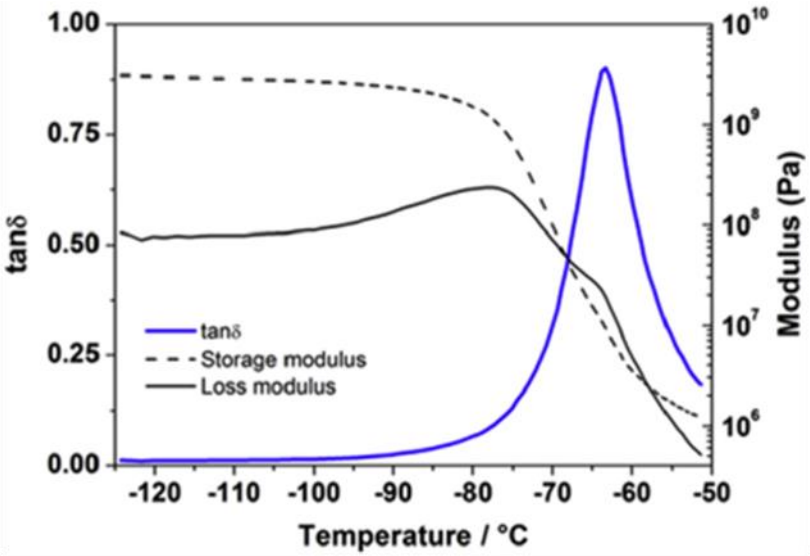

Fig. 5.18 DMTA analysis of the PEO-based XPE.

During sample preparation, PC and $NaClO_4$ salt were added to the PEO matrix, and PC acted as plasticizer and decreased the T_g; this is commonly explained considering that the addition of small molecules facilitates the movement of polymer chains, increasing the free volume inside the polymer matrix. The measured T_g of -63 °C indicates that the XPE at the operating temperature of 25 °C is 89 °C above its T_g, and this favours high degree of segmental motion [176-178]. The shift of the T_g to lower values with respect to pristine PEO indicates a higher elasticity of the polymer chains, nurturing the ionic transport through the polymer electrolyte. The crosslinking process further enhances the amorphous characteristics by restricting the recrystallization process, which in turn increases the amorphous characteristics leading to a crosslinked, yet soft, polymer matrix. Similar characteristics were also observed in similar systems [179,180]. These results indicate that the XPE might be safely used in sodium-based batteries in the temperature range between -50 and 100 °C, which is well above their operational temperature upon standard usage.

The images obtained by FESEM analysis (Fig. 5.19) reveal a high degree of structural homogeneity at high magnification. This confirms that the XPE is almost completely reticulated and PC molecules are homogeneously encompassed in the crosslinked polymer matrix. Fig. 5.19 A and B exhibit how the membrane structure is homogeneous without any evidence of aggregates, crystallites, liquids vesicles or pores formation, both in top-view and cross-sectional setup.

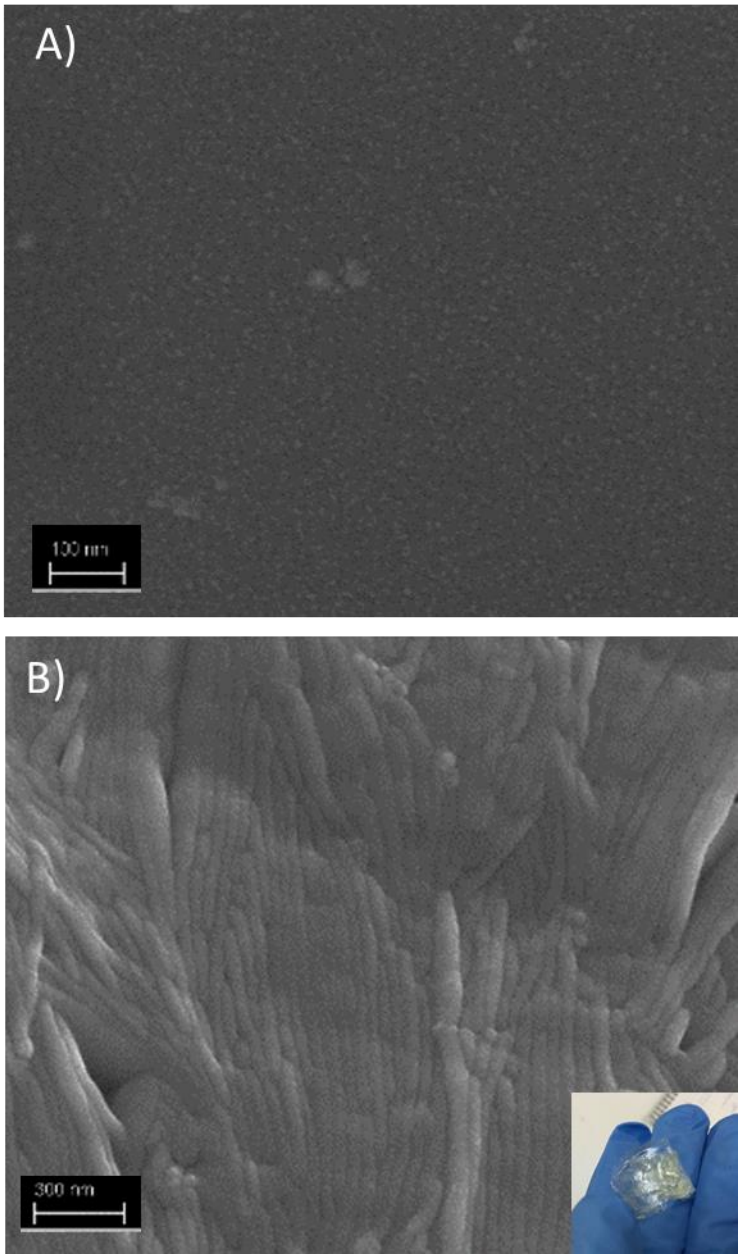

Fig. 5.19 FESEM images of the XPE membrane before (A) and after (B) gel content.

The insoluble fraction of the UV-cured polymer electrolyte was determined as described in the experimental section. XPE showed a gel-content of 100% with respect to the amount of PEO in the matrix. This result indicates that the PC molecules did not take part in the crosslinking process and the crosslinking occurred between the PEO chains, as also demonstrated elsewhere [179,180]. It is worth mentioning that the polymer electrolyte retained its structure even after the

extraction process (see inset of Fig. 5.19 B), indicating that the 45 wt% of PEO was sufficient to impart excellent mechanical stability and integrity to the polymer matrix. As a further confirmation, when the test was carried out on a non-crosslinked sample, after the extraction process no evidence of PEO matrix was observed. This demonstrates the importance of polymer crosslinking process and the efficiency of the light-induced process in retaining the physical characteristics of the final XPE. It is interesting to note that once the plasticisers are extracted (inset of Fig. 5.19 B) from the XPE, the membrane is less flexible, translucent and tougher/stiffer than the XPE itself. This also confirms that PC and $NaClO_4$ are vital to plasticize the polymer matrix and they play a crucial role in increasing the flexibility, plasticisability and ionic conductivity of the final XPE.

The ionic conductivity values were calculated between -40 and 90 °C using EIS analysis as explained in the experimental section. The resulting Arrhenius plot is shown in Fig. 5.20. The XPE membrane showed a conductivity close to 1 mS cm^{-1} at ambient temperature, thus resulting among the highest values reported so far on crosslinked electrolytes proposed for NIBs [181-183]. For a polymer electrolyte, the nature of its phases is of utmost importance, especially when it is considered that the increase in the amorphous phase fraction over its crystalline counterpart enhances the ionic mobility [184]. As expected, in the system under study the presence of PC (and the sodium salt) as plasticizer and solvent, along with the crosslinking between the polymer chains, guaranteed the proper amorphisation of the polymeric system. Indeed, the temperature dependence of the ionic conductivity shown in the Arrhenius plot exhibited the typical Vogel-Tamman-Fulcher (VTF) behaviour, which is typically associated with amorphous polymer electrolytes. Moreover, considering the remarkable values obtained for a truly quasi-solid system (at ambient temperature the lowest value achieved was 0.8 mS cm^{-1}), the ionic conductivity behavior of the XPE was also investigated down to very low -40 °C temperature (Fig. 5.20). Noteworthy, the XPE demonstrated ionic conductivity values exceeding 0.1 mS cm^{-1} at around 0 °C and above 10^{-6} S cm^{-1} even at -40 °C. Such a result bodes well with the application of the proposed polymer electrolyte in energy storage systems even in geographic areas where the temperature fluctuations are extremely relevant.

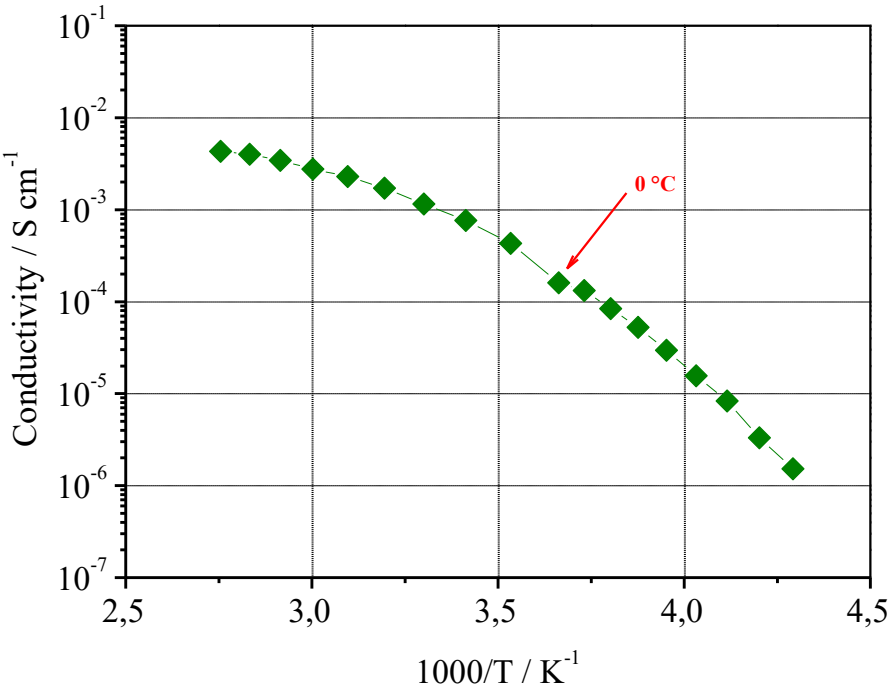

Fig. 5.20 Arrhenius plot showing the ionic conductivity of the XPE in the range of temperatures from -40 to 90 °C.

The study of the electrochemical stability window (ESW) is necessary in order to evaluate the stability of the XPE towards oxidation as well as reduction reactions, so that it can be safely applied in various battery systems operating in a broad potential range. Fig. 5.21 shows the cathodic reduction (C.S.W., red curve) and anodic oxidation (A.S.W., blue curve) reactions for our polymer electrolyte. The XPE was stable towards cathodic potentials below 0.0 V vs. Na^+/Na, where the deposition of Na started occurring, and facilitated the plating and stripping of sodium ions to and from the sodium metal electrode surface. No foreign peaks corresponding to any unwanted side reactions were observed, thus confirming that the electrolyte was free of impurities and stable towards sodium metal. It was also stable in the anodic potential scan, where no relevant onset of current was observed until 4.7 V vs. Na^+/Na. The graph was neat without any peaks indicating that the XPE was free of moisture, thus confirming the validity of the preparation process adopted. A degradation reaction took place above 4.7 V, indicated by the onset of the current flow. It can therefore be concluded that the XPE under study has a wide stability window of 4.7 V and it can be safely used in NIBs operating in a wide potential range.

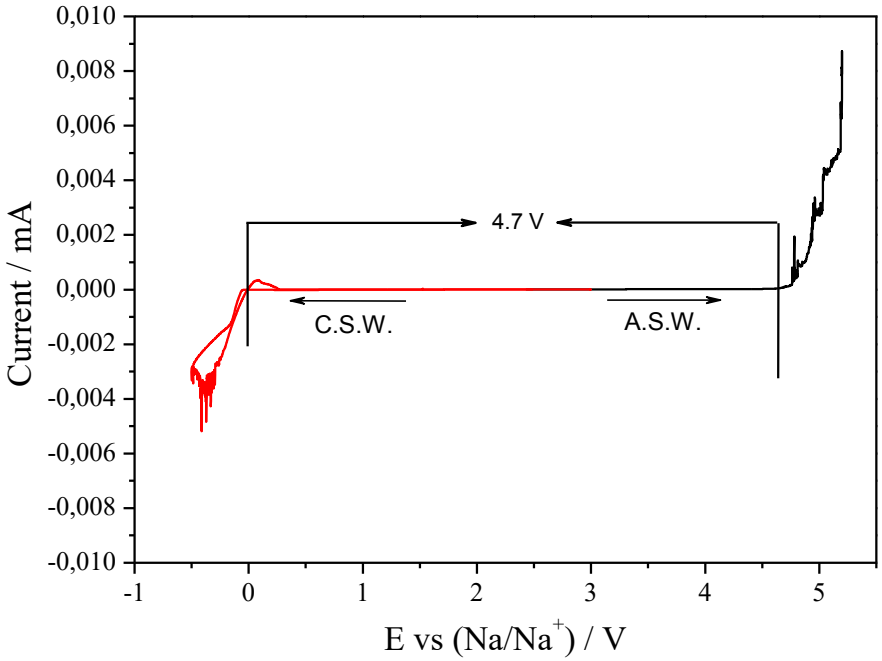

Fig. 5.21 Electrochemical stability window (ESW) of the XPE. The red branch represents the cathodic (reduction) potential scan, while the black branch is relative to the anodic (oxidation) potential scan (black line). Data were recorded at ambient temperature.

Estimation of t_{Na^+} was performed by coupling AC current and DC polarization techniques as described in the experimental section. This parameter is very important to test the performance of a polymer electrolyte in view of its application in rechargeable batteries. According to the technique proposed by Bruce and Evans [185], for a symmetric cell of Na|XPE|Na, a DV of 20 mV for 4000 s was applied in order to monitor the resulting initial and steady state current as a function of time. The method also includes the measurement of the AC impedance before and after cell polarization and the values of the electrode-electrolyte contact resistances are estimated from the corresponding Nyquist plots. Using Equation 2 (section 5.1.1.3), the value of t_{Na^+} for the XPE was found to be ~ 0.32 at ambient temperature. This value may account for the fast transport of sodium ions inside the polymer electrolyte.

Besides the ionic conductivity, the electrochemical stability window and the transference number, interfacial stability is another parameter that gives important information on the characteristics of a polymer electrolyte and its compatibility with the electrodes. Indeed, the compatibility of the XPE with the sodium metal

electrode is a fundamental parameter to guarantee acceptable performances in electrochemical devices (i.e., batteries) especially when long-term cyclability and reliability are envisaged. This is well known in LIBs, and as demonstrated in the previous Chapters of this thesis, the electrolyte reactivity towards sodium metal electrode should be curbed similarly to achieve substantial cycling [186,131]. Indeed, when an electrolyte (liquid or solid) is in contact with a metal electrode, a solid electrolyte interface (SEI) forms: such a passivation layer is attributable to the reactivity of some of the components of the separating electrolyte with the bulky metal surface. The interface behaviour was evaluated by following the evolution of the overall resistance of a symmetrical Na|XPE|Na cell at ambient temperature under OCV condition [187]. In this experiment, the interfacial resistances are typically obtained from the intercept at low frequencies of the real axis of the Nyquist plot that corresponds to the charge transfer resistance (R_{ct}) (Fig. 5.22 B). The global behaviour is shown in Fig. 5.22 A, in whichthe time evolution of the charge transfer resistance is plotted [167]. The formation of the passivation layer is a key point for the preservation of the sodium metal electrode during the repeated charge/discharge cycles, which often induces dendritic growth that eventually leads to short-circuit, detrimental for the battery life. Initially, the value of the R_{ct} slightly increased, indicating the beginning of the SEI layer formation. After 24 h, R_{ct} decreased close to initial values and remained stable up to 200 h. The resistance was stabilized around 1 kΩ. As already reported by Slater *et al.* [188], the reactivity of Na metal with organic electrolyte solvents is more problematic than Li metal electrode. Indeed, it is very critical to use sodium, due to its complicated manipulation process for reducing from ingots into thin foils to be then contacted to the stainless steel current collector. As a result, the obtained interfacial stability is appreciable for the use of this XPE in NIB configuration [188], and the fluctuations can be most likely ascribed to the raw surface of the manipulated sodium metal electrode.

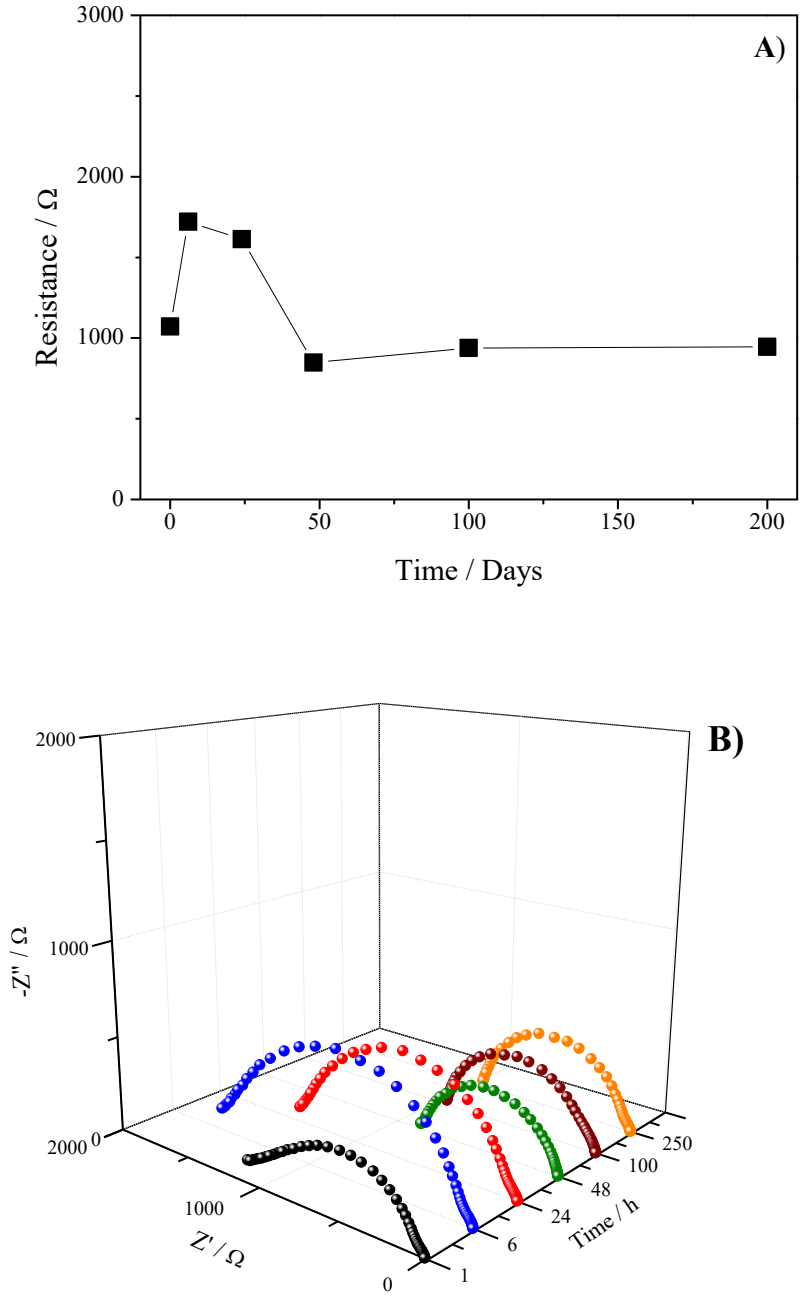

Fig. 5.22 Interfacial stability (R_{ct} evolution time overview) of the XPE at ambient temperature in a Na/XPE/Na symmetrical configuration. The resistance values shown in (A) were extracted from the single Nyquist plots of the EIS measurements (B).

Considering the satisfactory results obtained from the morphological, physico-chemical and electrochemical characterization of the newly proposed crosslinked polymer electrolyte membrane, XPE was finally investigated for its practical operation in sodium batteries. Therefore, it was assembled in a lab-scale TiO_2|XPE|Na sodium polymer cell (where the crosslinked membrane acted as the separating electrolyte), and its electrochemical behavior was investigated by means of constant current (galvanostatic) discharge/charge cycling at different current densities (up to 0.5 mA cm^{-2}) at ambient temperature; the very long-term response of the cell was evaluated as well. Fig. 5.23 shows the response of a lab-scale polymer cell, which delivered a high specific capacity of ~410 mAh g^{-1} during the initial discharge cycle (~250 mAh g^{-1} during initial charge), when applying a low current density of 0.1 mA cm^{-2}, which corresponds to about 0.04C rate vs. the TiO_2 active material weight.

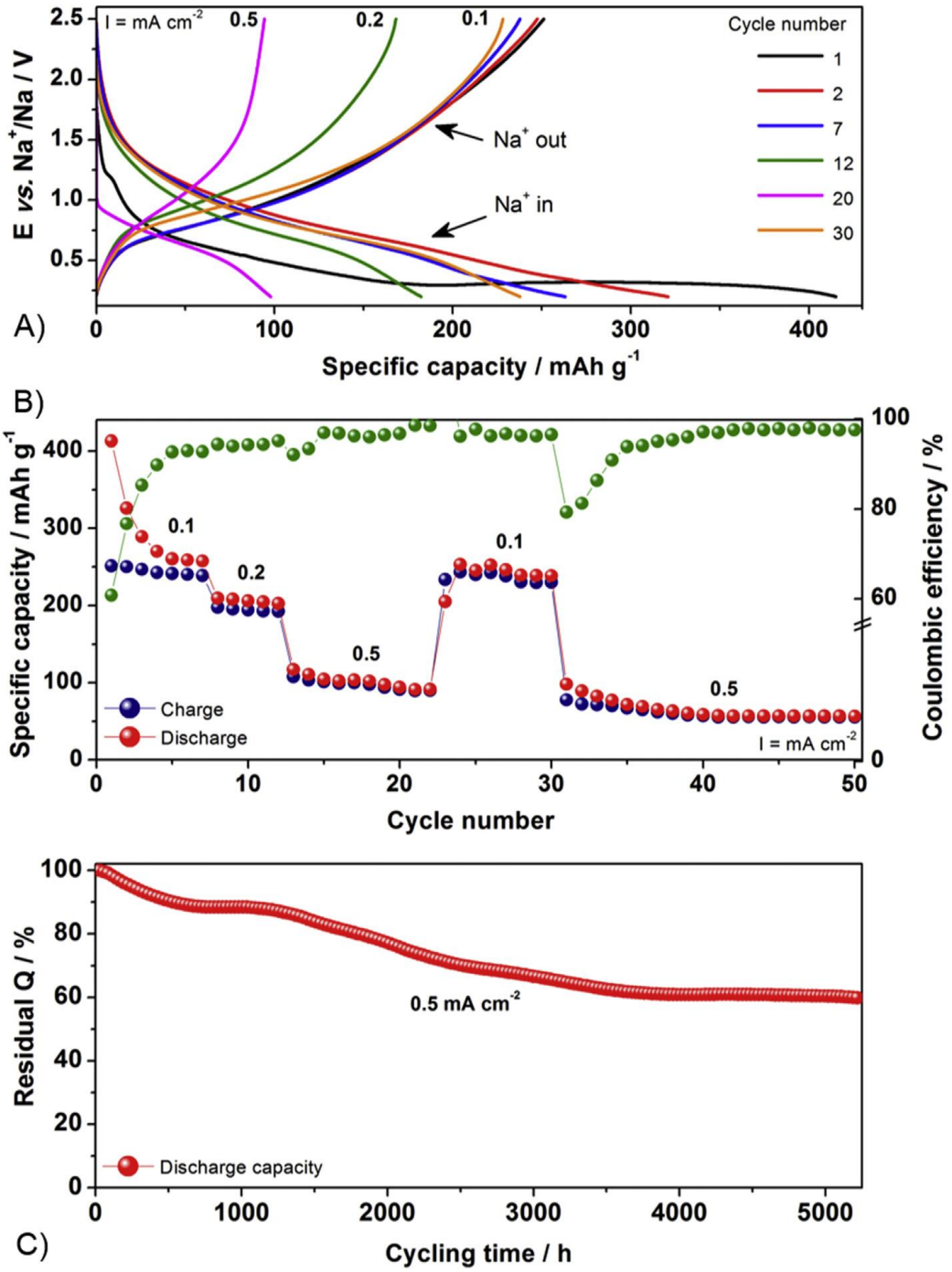

Fig. 5.23 Ambient temperature constant current cycling behaviour of the lab-scale TiO_2|XPE|Na cell at different current densities (from 0.1 to 0.5 mA cm^{-2}): A) Discharge/charge potential vs. specific capacity profiles, B) Specific capacity and Coulombic efficiency (green spheres, right axis) vs. cycle number, C) Residual discharge capacity upon long-term (about 1000 cycles corresponding to about 5250 h) cycling at 0.5 mA cm^{-2}. (Taken from [146])

The excess of capacity consumption during the first discharge (TiO_2 sodiation) causes the classical irreversible capacity loss [44]. Indeed, during this step - as expected from the previously discussed interfacial stability test - the SEI formation occurs and, consequently, the discharge time is much longer than the theoretical value reported in the literature for a complete sodiation of the TiO_2 working electrode [189,190]. Even though such an irreversible capacity loss might be considered detrimental from the discharge/charge point of view, it represents an important point for practical application of these batteries. Indeed, the formation of the SEI layer protects the surface of the sodium metal electrode from side reactions that normally occur between the metal surface and the electrolyte medium upon prolonged cycling.

The discharge capacity decreased upon initial cycling, achieving an almost stable regime at about 260 mAh g^{-1} after 5 cycles, thus a rather short "activation" process was found to be necessary before cell equilibration [191]; on the contrary, a stable specific capacity of about 245 mAh g^{-1} was achieved upon charging at low 0.1 mA cm^{-2}, which is remarkable for a truly quasi-solid Na polymer cell. The capacity fading is similar to what previously observed [192]. After the gradual capacity fading upon initial cycling at low current regime, which is likely ascribable to surface reactions and the structural adjustments during the insertion/extraction of "big" sodium ions in/from the TiO_2/C active material particles, the cell demonstrated stable behavior at each of the tested currents and also delivered an overall excellent reversible cycling. In particular, a 15% decrease in specific capacity was experienced while doubling the current density; still sufficient and stable capacity slightly exceeding 100 mAh g^{-1} was achieved at relatively high 0.5 mAh cm^{-2}, which corresponds to about 0.2C rate.

The cell did not experience any abnormal drift upon cycling at higher current density, as confirmed by the full restoring of the capacity (> 250 mAh g^{-1}) when the current was decreased back to 0.1 mA cm^{-2} after about 25 cycles, thus accounting for the structural stability and mechanical integrity of the electrode/electrolyte materials after the initial rearrangements were completed. Thereafter, the current density was again increased to 0.5 mA cm^{-2}, and the Na polymer cell still provided slightly more than 60 mAh g^{-1} after 50 cycles. Sufficient performance even at higher current regime may be ascribed to the efficient ionic mobility and Na^+ transport in the separating polymer electrolyte and the favourable interfacial charge transport between electrodes and electrolyte in the cell. Overall, the Coulombic efficiency approached 99% at higher current densities, thus giving a clear insight into the good reversibility of the electrochemical process in the cell and the stability of the formed

SEI layer as well as of the structural/morphological and physicochemical properties of the electrode/electrolyte materials [189].

Typical charge/discharge potential vs. specific capacity profiles of the lab-scale Na polymer cell are shown in Fig. 40. They resemble those of remarkably reversible processes and were found clearly in agreement with the literature data for nanostructured TiO_2 electrodes [189,190,192,193], showing reproducible and reasonably well defined S-shaped curves averagely centred at about 0.92 V vs. Na^+/Na. As already pointed out by Ruffo and co-workers, such a value is definitely lower if compared to the corresponding insertion/intercalation potential of lithium ions inside amorphous/crystalline titania/titanates [194], which is actually well confined in the stability window of the selected polymer electrolyte and enlightens even more the appealing features of TiO_2 nanostructures as safe NIB anodes. The very long-term cycling test, shown in Fig. 41, finally demonstrates the promising prospects of the proposed XPE. The results are here reported in terms of residual normalised discharge capacity vs. number of hours of consecutive continuous cycling, which allows to highlight the remarkable stability of the novel quasi-solid polymer electrolyte under study in connection to the very stable TiO_2 nanostructured electrode active material particles, which delivered almost 60% of the initial capacity after about 5250 h resulting from 1000 reversible cycles at 0.5 mA cm^{-2}.

5.2.1.5 Conclusions

A crosslinked polymer electrolyte was proposed for safe sodium-ion batteries conceived for large-scale energy storage systems, which are now highly requested to be coupled with photovoltaic and wind farms. The proposed polymer electrolyte was obtained by light-induced crosslinking of a poly(ethylene oxide) matrix, which is a rapid and solvent-free process easily up scalable for large industrial production as it allows to produce ready-to-use polymer electrolytes in a single step. Besides showing excellent thermal properties (T_g = -63 °C, first TGA peak > 100 °C), the polymer electrolyte is also characterized by an ionic conductivity exceeding 1 mS cm^{-1} at 25 °C (0.1 mS cm^{-1} at 0 °C) and an electrochemical stability window as wide as 4.7 V vs. Na^+/Na.

The polymer electrolyte was assembled in TiO_2-based labscale sodium cells, which delivered stable specific capacity of about 250 mAh g^{-1} at ambient temperature upon constant current cycling at 0.1 mA cm^{-2}. The stability of the light-designed electrolyte was also confirmed by very long-term cycling test that

exceeded 5200 h of continuous operation, which is definitely remarkable for a truly quasi-solid system. The present findings demonstrate that photocured systems based on a simple, but efficient poly(ethylene oxide) matrix, can be a strong solution to the request of industrially-processable polymer electrolytes for sustainable sodium-based batteries.

Chapter 6

Organic electrodes for secondary Na-ion cells

6.1 General context

Nowadays, active materials for batteries are based on inorganic chemistry. In a recent work, Poizot and Dolhem [5] gave an overview on the state of art of the materials actually in use, focusing the attention on the cost in terms of energy and pollution related to the use of these materials. In the article they summarized the concepts in a picture (Fig. 6.1) which can be described as follow: the entire process starts with the mining of the precursors (ores); after the extraction of the mineral materials, a second step is necessary for the refinement and the production of the redox active materials, which in general requires elevated temperatures and the use of chemicals; the third step is the battery manufacturing; then batteries are ready to serve at several purposes for which they have been developed and sent to the market. After full utilization, all batteries must be collected and recycled. Aside the battery usage, all the other processes, including the recycling step, are energetically expensive and pollutant. Basically, we spend a lot of energy to produce energy. Moreover, the recycling process is by now mandatory, especially in the countries belonging to the European Union; in this respect, a directive of 2006 cites as follows: *"recycling of 50 % by average weight of other waste batteries and accumulators"* [195].

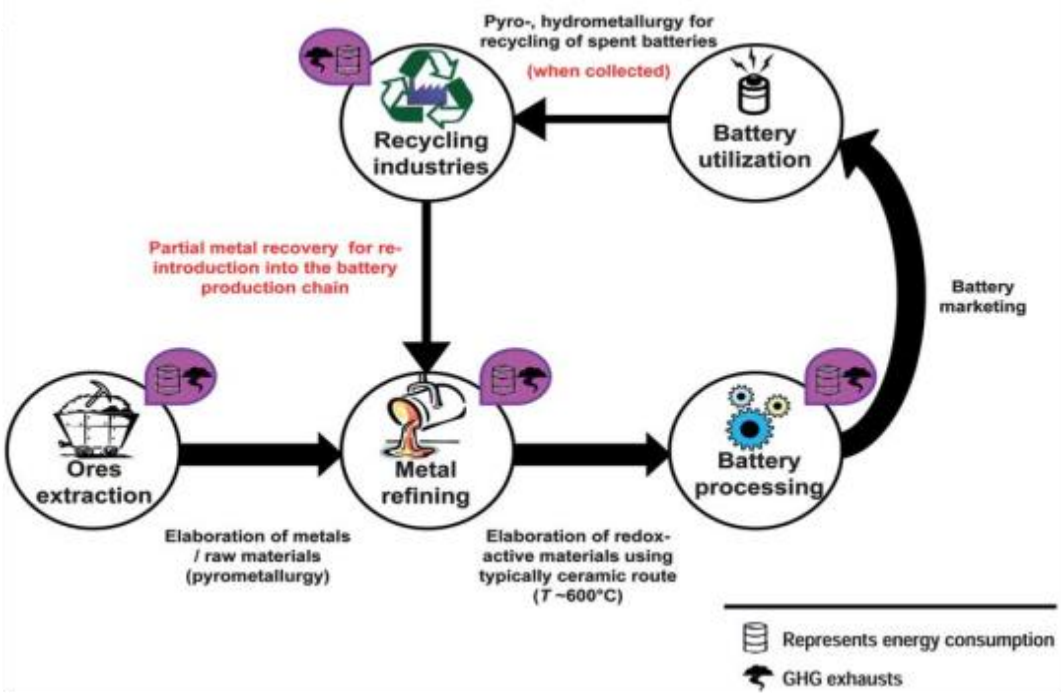

Fig. 6.1 Overview of the current battery technology using ores derivatives for the production of electrodes. (taken from [5])

In order to meet the energy demand with special attention to the environmental concerns, the substitution of inorganic compounds with organic ones might be a promising solution. In fact, the main idea of circular economy is to use organic materials prepared by a sustainable cycle life starting from CO_2 in the atmosphere. Tarascon *et al*., in 2008 described by a simple scheme (Fig. 6.2) the concept of "a sustainable battery" [196]. The main idea is the use of the modern green chemistry, starting from a renewable natural precursor (CO_2 indeed) for the synthesis of the active materials which are then used in the battery processing. After utilization and at the end-of-life, the battery is delivered to the recycling factory where, during the process, carbon dioxide is again released in the atmosphere. Such CO_2 in an ideal cycle is used anew in the biomass assimilation closing the circle. In such an ideal scenario, no additional carbon dioxide is produced, with a really ecofriendly concept.

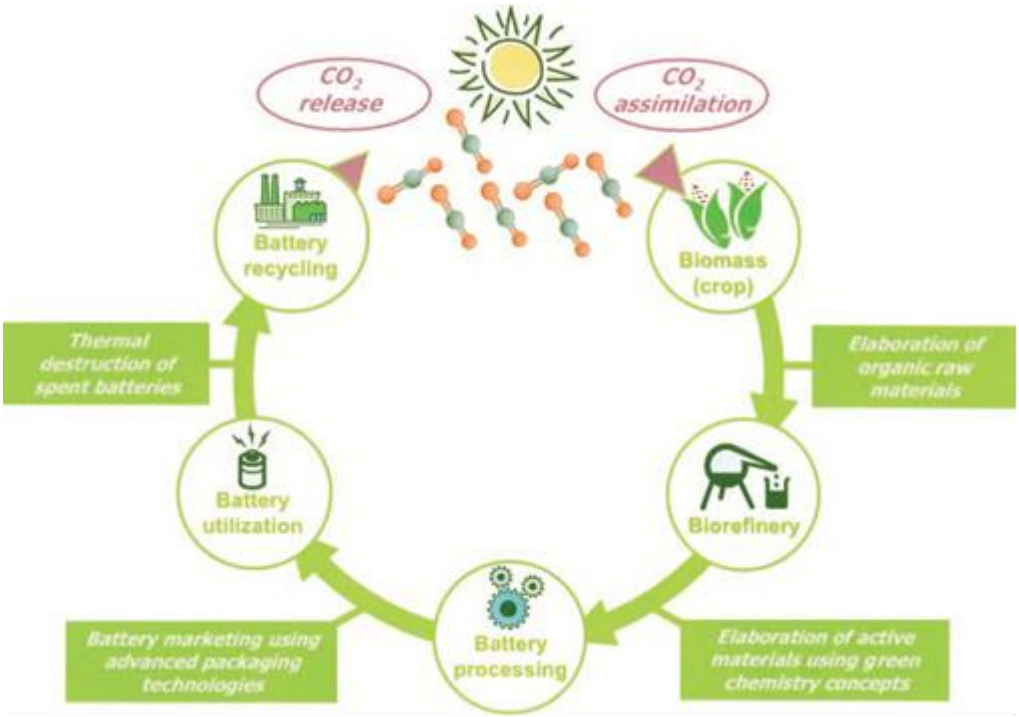

Fig. 6.2 Simple scheme of the cycle life for a sustainable secondary battery. In the ideal point of view, no additional CO_2 is produced. (Taken from [204])

In the last years, the scientific worldwide interest in organic electrode materials has grown very fast. This is due to the environmental impact factor, but also because organic materials are easy to synthesize, with the possibility of design many molecules, their abundance, recyclability, and compared to the inorganic counterpart, it is possible to form molecules with high theoretical capacity and tunable working redox potential.

The first example of an organic compound applied as electrode in a battery system dates back to 1969, when Williams et al. [197] investigated the dichloroisocyanuric acid (DCA) as cathode for lithium primary batteries. After this pioneering work, the scientific interest for such materials increased; discovery of redox activity in inorganic compounds, nevertheless during the seventies, which showed better performances in terms of energy density, stability against the common liquid electrolyte and temperature suddenly "freezed" the research on high performing organic electrodes. Organic compounds as electrodes display several drawbacks,

which make theme still less appealing for practical use in battery prototypes. Compared to the inorganic counterparts, organic electrodes are:

a) Less electronically conducting, so they need more conducting additive (e.g. carbon black) to enhance their performance, but at the same time the quantity of the active material in the composite electrode decreases, correspondingly reducing the gravimetrical capacity of the electrode.

b) They are less stable at higher temperatures, which limits their potential application to moderate temperatures.

c) They are highly soluble in the standard liquid electrolytes commonly used in battery technologies.

Despite their drawbacks, the scientific community in the last years designed several strategies to improve their performances in view of their practical application in real battery system.

The most widely reported redox organic compounds as electrodes in NIBs, are mainly based on C=O bond reaction (carbonyls), C=N bond reaction and doping reaction [198].

Carbonyls are typically divided into four categories: quinones, carboxylates, anhydrides and imides [199-201]. Quinones have the simplest structure with high theoretical capacity (Fig. 6.3), but the rapid dissolution in the conventional liquid electrolytes leads to serious capacity fading, because the dissolved species migrate between the electrodes which worsen the battery performances. In order to solve the problem, several strategies were applied. Among them the optimization of the electrolyte rending it highly viscous [202], the use of electron withdrawing groups in the structure (F^-, Cl^-) [203], the formation of salts using salt substituent (Na-enolate, -ONa) which increases the polarity of the material [204,205], the polymerization of the structures that results in materials with enhanced molecular weight .

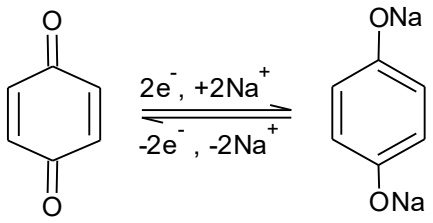

Fig. 6.3 Example of a simple quinone structure and relative double sodium insertion mechanism.

Carboxylates are the most widely reported electrodes in NIBs [206,207]. They are organic structures with one or more electron donor group (-ONa) connected to the carbonyl (Fig. 6.4). The redox potential of Na insertion for these materials is in general below 1 V vs Na^+/Na, so they can be employed as anodes in NIBs. In the field of sodium organic batteries, the most popular carboxylate compound is disodium terephthalate ($Na_2C_8H_4O_4$). This material is able to insert reversibly 2 Na– ions at 0.29 V vs Na^+/Na and shows a reversible capacity of 250 mAh g^{-1}. However, as it happens for the low molecular weight organic materials, their solubility in the electrolytes leads to capacity fading that results in a Coulombic efficiency around 50 % during the first cycle. In order to mitigate this effect, atomic layer Al_2O_3 deposition and the build of nanostructured electrodes (nano-sheets) was applied, with an improvement of the performances [208]. The inorganic coating acts as a protecting layer, which prevents high dissolution. Nanostructuration enhances electronic conductivity and cation migration.

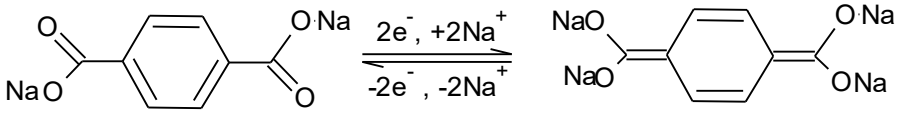

Fig. 6.4 Example of a carboxylate structure and relative double sodium insertion mechanism.

Also for these compounds, several modifications were investigated, and different substituents were explored, such as $-NH_2$, -Br, $-NO_2$; also new structures were synthesized, with an extended conjugated system that enhances the conductivity of the organic compound.

Anhydrides commonly have large conjugated structures with adjustable amount of Na-ion insertions by cutting off different discharge voltages. Fig. 6.5 shows an example of a simple anhydride organic compound and the double sodium ion insertion mechanism for this molecule.

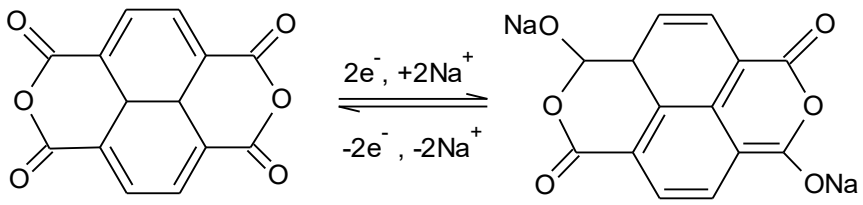

Fig. 6.5 Example of an anhydride structure and relative double sodium insertion mechanism.

Fig. 6.6 shows a recent example of an anhydride and the relative electrochemical reactions proposed for the 3,4,9,10-perylene-tetracarboxylicacid-dianhydride (PTCDA), well-known organic pigment, also known as "red 224", which has an aromatic core and two anhydride groups ($C_{24}H_8O$) [200]. As shown in the picture, the compound presents a reversible process between 1-3 V vs Na^+/Na for 2 electrons. In this potential range, the material delivers a capacity of 145 mAh g^{-1} at 10 mA g^{-1}. Other 2 irreversible processes occur upon material discharging to 0.01 V, and an extremely high capacity of 1017 mAh g^{-1} was obtained in the first cycle. However, a low reversible capacity was observed in this potential range, coupled with a completely destroyed crystal structure of PTCDA.

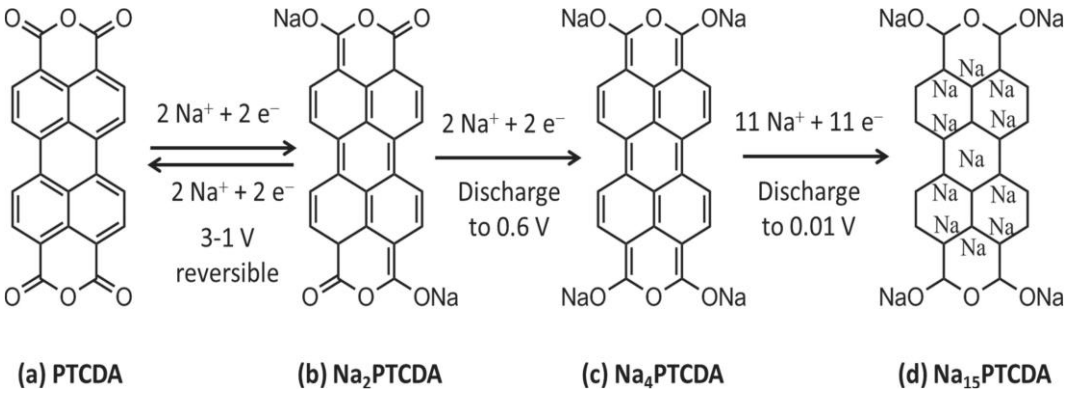

Fig. 6.6 The proposed reaction mechanism of PTCDA (Taken from [200]).

Among the C=O bond reaction materials, one should also consider imide and polyimide compounds. In general the diimide salts are employed (Fig. 6.7), because simple small imide shows high solubility in aprotic electrolyte. However, the problem of dissolution still remains, and the synthesis of polyimide was investigated to inhibit this effect [209]. Such polyimides often exhibit a long cycling life, which may even reach 5000 cycles without evident capacity fading. The main issue of polyimides is their limited theoretical capacity, which is in general lower than 150 mAh g^{-1}. In order to enhance the specific capacity, Xu and co workers

recently proposed the copolymerization of imide with 2,6-diaminoanthraquinone, which led to double the theoretical capacity of the new polyimide proposed [199].

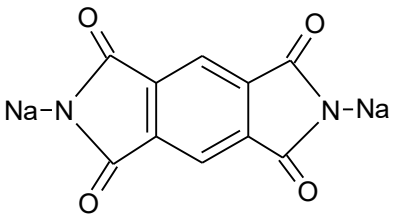

Fig. 6.7 Molecular structure of the diimide salt [210].

Recently, a new type of unexplored organic electrode materials based on Schiff functional group ($R^1HC=NR^2$) were proposed [211]. The electrochemical activity of these materials derives from the C=N double bond. Interesting is the possibility to tune the redox voltage potential by lengthening the conjugation chain, formation of intramolecular hydrogen bonds or by introducing electron donor or acceptor groups in the aromatic rings. Furthermore, the synthesis of Schiff bases is a simple condensation reaction from aldehydes and amines, which release H_2O as a by-product, and this adds value to the environmental aspects of the material. Castillo-Martinez and co workers [201] proposed polymeric Schiff bases as negative electrode material for NIBs. All of these materials have in common the (N=CH-Ar-HC=N) repeating unit, that is considered the active center when the molecule is conjugated. The conjugation is fundamental, because the corresponding isomer in a nonconjugated system is electrochemically inactive. They obtained capacities of 350 mAh g^{-1}, upon cycling at 26 mA g^{-1} the poly-[N,N'-p(benzylidene)phenylenediamine], which corresponds to more than one sodium atom per azomethine C=N unit.

The last class of organic materials used as electrode for NIBs are based on doping reactions. Three different types of compounds belong to this category: organic radical compounds, conductive polymers, and microporous polymers. Among the radical polymers, poly (2,2,6,6-tetramethylpiperidinyloxy-4-yl methacrylate) (PTMA), a derivative of polymethacrylate with a 2,2,6,6-tetramethyl-1-piperidinyloxy (TEMPO) radical in the repeating unit, was first reported by Nakahara *et al.* as the cathode-active material for lithium ion batteries [212]. In the field of NIBs, the first work was reported by Dai *et al.* [213], studying a polynorbornene derivative radical polymer as the cathode active material. The battery delivered a discharge capacity of 75 mAh g^{-1} at the 1st cycle with a capacity retention of 48 mAh g^{-1} at the 50th cycle. More recently Kim *et al.* [214]

investigated a PTMA encapsulated in carbon nanotubes (CNT). The are two beneficial effects of the use of CNT: a) the confinement of the active material prevents its dissolution in the liquid electrolyte, b) the global performances in cell are enhanced, allowing a better stability, discharge capacity, cyclability, and rate capability. The electrode delivered an initial discharge capacity of 222 mAh g^{-1} at a 0.1C-rate, with a capacity retention of around 93 % after 100 cycles at 0.5C, which indicates that such hybrid material is a good candidate as positive electrode for sodium batteries.

The first examples of conductive polymer used as electrodes in NIBs, i.e. polyacetylene and poly-paraphenylene were reported in 1985 by Shacklette *et al.* [215]. At present, the mostly investigated conductive polymers are polypyrrole (PPy), polyaniline (PAn), polythiophene (PTh), and their derivatives [216,217]. However, although these polymers have a theoretically high redox capacity, their practical capacity is usually very low and decreases gradually upon charge–discharge cycling, possibly because of a low p-doping level of counter anions in the polymeric matrixes, and a diffusive dissolution of the anions to the electrolyte [218]. To bypass these issues, one possible way is the doping by anions: acting as redox-active sites, they contribute to the overall capacity, and also enhance the electronic conductivity of the polymer. Zhou *et al.* [218] studied the doping of PPy and PTh with $Fe(CN)_6^{4-}$. In this work, they mainly investigated the behaviour in LIBs, with just only one measurement with sodium using a solution 1 M $NaPF_6$ in EC:DMC:EMC 1:1:1 for PPy-based electrode. An extensive research on $Fe(CN)_6^{4-}$-doped polypyrrole for NIBs was delivered by the same group in the following years [219]. The beneficial effect of the doping is confirmed also in the case of sodium batteries.

Thus, although organic electrode materials in rechargeable NIBs are still at their preliminary stage of development, the variety and designability of such materials are definitely promising. The practical use of organic materials in the field of sodium rechargeable batteries can have different beneficial effects, not only on the environmental point of view, but also for the realization of flexible, high weight and low-cost electrodes.

The last years of my PhD experience was focused on the development and thorough characterization of a carboxylate organic electrode material, the disodium benzenediacrylate (Na_2BDA), to be used as anode in sodium-ion batteries. The material was developed and optimized during a 5 months stage at the Ångströmlaboratoriet under the supervision of Prof. Daniel Brandell at the Uppsala

University. After proper optimization and characterization, I thoroughly studied the electrochemical response of the electrode under different condition, with the main goal to find the best liquid electrolyte to be used in order to fully exploit the material's specific capacity and durability.

6.2 Na_2BDA as anode for Na-based organic batteries: an electrolyte study.

6.2.1 Introduction

One of the most dramatic issues related to the use of organic compounds as functional electrode materials for batteries is their high solubility in the conventional aprotic liquid electrolyte. Several strategies have been proposed over the years to overcome this issue, including materials' polymerization, grafting of insoluble particles onto the electrodes' surface, and even moving towards all-solid-state cell configurations. Unfortunately, up to now none of these approaches led to excellent results.

However, to fully exploit the capabilities of electrodes materials and, in particular, organic electrode materials the correct choice of the most suitable electrolyte is one of the most important steps of research and development.

This is particularly appropriate for disodium benzenediacrylate (Na_2BDA), a new material with very interesting prospects as anode for Na-based organic batteries. In this respect, the following sections will detail about an extensively study on the behavior of Na_2BDA in different liquid electrolyte media; the differences in performance that occur using different binder, and how a simple calendaring process could improve the global capacity output of the electrode will be also discussed with the aim of enhancing the effective materials' utilization and long term stability.

6.2.2 Experimental

6.2.2.1 Synthesis of Disodium benzenediacrylate

The disodium benzenediacrylate (Na_2BDA) was synthetized by proper modification of the procedure reported in the literature by Y. Park *et al.* [220]. In brief, 1.1349 g of 1,4-benzenediacrylic acid (98 % purity, Alfa Aesar) were added to a solution of sodium hydroxide (NaOH, 98 % purity, purchased from VWR

International) prepared dissolving 1.4080 g of NaOH in 5 ml of deionized water at around 50-60 °C. Deionized water was gradually added up to 40 ml to fully dissolve the residue; then ethanol (99.5 % purity, purchased from Sovelco) was added at 90 °C until the material precipitation started (the brownish-yellow solution became transparent and a white product appeared). The solution was maintained at 90 °C overnight under reflux. The formed crystals were hot-filtered and dried at 100 °C in an oven. The final product obtained was a crystalline solid white powder, the structure of which is shown in Fig. 6.8 A. In Fig. 6.8 B are shown some digital

A) ›s of the real synthesis reaction.

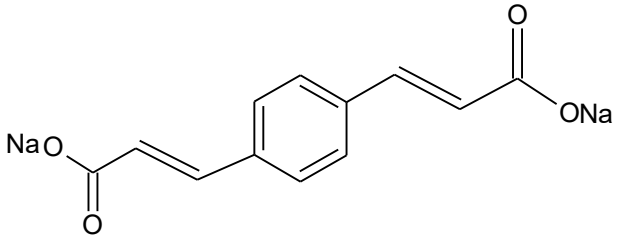

B)

Fig. 6.8 Disodium benzenediacrylate (Na_2BDA) chemical structure (A); digital photographs of the synthesis of the Na_2BDA (B).

6.2.2.2 Characterization

In order to verify the success of the synthesis, IR spectra were recorded, using a Perkin Elmer Spectrum One FT-IR spectrometer equipped with an attenuated total reflectance (ATR) probe. Data were collected in the wavelength range from 4000

to 600 cm^{-1}. The purity of the material (Na_2BDA) was also verified by ^{13}C-NMR spectroscopy using a JEOL ECP-400 spectrometer at 100 MHz. The resulting spectra was recorded at room temperature.

6.2.2.3 Preparation of the composite electrodes

The Na_2BDA composite electrode was prepared mixing the active material with C65 as conductive additive and a water solution of sodium carboxymethyl cellulose (CMC, M_w = 700000, purchased from Sigma Aldrich) 1.5 % w/w as binder, in the ratio 60:35:5. The slurry was ball milled in a planetary Ball Mill by Retsch for 1 h and then coated onto a copper foil current collector using RK K control coater at 50 °C (electrode labelled FC_01_01).

The same procedure was adopted for the preparation of an Na_2BDA composite electrode with PVdF binder. Since the PVdF binder shows very high swelling capability, it tends to lose its mechanical benefits when in contact with liquid electrolytes, thus the percentage of binder used was higher (10 %) in the composite electrode preparation, compared to the corresponding 5 wt. % of CMC. Therefore, the final ratio used was 60:30:10 (electrode labelled FC_01_2)

After complete coating of the current colelctor, dried discs of 20 mm of diameter were punched out using a Hosen puncher. The discs were transferred in an argon-filled dry glove box (MBraun) and dried in vacuum at 100 °C for 12 h.

A portion of the FC_01_01 electrode was calendared using a Gelon coating machine GN-DYG135 equipped with a 300 mm coating width oven lab. After the calendaring process, the sample was labelled FC_01_01_C.

6.2.2.4 Electrochemical characterization

The main goal of this experimental work was the proper selection of the best liquid electrolyte for the Na_2BDA organic electrode. For this reason several electrolyte solutions were prepared, with different sodium salts and different solvents (see Table 3).

Table 2 List of the electrolyte solutions prepared and tested with the Na_2BDA organic electrode.

ELECTROLYTE
1 M $NaClO_4$ in PC
1 M $NaClO_4$ in EC:DEC 1:1
1 M NaFSI in PC
1 M NaFSI in EC:DEC 1:1
1 M NaFSI in TEGDME
1 M $NaPF_6$ in PC
1 M $NaPF_6$ in EC:DEC
1 M NaTFSI in PC

Galvanostatic discharge (Na^+ deinsertion) / charge (Na^+ insertion) cycling tests were performed in half-cell configuration with coffee bag cells (Fig. 6.9), using the battery testing system BT 2043 by Arbin instrument. The cells were assembled swelling the electrolytes solutions in glass-fiber separator (Whatman®) and sandwiching the swelled separator between the electrode sample (WE) and the Na metal (99.8 %, Sigma Aldrich) counter electrode. Thus, all potential values given in this section of the monograph refer to the Na^+/Na reference couple.

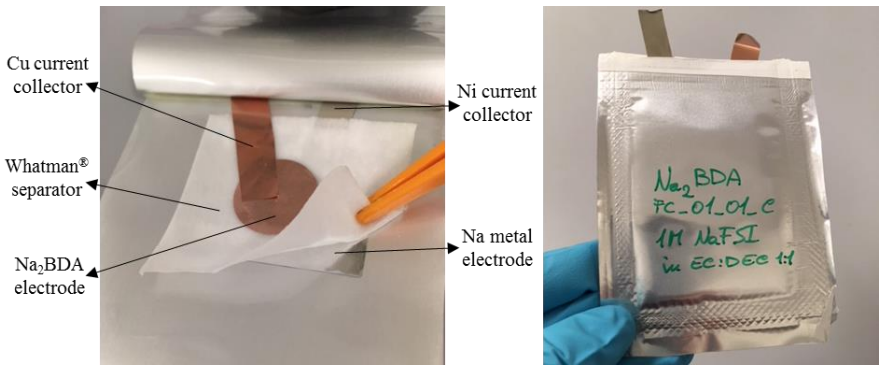

Fig. 6.9 Digital photographs of a coffee bag cell. On the right is showed the "open" bag with in evidence all the materials used and how the components are sandwiching. On the left the picture shows the final aspect of the coffee bag.

6.2.3 Results and discussion

In order to evaluate effective formation of the desired Na_2BDA materials, thus confirming successful reaction, FT-IR analysis was performed. Fig. 6.10 shows the FT-IR spectrum in the wavelength between 1700 and 800 cm^{-1}, which is the most interesting portion of the spectrum in which the fundamental peaks appeared. The picture displays several characteristic peaks, which can be assigned as follows: 1639 cm^{-1} assigned to C=C symmetric stretch, 1553–1510 cm^{-1} to C=O stretch vibrations, 1422–1390 cm^{-1} to C=C stretching from the phenylene group, 1250 cm^{-1} to C–O stretch, 969 cm^{-1} to C–H stretch characteristic of the alkene group and 850 cm^{-1} to the bending of the 1,4-disubstituted aromatic rings.

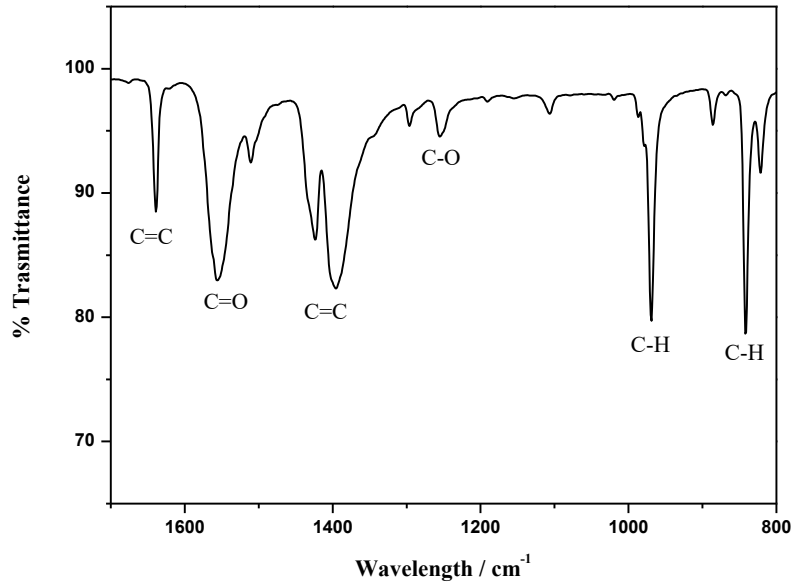

Fig. 6.10 FT-IR spectrum of Na_2BDA and relative assignment of typical stretching and/or bending peaks.

The purity of the material (Na_2BDA) was also confirmed by ^{13}C-NMR spectroscopy. The spectra show single phase signals from the carboxylate as well as the phenylene groups of the disodium benzenediacrylate (Fig. 6.11). The NMR 13C NMR (100 MHz, D_2O) d (ppm): 125.0 (HC=CH–CO2), 128.3 (CH, phenylene), 136.5 (C–CH=CH–CO2), 140.2 (CH=CH–CO2), 175.7 (CO2).

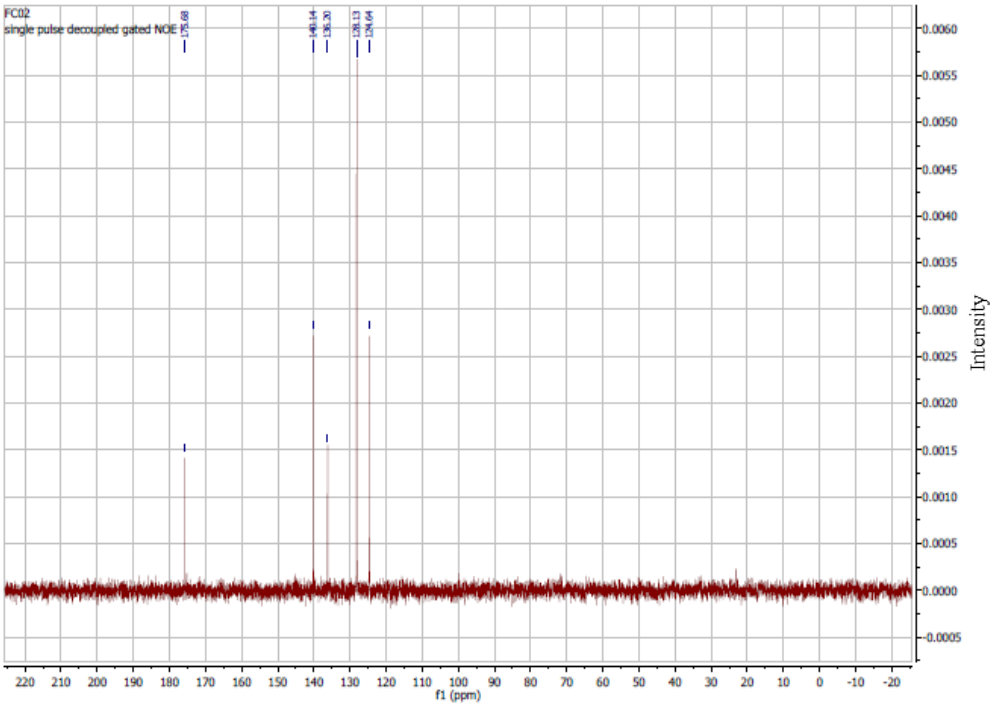

Fig. 6.11 ^{13}C-NMR apt spectrum of Na_2BDA in D_2O at 100 MHz. The analysis confirmed the complete formation of the disodium benzenediacrylate.

The electrochemical behavior of the electrodes FC_01_01_C and FC_01_02 prepared using different binders is shown in the following Fig. 6.12 (A,B) , where the cyclic voltammetry (CV) profiles are shown, which were recorded at ambient temperature in a two-electrodes cell assembled with Na metal acting as both the counter and the reference electrode.

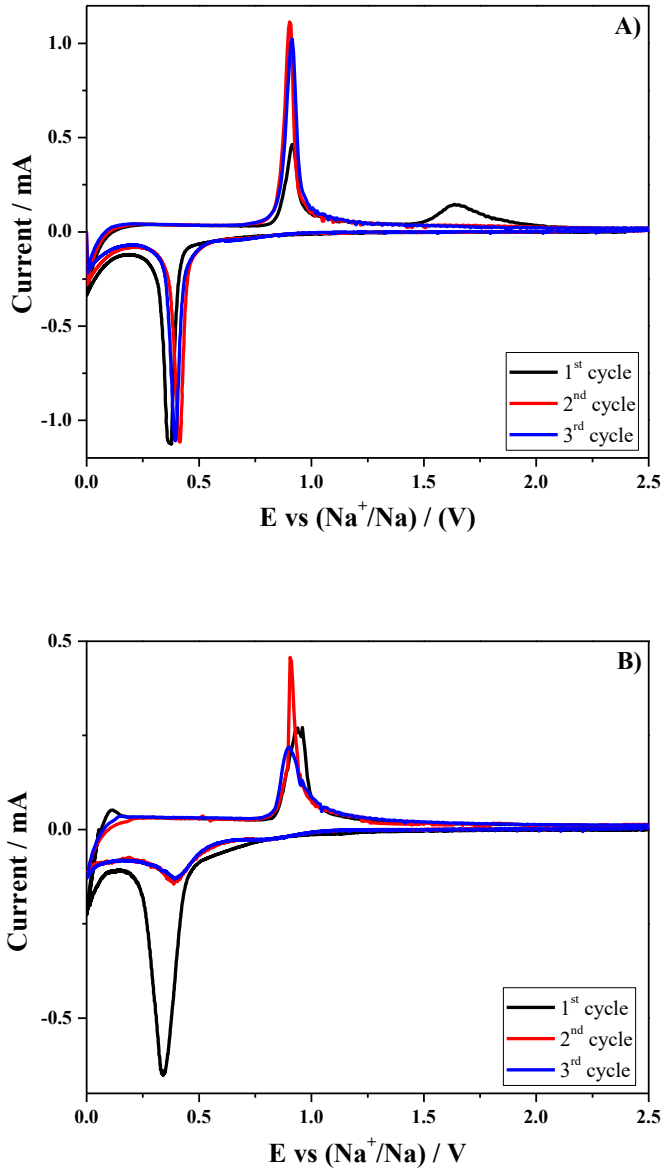

Fig. 6.12 Cyclic voltammetry (CV) of the Na_2BDA composite electrodes prepared with different binders: Na-CMC (A) and PVDF (B). Scan rate = 0.100 mV s^{-1} and potential scan range = 0.0 – 2.5 V vs. Na^+/Na.

Overall, the reduction and oxidation peaks appeared well centered at potential values of about 0.4 and 0.9 V vs. Na^+/Na, respectively. The potential values are in good agreement with the results reported in the literature [221] [222], reflecting the

typical electrochemical response towards sodium de-insertion/insertion of Na_2BDA. Comparing the voltammograms of samples FC_01_01 and FC_01_02, it is clearly evident that the electrode prepared with Na-CMC binder exhibits an enhanced electrochemical behavior, with the reduction and oxidation processes perfectly reversible after the second cycle; the peaks are also sharp and intense accounting for the good electronic conduction within the active material grains. On the contrary, the composite electrode prepared with PVdF binder showed a remarkable decrease in the intensity of the redox/oxidation peaks upon cycling. The FC_01_01 electrode displays a peculiar shoulder at about 1.6 V vs. Na^+/Na during the first oxidation cycle (the anodic sweep towards higher potential values). Compared with previous literature reports [221], in the present case, this peak is more clearly pronounced and it is attributed to the presence of Na-CMC; it might be ascribed to some residual water and/or a sort of oxidation/passivation of CMC moieties. The overpotential (potential difference between anodic and cathodic peaks) is extremely low, indicating the good reversibility of the sodium extraction/insertion reactions of the FC_01_01 electrode. The voltammetric profiles did not undergo substantial differences with cycling, accounting for the excellent stability of the prepared electrode and revealing that only the main electrochemical reaction occurred, without secondary processes. The typical shoulder detailed in the literature in the cathodic branch at about 0.3 V vs. Na^+/Na [221] associated to the formation of the passivating film onto the electrode surface with the partial decomposition of the electrolyte solvent is clearly distinguished in both the samples under investigation. The formation of SEI occurs in both cases, most probably at the same voltage of the reduction process thus the signals are overlapped.

In order to find the most suited electrolyte for the Na_2BDA organic electrode, the different liquid formulation selected (see Table 3) were tested in Na metal cell in terms of discharge/charge galvanostatic cycling at C/4 current rate. The current rate was selected according to earlier works where the material was investigated from lower current regimes (C/40 and C/10) to C/4 and the results already obtained revealed the improvement of the performances when testing the cells at faster rate. Indeed, capacity fading at C/4 is less pronounced compared to C/10 or C/40 rates, resulting in specific capacity values that are double after 40 cycles at higher current regime. The reason for such behavior of Na_2BDA is that the material has more of time to dissolve or react chemically with the electrolyte or polymerize when cycling at C/40 or C/10, forming secondary products that lead an increased loss of active material. When cycling at C/4 or even higher rates, on the other hand, there is less time for the radicals to take part in side-reactions, thus resulting in an increased

cycling performance. The cycling behavior was tested in lab-scale coffee bag cells in terms of galvanostatic discharge/charge measurements performed at ambient temperature setting the voltage cut-offs from 0.1 to 2 V vs. Na^+/Na. The resulting specific capacity vs. cycle number plots for the samples prepared with Na-CMC and PVdF binders using the 1M NaFSI in EC:DEC 1:1 electrolyte formulation are shown in Fig. 6.13 A e B. The NaFSI based electrolyte formulation was used based on previous literature reports [221].

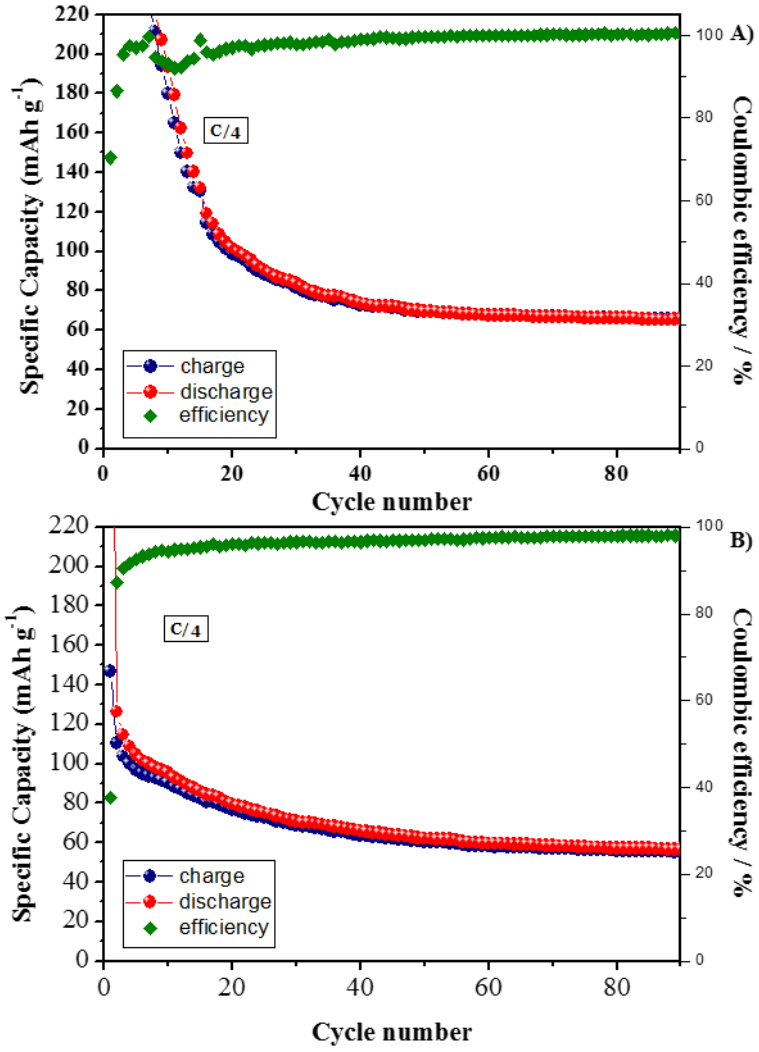

Fig. 6.13 Constant current charge/discharge cycling test at ambient temperature and using the 1M NaFSI in EC:DEC 1:1 electrolyte formulation of the Na_2BDA composite electrodes prepared with different binders: A) Na-CMC and B) PVDF.

Both the samples showed the typical initial irreversible specific capacity loss. It occurs in all the samples tested and is in fair agreement with the results reported in the literature [221]. All the half-cells assembled with the FC_01_01 sample, after the initial "formation" cycles, demonstrated a good stabilization of the specific capacity after 20 cycles and, correspondingly, a rapid increase in the Coulombic efficiency from 70 % to above 95 % (the Coulombic efficiency then stabilizes and effectively approaches 100% after about 50 cycles.. The reason for such behavior lies in the specific decomposition reaction or dissolution of the material in the electrolyte, but also in the formation of the SEI layer on the electrode surface during initial cycling. It was established that a strong contribution to the capacity fading is due to the salt degradation; in the case of NaFSI, the degradation products increase upon cycling but, differently from its lithium analogue (LiFSI), the formation of the passivation layer is faster, and the salt degradation stabilizes after the first cycle [221,222]. Anyway, after the initial stabilization period, the reversible specific capacity at C/4 was found to be around 70 mAh g^{-1} at the 40^{th} cycle in the case of the composite electrode prepared with Na-CMC aqueous binder. The composite electrode prepared with PVdF binder showed a drastically different behavior; indeed, the initial specific capacity output is definitely lower, and the capacity fading is less pronounced but proceeds for a more extended number of cycles (stabilization after > 50 cycles). Moreover, the Coulombic efficiency always stands below 98%, which is lower if compared to the FC_01_01 cells and the specific capacity output is also about 10% lower. As a result, the beneficial effect of the use of Na-CMC as binder are clearly evidenced: Na-CMC not only contributes to the improvement of the cycling performances, but also, being an aqueous binder and a natural cellulose derivative, accounts for the realization of an ecofriendly organic-based battery.

One method widely used for improving inorganic materials based LIB electrodes is calendering, where the electrodes are compacted by controlled pressure, sometimes also at elevated temperatures [223,224]. The selected height before applying pressure was 15 μm without considering the Cu current collector; after calendering, it resulted in the final electrode height of 5 μm. In order to confirm the trend already reported in the literature [224], and in particular, to effectively demonstrate that the mechanical calendaring procedure may help in improving the performances of Na_2BDA organic material, calendered samples were subjected to galvanostatic cycling at ambient temperature. In Fig. 6.14, the galvanostatic discharge/charge cycles obtained at C/4 current rate are displayed, resulting from testing of the Na-CMC binded electrode in the half-cell configuration

FC_01_01_C|1M NaFSI in EC:DEC 1:1|Na, along with its Coulombic efficiency, that is the ratio of desodiation capacity to sodiation capacity

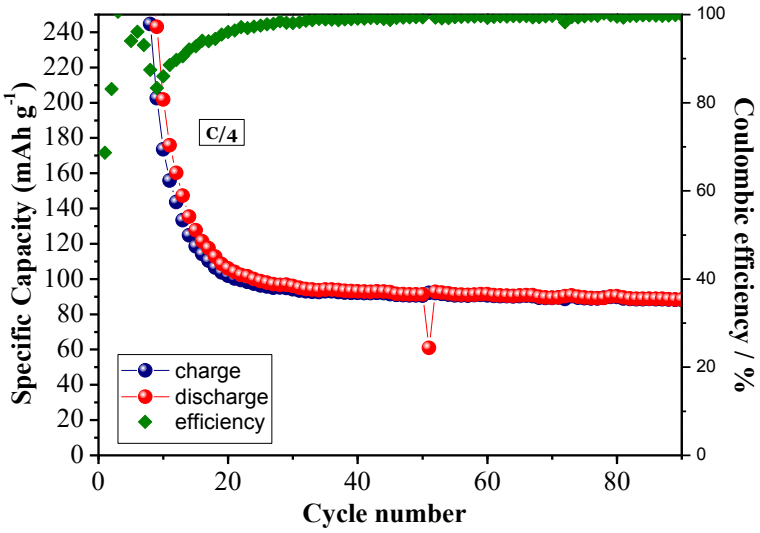

Fig. 6.14 Galvanostatic cycling test at C/4 current rate of the calendered Na-CMC binded Na_2BDA composite electrode, namely FC_01_01_C.

The sample showed the initial pronounced capacity fading, which stabilized after 20 cycles, then resulting in good cyclability. Interestingly, after the initial stabilization period, the cell was able to deliver 90 mAh g^{-1} with very stable cycling for 100 cycles; it corresponds to a remarkable 25 % improvement if compared to the non calendered sample (Fig. 6.13 A), thus evidencing the importance of mechanical calendering also for the stabilization of organic electrodes.

The calendered samples were then tested with the different liquid electrolyte formulations prepared (see Table 3) at the same current rate (C/4) in the voltage range 0.1-2 V vs. Na^+/Na. Fig. 6.15 shows some representative results of the galvanostatic cycling with the following electrolyte solutions: 1M NaTFSI in PC (Fig. 6.15 A), 1M $NaPF_6$ in PC (Fig. 6.15 B), 1M $NaPF_6$ in EC:DEC 1:1 (Fig. 6.15 C) and 1M $NaClO_4$ in PC (Fig. 6.15 D).

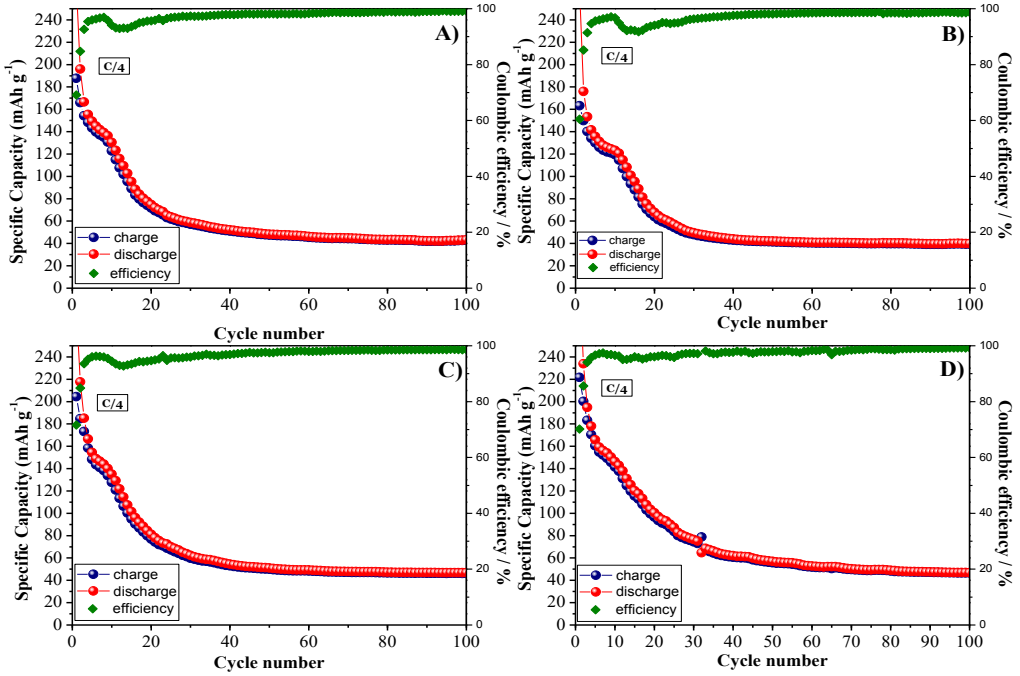

Fig. 6.15 Constant current charge/discharge cycling test at C/4 current rate of the calendered Na-CMC binded Na_2BDA composite electrode, namely FC_01_01_C, using A) 1M NaTFSI in PC, B) 1M $NaPF_6$ in PC, C) 1M $NaPF_6$ in EC:DEC 1:1, and D) 1M $NaClO_4$ in PC.

The calendered Na-CMC binded organic electrode showed rather similar cycling behavior with the different electrolyte formulations: typical irreversible specific capacity loss during initial cycling followed by rapid specific capacity decay prolonged for several cycles (25-30). The reversible specific capacity finally stabilizes at different values, as resumed in Table 4.

Table 4 Stable specific capacity value of the tested cells with different electrolyte solutions.

ELECTROLYTE (salts and solvents used)	**CAPACITY RETENTION (mAh g^{-1})**
1 M $NaClO_4$ in PC	50
1 M $NaClO_4$ in EC:DEC 1:1	55
1 M NaFSI in PC	70
1 M NaFSI in EC:DEC 1:1	90
1 M NaFSI in TEGDME	70 (after 20 cycles)
1 M $NaPF_6$ in PC	50
1 M $NaPF_6$ in EC:DEC	40
1 M NaTFSI in PC	55

From an analysis of the data obtained, it is clear that the lab-scale cell FC_01_01_C|1M NaFSI in EC:DEC 1:1|Na provides the best cycling behavior, with a stable reversible specific capacity of about 90 mAh g^{-1}. As a result, it is confirmed that the choice of the electrolyte is truly fundamental to effectively exploit the full capability of an organic electrode. Remarkably, data obtained during my PhD work are considerably better with the literature findings [221] for all the electrolyte systems analyzed, at the same conditions, with the exception of the electrolyte 1M $NaClO_4$ in PC. For example, the cell assembled with 1 M NaFSI in EC:DEC 1:1 presented in the work of Mihali [221] demonstrated a specific capacity of 80 mAh g^{-1} after 40 cycles (in the publication only specific capacity values up to 40 cycles are shown). It means 10 mAh g^{-1} less than the calendered FC_01_01_C electrode under study, which also delivered stable specific capacity after only 20 cycles, the specific capacity was then highly stable for 100 cycles.

The above presented results confirmed that the organic Na_2BDA material has promising prospects as electrode for NIBs and the liquid electrolyte solution which synergistically operates better with this active electrode material is the 1M NaFSI in EC:DEC 1:1. Moreover, the calendering process demonstrated to be useful in enhancing the electrochemical performance, improving the cohesion between the active material particles and preventing, at least partially, the destruction of the organic electrode, also reducing the dissolution of the material in the liquid electrolyte.

Considering that the cell FC_01_01_C|1M NaFSI in EC:DEC 1:1|Na demonstrated the best performances at C/4 current rate, it was further studied in terms of its rate capability at ambient temperature and different C-rates up to 5C. In general, the specific capacity decreases when the C-rate increases and a limited decrease in capacity at high current accounts for good electronic conductivity and cycling response of the sample under testing. Fig. 6.16 shows the electrochemical discharge/charge galvanostatic cycling behavior of the sample in terms of rate capability at different current regimes, from C/5 to 5C.

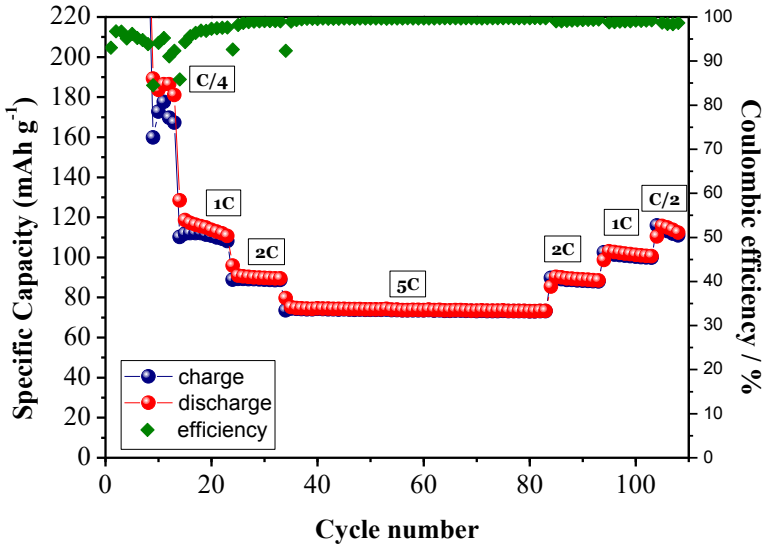

Fig. 6.16 Rate capability test at different current regimes of the calendered Na-CMC binded Na_2BDA composite electrode, namely FC_01_01_C, using 1M NaFSI in EC:DEC 1:1 electrolyte solution.

As expected a pronounced capacity fading occurred during the first cycles at lower C/4 rate. However, already after only 8 cycles at 1C rate the specific capacity stabilized, and the cell delivered around 110 mAh g^{-1}. to the capacity fading upon increasing the current rate was found to be limited and, at 5C current rate, corresponding to 66 μA g^{-1}, the cell still delivered a specific capacity of ~ 74 mAh g^{-1}, which is then maintained very stably for 50 cycles with a Coulombic efficiency higher than 99.5 %, which indicates the excellent reversibility of the reduction/oxidation processes in the active material. The cell also demonstrated no abnormal drift and/or degradation after cycling at very high current as demonstrated from the full recovery of specific capacity when the current regime was gradually decreased at 2C (89 mAh g^{-1}) and 1C (103 mAh g^{-1} after 100 cycles). This is definitely remarkable for a fully organic electrode specifically conceived for application in NIBs.

At this stage of development, the Na_2BDA was demonstrated to be strongly affected by the selected liquid electrolyte, and its galvanostatic cycling behavior was demonstrated to be enhanced under high current regimes at ambient temperature, because the contact time with the liquid electrolyte is reduced, thus reducing the possibility to chemically react with the electrolyte components and get dissolved. In order to confirm this hypothesis, a very long-term (> 3500 cycles)

galvanostatic charge/discharge test was performed at 5C current rate on the Na_2BDA|1M NaFSI in EC:DEC 1:1|Na cell. The response of the cell in terms of specific capacity vs. cycle number is shown in Fig. 6.17.

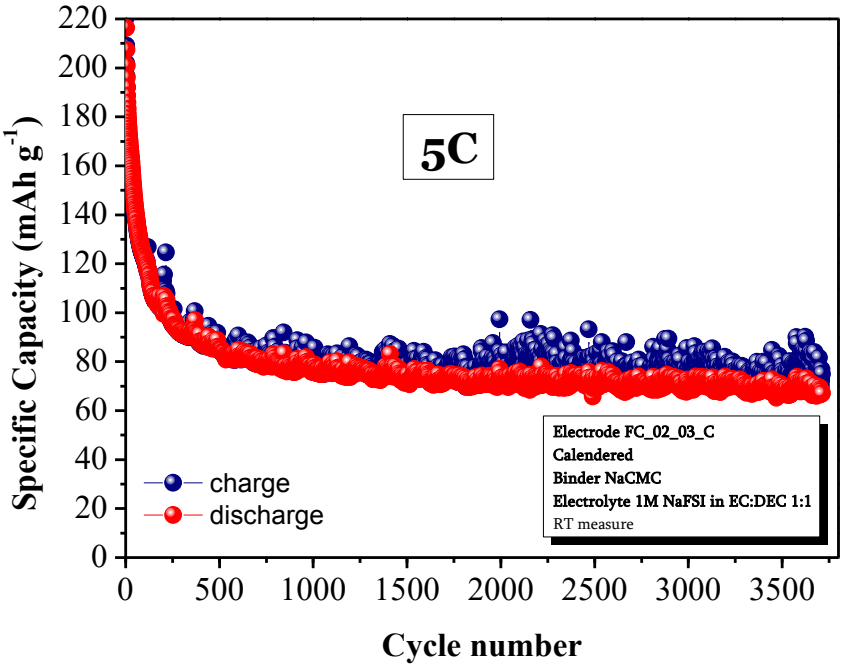

Fig. 6.17 Very long-term cycling performance at 5C (> 3500 cycles) of the calendered Na-CMC binded Na_2BDA composite electrode, namely FC_01_01_C, using 1M NaFSI in EC:DEC 1:1 electrolyte solution.

During the initial cycles, the typical irreversible capacity loss was observed. The Coulombic efficiency increased from 59 to 95 % after 5 cycles, reaching 98 % after 14 discharge/charge cycles and exceeding 99 % at the 50^{th} cycle, which indicates the overall good reversibility of the reduction/oxidation processes. in order to get a more deep insight in the long-term cycling behavior, Fig. 6.18 shows different portions of the measurement extracted at intervals of 100 cycles, namely 0 to 100 cycles in Fig. 6.18 A, 200 to 300 cycles in Fig. 6.18 B and 800 to 900 cycles in Fig. 6.18 C. As evidenced in Fig. 6.18 A, the specific capacity is not yet stabilized at a constant value after 100 cycles; a slight decrease in capacity is still evident in Fig. 6.18 B and, after 300 cycles the capacity reached 100 mAh g^{-1}. Cycle by cycle, the specific capacity monotonously decreased slightly but, after 900 cycles, the Na_2BDA|1M NaFSI in EC:DEC 1:1|Na cell demonstrated a truly stable cycling behavior at about 80 mAh g^{-1}.

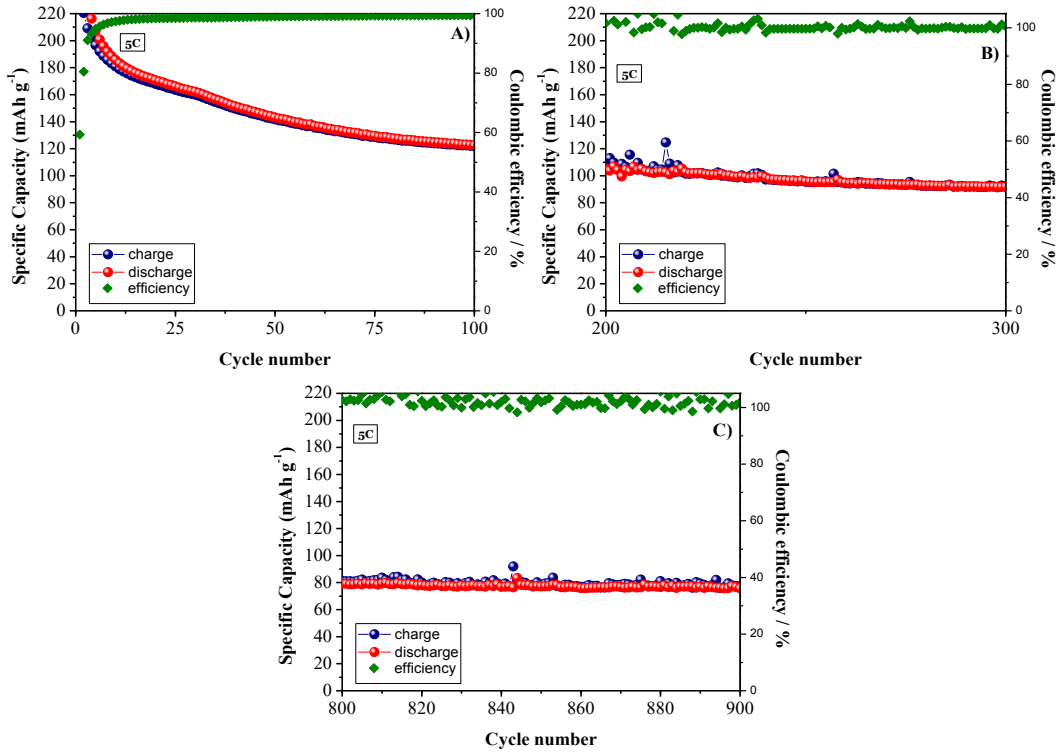

Fig. 6.18 Specific capacity vs. cycle number plots extracted at different intervals from the very long term galvanostatic charge/discharge cycling test: a) from 0 to 100 cycle, b) from cycle 200 to cycle 300, and c) from cycle 800 to cycle 900 when the cell stabilized its behavior at a specific capacity value of 80 mAh g^{-1}.

Fig. 6.19 shows the discharge/charge potential vs. specific capacity profiles, extracted from the very long-term cycling test at 5C rate. They clearly evidence that the cell demonstrated an outstanding capacity retention, with a very limited capacity fading below 10% from cycle 500 to cycle 3700, which is really outstanding for an organic electrode. It is also clear that the potential plateau underwent severe modification before cycle 500, which likely accounts for a structural modification of the material and is now under investigation.

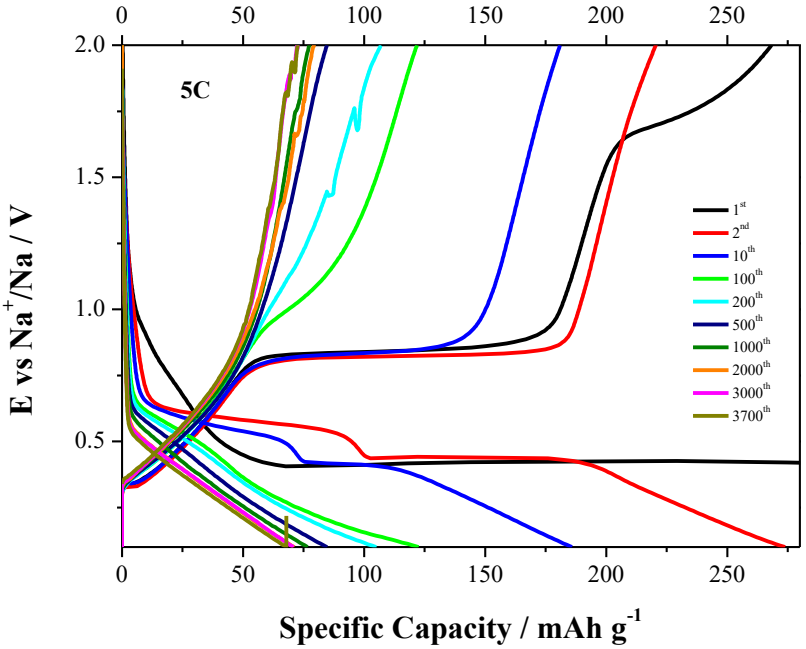

Fig. 6.19 Discharge/charge potential vs. specific capacity profiles extracted from the very long-term galvanostatic cycling test at 5C of the calendered Na_2BDA composite electrode.

This last measurement confirms the assumptions made, namely that the Na_2BDA is able to work at high current regime upon very long-term cycling. It is also confirmed that the contact time with the liquid electrolyte is detrimental for the cell performances, leading to dissolution of the organic material resulting in the decrease of the specific capacity delivered.

6.2.4 Conclusions

An organic battery electrode material, namely Na_2BDA, was synthesized, and its electrochemical behavior thoroughly studied in Na metal lab-scale cells. Different aspects of the electrode preparation as well as the cell assembly procedures were thoroughly investigated in order to have a comprehensive insight on the prospects of this material as potential new low-cost and stable Na-ion battery electrode. At first, the use of different binders (i.e., Na-CMC and PVdF) was investigated in terms of cyclic voltammetry (CV) and galvanostatic discharge/charge cycling. The composite electrode prepared with the aqueous binder Na-CMC demonstrated enhanced performance.

Then, the Na-CMC based electrode was subjected to a mechanical calendering step and compared with its non-calendered counterpart. It confirmed the beneficial effects of the calendering process, which enhanced the cohesion between the active material particles and also helped in preventing the severe dissolution of the material in the liquid electrolyte, that is one of the main drawbacks associated to the use of organic electrode materials in rechargeable batteries.

An extensive study of the cell performance in different liquid electrolyte solutions was also performed. This study lead to conclude that 1M NaFSI in EC:DEC 1:1 is the best liquid electrolyte solution among those investigated. The corresponding cell delivered a stable specific capacity of 90 mAh g^{-1} at C/4 current rate, with an almost ideal Coulombic efficiency after only 20 cycles.

The calendered Na-CMC based composite electrode was then assembled in Na metal test cell with the best liquid electrolyte formulation and subjected to a rate capability test up to very high 5C rate. Remarkably, it delivered good cycling performance at different current regimes, particularly at very high 5C rate, which proved the ability of Na_2BDA to be implemented in high power devices. It was also confirmed by a subsequent very long-term galvanostatic cycling test at 5C and ambient temperature, where the cell, after the initial "formation" steps, provided very stable cycling behavior for over 3700 cycles, with extremely limited capacity fading (final specific capacity around 70 mAh g^{-1}).

The results obtained demonstrated that, upon proper optimization of the solubility issue in common liquid electrolytes, the disodium benzenediacrylate can be effectively used as a "high current" electrode material in NIBs. Further efforts should be done on this way. One of the hypothesis is to switch on an all-solid-state polymeric configuration, by using some of the polymer electrolytes described in this PhD Thesis, which will prevent the dissolution of the organic material and should guarantee very stable cycling at improved specific capacity.

Concluding remarks

In the present global environmental emergency, which jeopardizes the future of our present society, it is truly mandatory to find an alternative to the non-renewable resources for mass energy production. The massive exploitation of renewable energy coming from Sun and wind is the most valuable solution. Clearly, renewable resources are discontinuous and require a high energy, low cost and safe energy storage system to be fully exploited. This goal can be achieved using rechargeable batteries, and lithium ion batteries represent the actual system of choice in this respect. As a result, in the last years the lithium demand grew extremely fast, which generated an increase of the prize of lithium metal. Sodium is the most suited alternative, due to its very similar characteristics to lithium. Moreover, the actual battery technology uses organic solvents with dissolved salts as electrolytes, which are toxic and volatile, and sometimes lead to undesirable events, such as battery failures and even explosions in the worst cases. The most effective alternative to fabricate safe devices is moving towards an all-solid configuration by developing suitable polymer electrolytes. High CO_2 production during battery manufacturing is rapidly emerging as another ecological issue, starting from the extraction of ores for the electrodes preparation, moving towards all the different steps of battery production, which are also very expensive in terms of energy consumption. Some research groups proposed the use of organic materials as valid alternative to commonly used inorganic electrodes; indeed, the production organic electrodes can directly start from the sequestration of CO_2 contained in the atmosphere and its relative conversion, thus resulting following the principles of circular economy.

Taking into account the abovementioned scenario, and the challenges and expectations particularly for large-scale energy storage devices in the near future, the target of this PhD Thesis was the study and the development of novel polymer electrolytes and organic electrodes to fabricate high energy, safe and ecofriendly sodium-ion batteries.

The experimental research work started from the development of different polymer electrolytes following a precise path towards the realization of highly conducting, safe systems for ambient temperature application. At first, a polymer electrolyte was prepared by simple casting procedure, using poly(ethylene oxide) - PEO blended with sodium carboxymethyl cellulose (Na-CMC) and sodium perchlorate. The results obtained demonstrated the possibility to use a solid polymer

blend, prepared by a very simple, fast, low cost and green aqueous procedure. The cellulose derivative was selected to improve the mechanical features of the final membrane. The electrochemical behavior in Na-metal cells was successfully demonstrated with different working electrodes (TiO_2 and $NaFePO_4$), confirming the possibility to use this PEO-based polymer electrolyte in lab-scale sodium battery prototypes at moderate temperatures.

The following steps of my research work were devoted to the development of crosslinked systems by means of free-radical photopolymerization (UV-curing), which is widely used in different industrial fields (e.g, inks, coatings, etc.) and can be easily employed for the preparation of different kinds of polymer electrolytes (SPEs, GPEs, CPEs) in a single step, without the use of any solvent, thus being rapid, sustainable and ecofriendly. A highly crosslinked methacrylic-based polymer (BEMA-PEGMA) electrolyte was firstly prepared. It exhibited good thermal characteristics, high ionic conductivity at ambient temperature, and wide electrochemical stability window. In a second stage of development, profoundly ion-conducting, self-standing, and tack-free ethylene oxide-based crosslinked polymer electrolytes intimately encompassing a fixed amount of cyclic carbonate and sodium salt were successfully prepared via a rapid and easily up scalable process including a UV irradiation step. They were thoroughly characterized in terms of their physical, chemical, and morphological properties and intimate electrode/electrolyte interfacial characteristics. The novel PEO-based crosslinked truly quasi-solid electrolytes showed very high ionic conductivity (1 mS cm^{-1} at 25 °C) and very wide electrochemical stability window (4.7 V vs Na^+/Na). Both the photopolymer electrolytes were tested for their reversible constant charge/discharge behaviour in lab-scale Na metal cells using nanosized commercial TiO_2 as working electrode. The BEMA-PEGMA photopolymer electrolyte showed a reasonably high specific capacity and rate capability upon prolonged cycling (250 cycles) at ambient temperature. The cells assembled with the crosslinked PEO-based electrolyte delivered a stable specific capacity of 250 mAh g^{-1} at ambient temperature and demonstrated to be very stable upon prolonged galvanostatic cycling at 0.1 mA cm^{-2} for more than 6 months of continuous operation. The reported results enlightened the promising prospects of the materials to be successfully implemented as stable, durable, and efficient electrolytes in the next-generation of large-scale energy storage devices from renewables, with very promising industriability prospects thanks to the use of UV-induced radical polymerization.

The final part of my three years PhD thesis work was focused on the development and electrochemical characterization of a carboxylate organic electrode for NIBs, the disodium benzenediacrylate (Na_2BDA). The material was synthesized and optimized during a 5 months' stage of research at the Ångströmlaboratoriet of Prof. Daniel Brandell at the Uppsala University, Sweden. The main target was to find the most suited liquid electrolyte to exploit the full potential of the material. Such a study is fundamental particularly for organic electrodes, due to their high solubility in liquid electrolyte media, which always leads to rapid decay in electrochemical performances. The higher specific capacity and better capacity retention was obtained with the 1M NaFSI in EC:DEC 1:1 electrolyte solution that was then employed for further studies. The use of different (aqueous Na-CMC and non-aqueous PVdF) binders was also investigated during electrode preparation in order to understand if the cell performances are affected to the composite electrode formulation. The Na-based cells assembled with the Na-CMC binded electrodes ensured a more efficient cohesiveness of the active material particles, particularly after proper mechanical calendering, thus allowing enhanced electrochemical behaviour as confirmed by cyclic voltammetry and higher specific capacity output. The electrochemical study was also extended to severe rate capability test at ambient temperature as well as very long-term constant current cycling up to 5C current rate. The results obtained confirmed the solubility of Na_2BDA in common liquid electrolytes, especially for prolonged contact time when cycling at low C-rates; however, such issue was definitely mitigated in the present work by using calendered Na-CMC based electrodes and cycling at very high C-rates. This allowed very long-term stability of the newly developed organic electrode as demonstrated by the very stable capacity output in Na metal cell upon prolonged constant current discharge/charge cycling for over 3700 cycles at ambient temperature.

Summarizing, the promising prospects of practical application of safe and ecofriendly polymer electrolytes in sodium based rechargeable batteries was effectively demonstrated. This is particularly effective when exploiting UV-induced photopolymerization that, compared to other techniques, is highly advantageous due to its easiness, amenability, eco friendliness, energy efficiency and rapidity in processing, thus easily scalable to the industrial level. Moreover, organic materials were successfully demonstrated as valid alternatives to common inorganic electrodes in NIBs, especially when the severe solubility issues in common liquid electrolytes are prevented. To my knowledge, the best alternative is represented by polymer electrolytes, which should avoid the solubility issue, also

providing a series of other appealing characteristics, such as safety, eco-compatibility, and easiness in design.

Appendix A

List of Figures

List of Tables

Appendix B

OPEN CIRCUIT VOLTAGE (OCV) = is the potential difference across the terminals of the battery when no current is being drawn:

$$V_{OC} = -\frac{1}{nF} \cdot (\mu_A - \mu_C)$$

where (μ_A - μ_C) is the difference in the electro-chemical potential of the anode and the cathode.

CAPACITY (Q) = total amount of electric charge supplied by the system or by the electrode materials and it is usually expressed in terms of Coulomb (C) or Ampere hour (Ah); 1 Ah = 3600 C. It can be calculated as the product of the current by the time:

$$Q = i \cdot t$$

SPECIFIC CAPACITY = capacity per unit mass (Ah g^{-1}) or per unit volume (Ah dm^{-3}).

THEORETICAL CAPACITY (Q_t) = maximum amount of charge that can be extracted from a battery with respect of the amount of active material it contains and it can be calculated as follows:

$$Q_t = x \cdot n \cdot F$$

where x is the amount of active material in moles, n are the equivalents exchanged and F is the Faraday constant.

CHARGE EFFICIENCY (Y) (or COULOMBIC EFFICIENCY) = percent ratio of capacity supplied in discharge (Q_d) and capacity accumulated during the previous charge (Q_c):

$$Y\ (\%) = \frac{Q_d}{Q_c} \cdot 100$$

C-RATE = measures the applied current to charge or discharge a battery; it is expressed in fractions or multiples of C. A C-rate of 1C corresponds to the current required to fully discharge a battery in 1 hour, 0.5C or C/2 refers to the current to discharge in two hours and 2C to discharge in half an hour.

ENERGY (E) = is the amount of energy which an electrochemical power source can supply, expressed in Joule (J) or more commonly in Watt hour (Wh), is related to the capacity through the equation:

$$E = Q \cdot V$$

where V is the average operating potential delivered by the system.

SPECIFIC ENERGY (or usually **ENERGY DENSITY**) = energy output from a battery per unit mass (Wh g^{-1}) or per unit volume (Wh dm^{-3}). From the energy and the theoretical capacity equations, derive the equation:

$$E_t = \int_0^{Q_d} V_{(q)} \cdot dq \cong x \cdot n \cdot F \cdot \bar{V}$$

where V(q) is the working potential expressed as a function of the supplied electric charge q.

POWER (P) = delivered by a material or a power source is defined as the average working potential multiplied by the flowing current:

$$P = I \cdot \bar{V} = \frac{Q \cdot \bar{V}}{t} = \frac{E}{t}$$

The theoretical power can be obtained from the specific energy and the power as follows:

$$P_t = \frac{\int_0^{Q_d} V_{(q)}\, dq}{t_d} = \frac{x \cdot n \cdot F \cdot \bar{V}}{t_d}$$

where t_d is the time to fully discharge. It can be expressed for unit mass (W Kg^{-1}) or per unit volume (W dm^{-3}).

PASSIVATION = formation of a surface layer which impedes the electrochemical reactions at the electrodes.

CYCLE LIFE = measure of the ability of a secondary battery to withstand subsequent charge/discharge cycles. It usually describes the number of charge/discharge cycles that give rise in a battery to the capacity fade at a fixed

percentage of the original capacity (usually 80%). The cycle life depends on the working conditions, e.g. charge/discharge rate.

SHELF LIFE = period of time over which a battery can be stored and it still meets specified performance criteria without significant deterioration.

SELF-DISCHARGE = loss of capacity of a battery under opencircuit conditions as a result of internal chemical reactions and/or short-circuits

References

[1] D. Larcher and J-M. Tarascon, ‘Towards greener and more sustainable batteries for electrical energy storage’, *Nat. Chem.*, vol. 7, no. 1, pp. 19–29, Nov. 2014.

[2] E. M. Erickson *et al.*, ‘Development of advanced rechargeable batteries: a continuous challenge in the choice of suitable electrolyte solutions’, *J. Electrochem. Soc.*, vol. 162, no. 14, pp. A2424–A2438, 2015.

[3] Z. Yang *et al.*, ‘Electrochemical Energy Storage for Green Grid’, *Chem. Rev.*, vol. 111, no. 5, pp. 3577–3613, May 2011.

[4] V. Palomares, P. Serras, I. Villaluenga, K. B. Hueso, J. Carretero-González, and T. Rojo, ‘Na-ion batteries, recent advances and present challenges to become low cost energy storage systems’, *Energy Environ. Sci.*, vol. 5, no. 3, p. 5884, 2012.

[5] P. Poizot and F. Dolhem, ‘Clean energy new deal for a sustainable world: from non-CO_2 generating energy sources to greener electrochemical storage devices’, *Energy Environ. Sci.*, vol. 4, no. 6, p. 2003, 2011.

[6] International Energy Agency, ‘TheFutureofTrucksImplicationsforEnergyandtheEnvironment.pdf’. 2017.

[7] International Energy Agency, ‘TrackingCleanEnergyProgress2017.pdf’. 2017.

[8] J.-M. Tarascon and M. Armand, ‘Issues and challenges facing rechargeable lithium batteries’, *Nature*, vol. 414, no. 6861, pp. 359–367, 2001.

[9] B. Dunn and H. Kamath, ‘Electrical energy storage for the grid: a battery of choices’, *Science*, vol. 334, no. 6058, pp. 928–935, 2011.

[10] M. Pasta *et al.*, ‘Full open-framework batteries for stationary energy storage’, *Nat. Commun.*, vol. 5, Jan. 2014.

[11] EPRI (Electric Power Research Institute, ‘Electricity Energy Storage Technology Options’. 2010.

[12] R. Van Noorden, ‘A better battery’, *Nature*, vol. 507, no. 7490, p. 26, 2014.

[13] H. Vikström, S. Davidsson, and M. Höök, ‘Lithium availability and future production outlooks’, *Appl. Energy*, vol. 110, pp. 252–266, Oct. 2013.

[14] S Erturk, I Boztosun, Y Kucuk, M Karakoc, and S Aydin, ‘Failure of the standard coupled-channels method in describing inelastic reaction data: on

the use of a new shape for the coupling potential', *J. Phys. G Nucl. Part. Phys.*, vol. 31, pp. s1837–s1842, 2005.

[15] L. Oliveira, M. Messagie, S. Rangaraju, J. Sanfelix, M. Hernandez Rivas, and J. Van Mierlo, 'Key issues of lithium-ion batteries – from resource depletion to environmental performance indicators', *J. Clean. Prod.*, vol. 108, pp. 354–362, Dec. 2015.

[16] J.-M. Tarascon, 'Is lithium the new gold?', *Nat. Chem.*, vol. 2, no. 6, pp. 510–510, 2010.

[17] D. Kundu, E. Talaie, V. Duffort, and L. F. Nazar, 'The Emerging Chemistry of Sodium Ion Batteries for Electrochemical Energy Storage', *Angew. Chem. Int. Ed.*, vol. 54, no. 11, pp. 3431–3448, Mar. 2015.

[18] B. L. Ellis and L. F. Nazar, 'Sodium and sodium-ion energy storage batteries', *Curr. Opin. Solid State Mater. Sci.*, vol. 16, no. 4, pp. 168–177, Aug. 2012.

[19] D. Linden and T. B. Reddy, Eds., *Handbook of batteries*, 3rd ed. New York: McGraw-Hill, 2002.

[20] N. Yabuuchi, K. Kubota, M. Dahbi, and S. Komaba, 'Research Development on Sodium-Ion Batteries', *Chem. Rev.*, vol. 114, no. 23, pp. 11636–11682, Dec. 2014.

[21] Q. Ni, Y. Bai, F. Wu, and C. Wu, 'Polyanion-Type Electrode Materials for Sodium-Ion Batteries', *Adv. Sci.*, vol. 4, no. 3, p. 1600275, Mar. 2017.

[22] M. D. Tikekar, S. Choudhury, Z. Tu, and L. A. Archer, 'Design principles for electrolytes and interfaces for stable lithium-metal batteries', *Nat. Energy*, vol. 1, no. 9, p. 16114, Sep. 2016.

[23] Z. Tu, P. Nath, Y. Lu, M. D. Tikekar, and L. A. Archer, 'Nanostructured Electrolytes for Stable Lithium Electrodeposition in Secondary Batteries', *Acc. Chem. Res.*, vol. 48, no. 11, pp. 2947–2956, Nov. 2015.

[24] S. Choudhury *et al.*, 'Designing solid-liquid interphases for sodium batteries', *Nat. Commun.*, vol. 8, no. 1, Dec. 2017.

[25] A. Agrawal, S. Choudhury, and L. A. Archer, 'A highly conductive, non-flammable polymer–nanoparticle hybrid electrolyte', *RSC Adv.*, vol. 5, no. 27, pp. 20800–20809, 2015.

[26] S. Choudhury, R. Mangal, A. Agrawal, and L. A. Archer, 'A highly reversible room-temperature lithium metal battery based on crosslinked hairy nanoparticles', *Nat. Commun.*, vol. 6, p. 10101, Dec. 2015.

[27] D. H. C. Wong *et al.*, 'Nonflammable perfluoropolyether-based electrolytes for lithium batteries', *Proc. Natl. Acad. Sci.*, vol. 111, no. 9, pp. 3327–3331, Mar. 2014.

[28] H. Wu *et al.*, 'Stable Li-ion battery anodes by in-situ polymerization of conducting hydrogel to conformally coat silicon nanoparticles', *Nat. Commun.*, vol. 4, Jun. 2013.

[29] G. Zheng *et al.*, 'Interconnected hollow carbon nanospheres for stable lithium metal anodes', *Nat. Nanotechnol.*, vol. 9, no. 8, pp. 618–623, Jul. 2014.

[30] Z. W. Seh, J. Sun, Y. Sun, and Y. Cui, 'A Highly Reversible Room-Temperature Sodium Metal Anode', *ACS Cent. Sci.*, vol. 1, no. 8, pp. 449–455, Nov. 2015.

[31] S. Wei *et al.*, 'A stable room-temperature sodium–sulfur battery', *Nat. Commun.*, vol. 7, p. 11722, Jun. 2016.

[32] H. Pan, Y.-S. Hu, and L. Chen, 'Room-temperature stationary sodium-ion batteries for large-scale electric energy storage', *Energy Environ. Sci.*, vol. 6, no. 8, p. 2338, 2013.

[33] H. Moriwake, A. Kuwabara, C. A. J. Fisher, and Y. Ikuhara, 'Why is sodium-intercalated graphite unstable?', *RSC Adv.*, vol. 7, no. 58, pp. 36550–36554, 2017.

[34] J. Maibach, F. Jeschull, D. Brandell, K. Edström, and M. Valvo, 'Surface Layer Evolution on Graphite During Electrochemical Sodium-tetraglyme Co-intercalation', *ACS Appl. Mater. Interfaces*, vol. 9, no. 14, pp. 12373–12381, Apr. 2017.

[35] H. Kim, J. Hong, Y.-U. Park, J. Kim, I. Hwang, and K. Kang, 'Sodium Storage Behavior in Natural Graphite using Ether-based Electrolyte Systems', *Adv. Funct. Mater.*, vol. 25, no. 4, pp. 534–541, Jan. 2015.

[36] B. Jache and P. Adelhelm, 'Use of Graphite as a Highly Reversible Electrode with Superior Cycle Life for Sodium-Ion Batteries by Making Use of Co-Intercalation Phenomena', *Angew. Chem. Int. Ed.*, vol. 53, no. 38, pp. 10169–10173, Sep. 2014.

[37] M. M. Doeff, Y. Ma, S. J. Visco, and L. C. De Jonghe, 'Electrochemical insertion of sodium into carbon', *J. Electrochem. Soc.*, vol. 140, no. 12, pp. L169–L170, 1993.

[38] D. A. Stevens and J. R. Dahn, 'High Capacity Anode Materials for Rechargeable Sodium-Ion Batteries', *J. Electrochem. Soc.*, vol. 147, no. 4, pp. 1271–1273, 2000.

[39] H. Kang *et al.*, 'Update on anode materials for Na-ion batteries', *J. Mater. Chem. A*, vol. 3, no. 35, pp. 17899–17913, 2015.

[40] S. Komaba *et al.*, 'Electrochemical Na Insertion and Solid Electrolyte Interphase for Hard-Carbon Electrodes and Application to Na-Ion Batteries', *Adv. Funct. Mater.*, vol. 21, no. 20, pp. 3859–3867, Oct. 2011.

[41] J. Hu, B. Xu, S. A. Yang, S. Guan, C. Ouyang, and Y. Yao, '2D Electrides as Promising Anode Materials for Na-Ion Batteries from First-Principles Study', *ACS Appl. Mater. Interfaces*, vol. 7, no. 43, pp. 24016–24022, Nov. 2015.

[42] F. Bella, A. Lamberti, A. Sacco, S. Bianco, A. Chiodoni, and R. Bongiovanni, 'Novel electrode and electrolyte membranes: Towards flexible dye-sensitized solar cell combining vertically aligned TiO_2 nanotube array and light-cured polymer network', *J. Membr. Sci.*, vol. 470, pp. 125–131, Nov. 2014.

[43] J. P. Huang *et al.*, 'Electrochemical sodium storage of TiO_2 (B) nanotubes for sodium ion batteries', *Rsc Adv.*, vol. 3, no. 31, pp. 12593–12597, 2013.

[44] F. Bella *et al.*, 'Unveiling the controversial mechanism of reversible Na storage in TiO_2 nanotube arrays: Amorphous versus anatase TiO_2', *Nano Res.*, vol. 10, no. 8, pp. 2891–2903, Aug. 2017.

[45] R. Alcántara, M. Jaraba, P. Lavela, and J. L. Tirado, '$NiCo_2O_4$ Spinel: First Report on a Transition Metal Oxide for the Negative Electrode of Sodium-Ion Batteries', *Chem. Mater.*, vol. 14, no. 7, pp. 2847–2848, Jul. 2002.

[46] Q. Sun, Q.-Q. Ren, H. Li, and Z.-W. Fu, 'High capacity Sb_2O_4 thin film electrodes for rechargeable sodium battery', *Electrochem. Commun.*, vol. 13, no. 12, pp. 1462–1464, Dec. 2011.

[47] X. Lu *et al.*, 'Germanium as a Sodium Ion Battery Material: *In Situ* TEM Reveals Fast Sodiation Kinetics with High Capacity', *Chem. Mater.*, vol. 28, no. 4, pp. 1236–1242, Feb. 2016.

[48] B. Farbod *et al.*, 'Anodes for Sodium Ion Batteries Based on Tin–Germanium–Antimony Alloys', *ACS Nano*, vol. 8, no. 5, pp. 4415–4429, May 2014.

[49] A. Darwiche, C. Marino, M. T. Sougrati, B. Fraisse, L. Stievano, and L. Monconduit, 'Better Cycling Performances of Bulk Sb in Na-Ion Batteries Compared to Li-Ion Systems: An Unexpected Electrochemical Mechanism', *J. Am. Chem. Soc.*, vol. 134, no. 51, pp. 20805–20811, Dec. 2012.

[50] J. W. Wang, X. H. Liu, S. X. Mao, and J. Y. Huang, 'Microstructural Evolution of Tin Nanoparticles during In Situ Sodium Insertion and Extraction', *Nano Lett.*, vol. 12, no. 11, pp. 5897–5902, Nov. 2012.

[51] A. Ponrouch, D. Monti, A. Boschin, B. Steen, P. Johansson, and M. R. Palacín, 'Non-aqueous electrolytes for sodium-ion batteries', *J. Mater. Chem. A*, vol. 3, no. 1, pp. 22–42, 2015.

[52] C. Delmas, C. Fouassier, and P. Hagenmuller, 'Structural classification and properties of the layered oxides', *Phys. B C*, vol. 99, no. 1–4, pp. 81–85, 1980.

[53] N. Yabuuchi and S. Komaba, ‘Recent research progress on iron- and manganese-based positive electrode materials for rechargeable sodium batteries’, *Sci. Technol. Adv. Mater.*, vol. 15, no. 4, p. 043501, Aug. 2014.

[54] V. L. Chevrier and G. Ceder, ‘Challenges for Na-ion negative electrodes’, *J. Electrochem. Soc.*, vol. 158, no. 9, pp. A1011–A1014, 2011.

[55] E. Lee *et al.*, ‘New Insights into the Performance Degradation of Fe-Based Layered Oxides in Sodium-Ion Batteries: Instability of Fe^{3+}/Fe^{4+} Redox in α-$NaFeO_2$’, *Chem. Mater.*, vol. 27, no. 19, pp. 6755–6764, Oct. 2015.

[56] A. Sun *et al.*, ‘Synthesis, characterization, and electrochemical studies of chemically synthesized $NaFePO_4$’, *Mater. Sci. Eng. B*, vol. 177, no. 20, pp. 1729–1733, Dec. 2012.

[57] M. Avdeev *et al.*, ‘Magnetic Structures of $NaFePO_4$ Maricite and Triphylite Polymorphs for Sodium-Ion Batteries’, *Inorg. Chem.*, vol. 52, no. 15, pp. 8685–8693, Aug. 2013.

[58] P. Moreau, D. Guyomard, J. Gaubicher, and F. Boucher, ‘Structure and Stability of Sodium Intercalated Phases in Olivine $FePO_4$’, *Chem. Mater.*, vol. 22, no. 14, pp. 4126–4128, Jul. 2010.

[59] I. Hasa, J. Hassoun, Y.-K. Sun, and B. Scrosati, ‘Sodium-Ion Battery based on an Electrochemically Converted $NaFePO_4$ Cathode and Nanostructured Tin-Carbon Anode’, *ChemPhysChem*, vol. 15, no. 10, pp. 2152–2155, Jul. 2014.

[60] V. Palomares, M. Casas-Cabanas, E. Castillo-Martínez, M. H. Han, and T. Rojo, ‘Update on Na-based battery materials. A growing research path’, *Energy Environ. Sci.*, vol. 6, no. 8, p. 2312, 2013.

[61] M. H. Han, E. Gonzalo, G. Singh, and T. Rojo, ‘A comprehensive review of sodium layered oxides: powerful cathodes for Na-ion batteries’, *Energy Environ. Sci.*, vol. 8, no. 1, pp. 81–102, 2015.

[62] J. E. Weston and B. C. H. Steele, ‘Effects of inert fillers on the mechanical and electrochemical properties of lithium salt-poly (ethylene oxide) polymer electrolytes’, *Solid State Ion.*, vol. 7, no. 1, pp. 75–79, 1982.

[63] A. Bhide, J. Hofmann, A. Katharina Dürr, J. Janek, and P. Adelhelm, ‘Electrochemical stability of non-aqueous electrolytes for sodium-ion batteries and their compatibility with $Na_{0.7}CoO_2$’, *Phys Chem Chem Phys*, vol. 16, no. 5, pp. 1987–1998, 2014.

[64] G. G. Eshetu *et al.*, ‘Comprehensive Insights into the Reactivity of Electrolytes Based on Sodium Ions’, *ChemSusChem*, vol. 9, no. 5, pp. 462–471, Mar. 2016.

[65] J. Chen *et al.*, 'Sodium-difluoro(oxalato)borate (NaDFOB): a new electrolyte salt for Na-ion batteries', *Chem. Commun.*, vol. 51, no. 48, pp. 9809–9812, 2015.

[66] A. Plewa-Marczewska *et al.*, 'New Tailored Sodium Salts for Battery Applications', *Chem. Mater.*, vol. 26, no. 17, pp. 4908–4914, Sep. 2014.

[67] D. I. Iermakova, R. Dugas, M. R. Palacín, and A. Ponrouch, 'On the comparative stability of Li and Na metal anode interfaces in conventional alkyl carbonate electrolytes', *J. Electrochem. Soc.*, vol. 162, no. 13, pp. A7060–A7066, 2015.

[68] Snehashis Choudhury *et al.*, 'Designing solid-liquid interphases for sodium batteries', *Nat. Commun.*, vol. 8, no. 1, Dec. 2017.

[69] L. G. Chagas, D. Buchholz, L. Wu, B. Vortmann, and S. Passerini, 'Unexpected performance of layered sodium-ion cathode material in ionic liquid-based electrolyte', *J. Power Sources*, vol. 247, pp. 377–383, Feb. 2014.

[70] I. Hasa, S. Passerini, and J. Hassoun, 'Characteristics of an ionic liquid electrolyte for sodium-ion batteries', *J. Power Sources*, vol. 303, pp. 203–207, Jan. 2016.

[71] R.-S. Kühnel, M. Lübke, M. Winter, S. Passerini, and A. Balducci, 'Suppression of aluminum current collector corrosion in ionic liquid containing electrolytes', *J. Power Sources*, vol. 214, pp. 178–184, Sep. 2012.

[72] S. S. Zhang, 'A review on electrolyte additives for lithium-ion batteries', *J. Power Sources*, vol. 162, no. 2, pp. 1379–1394, Nov. 2006.

[73] S. Komaba, T. Ishikawa, N. Yabuuchi, W. Murata, A. Ito, and Y. Ohsawa, 'Fluorinated Ethylene Carbonate as Electrolyte Additive for Rechargeable Na Batteries', *ACS Appl. Mater. Interfaces*, vol. 3, no. 11, pp. 4165–4168, Nov. 2011.

[74] R. Dugas, A. Ponrouch, G. Gachot, R. David, M. R. Palacin, and J. M. Tarascon, 'Na Reactivity toward Carbonate-Based Electrolytes: The Effect of FEC as Additive', *J. Electrochem. Soc.*, vol. 163, no. 10, pp. A2333–A2339, 2016.

[75] S. F. Lux, F. Schappacher, A. Balducci, S. Passerini, and M. Winter, 'Low cost, environmentally benign binders for lithium-ion batteries', *J. Electrochem. Soc.*, vol. 157, no. 3, pp. A320–A325, 2010.

[76] N. Yabuuchi, K. Kubota, M. Dahbi, and S. Komaba, 'Research Development on Sodium-Ion Batteries', *Chem. Rev.*, vol. 114, no. 23, pp. 11636–11682, Dec. 2014.

[77] V. Palomares, M. Casas-Cabanas, E. Castillo-Martínez, M. H. Han, and T. Rojo, 'Update on Na-based battery materials. A growing research path', *Energy Environ. Sci.*, vol. 6, no. 8, p. 2312, 2013.

[78] I. Kovalenko *et al.*, 'A Major Constituent of Brown Algae for Use in High-Capacity Li-Ion Batteries', *Science*, vol. 334, no. 6052, pp. 75–79, Oct. 2011.

[79] S. Komaba *et al.*, 'Comparative Study of Sodium Polyacrylate and Poly(vinylidene fluoride) as Binders for High Capacity Si–Graphite Composite Negative Electrodes in Li-Ion Batteries', *J. Phys. Chem. C*, vol. 116, no. 1, pp. 1380–1389, Jan. 2012.

[80] A. Magasinski *et al.*, 'Toward Efficient Binders for Li-Ion Battery Si-Based Anodes: Polyacrylic Acid', *ACS Appl. Mater. Interfaces*, vol. 2, no. 11, pp. 3004–3010, Nov. 2010.

[81] J. Song, Z. Yu, M. L. Gordin, X. Li, H. Peng, and D. Wang, 'Advanced Sodium Ion Battery Anode Constructed *via* Chemical Bonding between Phosphorus, Carbon Nanotube, and Cross-Linked Polymer Binder', *ACS Nano*, vol. 9, no. 12, pp. 11933–11941, Dec. 2015.

[82] J.-Y. Hwang, S.-T. Myung, and Y.-K. Sun, 'Sodium-ion batteries: present and future', *Chem. Soc. Rev.*, vol. 46, no. 12, pp. 3529–3614, 2017.

[83] P. Arora and Z. (John) Zhang, 'Battery Separators', *Chem. Rev.*, vol. 104, no. 10, pp. 4419–4462, Oct. 2004.

[84] M. J. Martínez, S. Shimpalee, and J. W. Van Zee, 'Measurement of MacMullin Numbers for PEMFC Gas-Diffusion Media', *J. Electrochem. Soc.*, vol. 156, no. 1, p. B80, 2009.

[85] R. Marcilla, F. Alcaide, H. Sardon, J. A. Pomposo, C. Pozo-Gonzalo, and D. Mecerreyes, 'Tailor-made polymer electrolytes based upon ionic liquids and their application in all-plastic electrochromic devices', *Electrochem. Commun.*, vol. 8, no. 3, pp. 482–488, Mar. 2006.

[86] M. Watanabe and N. Ogata, 'Ionic conductivity of polymer electrolytes and future applications', *Polym. Int.*, vol. 20, no. 3, pp. 181–192, 1988.

[87] C. G. Granqvist *et al.*, 'Recent advances in electrochromics for smart windows applications', *Sol. Energy*, vol. 63, no. 4, pp. 199–216, 1998.

[88] B. Scrosati, Ed., *Applications of Electroactive Polymers*. Dordrecht: Springer Netherlands, 1993.

[89] Y.-F. Y. YAO and J. T. KUMMER, 'ION EXCHANGE PROPERTIES OF AND RATES OF IONIC DIFFUSION IN BETA-ALUMINA', *J. inorg, nucl. Chem*, vol. 29, pp. 2453–2475, 1967.

[90] D. Baril, C. Michot, and M. Armand, 'Electrochemistry of liquids vs. solids: polymer electrolytes', *Solid State Ion.*, vol. 94, no. 1–4, pp. 35–47, 1997.

[91] A. F. Diaz, K. K. Kanazawa, and G. P. Gardini, 'Electrochemical polymerization of pyrrole', *J. Chem. Soc. Chem. Commun.*, no. 14, p. 635, 1979.

[92] D. E. Fenton, J. M. Parker, and P. V. Wright, 'Complexes of alkali metal ions with poly (ethylene oxide)', *polymer*, vol. 14, no. 11, p. 589, 1973.

[93] M. B. Armand, 'Polymer electrolytes', *Annu. Rev. Mater. Sci.*, vol. 16, no. 1, pp. 245–261, 1986.

[94] C. Berthier, W. Gorecki, M. Minier, M. B. Armand, J. M. Chabagno, and P. Rigaud, 'Microscopic investigation of ionic conductivity in alkali metal salts-poly (ethylene oxide) adducts', *Solid State Ion.*, vol. 11, no. 1, pp. 91–95, 1983.

[95] J. L. Souquet, 'Ionic Transport in Amorphous Solid Electrolytes', *Annu. Rev. Mater. Sci.*, vol. 11, no. 1, pp. 211–231, Aug. 1981.

[96] C. Zhang, S. Gamble, D. Ainsworth, A. M. Z. Slawin, Y. G. Andreev, and P. G. Bruce, 'Alkali metal crystalline polymer electrolytes', *Nat. Mater.*, vol. 8, no. 7, pp. 580–584, Jul. 2009.

[97] K. Terabe, T. Hasegawa, T. Nakayama, and M. Aono, 'Quantized conductance atomic switch', *Nature*, vol. 433, no. 7021, pp. 47–50, Jan. 2005.

[98] K. West, B. Zachau-Christiansen, T. Jacobsen, and S. Atlung, 'A rechargeable all-solid-state sodium cell with polymer electrolyte', *Electrochem. Soc. J.*, vol. 132, no. 12, pp. 3061–3062, 1985.

[99] K. West, B. Zachau-Christiansen, T. Jacobsen, E. Hiort-Lorenzen, and S. Skaarup, 'Poly (ethylene oxide)-sodium perchlorate electrolytes in solid-state sodium cells', *Polym. Int.*, vol. 20, no. 3, pp. 243–246, 1988.

[100] S. A. Hashmi and S. Chandra, 'Experimental investigations on a sodium-ion-conducting polymer electrolyte based on poly (ethylene oxide) complexed with $NaPF_6$', *Mater. Sci. Eng. B*, vol. 34, no. 1, pp. 18–26, 1995.

[101] J. Serra Moreno, M. Armand, M. B. Berman, S. G. Greenbaum, B. Scrosati, and S. Panero, 'Composite PEOn:NaTFSI polymer electrolyte: Preparation, thermal and electrochemical characterization', *J. Power Sources*, vol. 248, pp. 695–702, Feb. 2014.

[102] A. Boschin and P. Johansson, 'Characterization of NaX (X: TFSI, FSI) – PEO based solid polymer electrolytes for sodium batteries', *Electrochimica Acta*, vol. 175, pp. 124–133, Sep. 2015.

[103] A. Boschin, M. E. Abdelhamid, and P. Johansson, 'On the Feasibility of Sodium Metal as Pseudo-Reference Electrode in Solid State Electrochemical Cells', *ChemElectroChem*, vol. 4, no. 10, pp. 2717–2721, Oct. 2017.

[104] X. Qi *et al.*, 'Sodium Bis(fluorosulfonyl)imide/Poly(ethylene oxide) Polymer Electrolytes for Sodium-Ion Batteries', *ChemElectroChem*, vol. 3, no. 11, pp. 1741–1745, Nov. 2016.

[105] O. Buriez *et al.*, 'Performance limitations of polymer electrolytes based on ethylene oxide polymers', *J. Power Sources*, vol. 89, no. 2, pp. 149–155, 2000.

[106] J. Mindemark, E. Törmä, B. Sun, and D. Brandell, 'Copolymers of trimethylene carbonate and ε-caprolactone as electrolytes for lithium-ion batteries', *Polymer*, vol. 63, pp. 91–98, Apr. 2015.

[107] B. Sun, J. Mindemark, K. Edström, and D. Brandell, 'Realization of high performance polycarbonate-based Li polymer batteries', *Electrochem. Commun.*, vol. 52, pp. 71–74, Mar. 2015.

[108] J. Mindemark, L. Imholt, J. Montero, and D. Brandell, 'Allyl ethers as combined plasticizing and crosslinkable side groups in polycarbonate-based polymer electrolytes for solid-state Li batteries', *J. Polym. Sci. Part Polym. Chem.*, vol. 54, no. 14, pp. 2128–2135, Jul. 2016.

[109] J. Mindemark, R. Mogensen, M. J. Smith, M. M. Silva, and D. Brandell, 'Polycarbonates as alternative electrolyte host materials for solid-state sodium batteries', *Electrochem. Commun.*, vol. 77, pp. 58–61, Apr. 2017.

[110] G. B. Appetecchi, F. Croce, P. Romagnoli, B. Scrosati, U. Heider, and R. Oesten, 'High-performance gel-type lithium electrolyte membranes', *Electrochem. Commun.*, vol. 1, no. 2, pp. 83–86, 1999.

[111] M. Watanabe, M. Kanba, K. Nagaoka, and I. Shinohara, 'Ionic conductivity of hybrid films based on polyacrylonitrile and their battery application', *J. Appl. Polym. Sci.*, vol. 27, no. 11, pp. 4191–4198, 1982.

[112] H. Hong, C. Liquan, H. Xuejie, and X. Rongjian, 'Studies on PAN-based lithium salt complex', *Electrochimica Acta*, vol. 37, no. 9, pp. 1671–1673, 1992.

[113] G. B. Appetecchi, F. Croce, and B. Scrosati, 'Kinetics and stability of the lithium electrode in poly (methylmethacrylate)-based gel electrolytes', *Electrochimica Acta*, vol. 40, no. 8, pp. 991–997, 1995.

[114] O. Bohnke, G. Frand, M. Rezrazi, C. Rousselot, and C. Truche, 'Fast ion transport in new lithium electrolytes gelled with PMMA. 1. Influence of polymer concentration', *Solid State Ion.*, vol. 66, no. 1–2, pp. 97–104, 1993.

[115] O. Bohnke, G. Frand, M. Rezrazi, C. Rousselot, and C. Truche, 'Fast ion transport in new lithium electrolytes gelled with PMMA. 2. Influence of lithium salt concentration', *Solid State Ion.*, vol. 66, no. 1–2, pp. 105–112, 1993.

[116] M. Alamgir and K. M. Abraham, ‘Li ion conductive electrolytes based on poly (vinyl chloride)’, *J. Electrochem. Soc.*, vol. 140, no. 6, pp. L96–L97, 1993.

[117] C. Capiglia, Y. Saito, H. Kataoka, T. Kodama, E. Quartarone, and P. Mustarelli, ‘Structure and transport properties of polymer gel electrolytes based on PVdF-HFP and $LiN(C_2F_5SO_2)_2$’, *Solid State Ionics*, vol. 131, pp. 291–299, 2000.

[118] A. Ciferri and A. Perico, Eds., *Ionic interactions in natural and synthetic macromolecules*. Hoboken, N.J: Wiley, 2012.

[119] M. Watanabe *et al.*, ‘High lithium ionic conductivity of polymeric solid electrolytes’, *Macromol. Rapid Commun.*, vol. 2, no. 12, pp. 741–744, 1981.

[120] H. S. Choe, J. Giaccai, M. Alamgir, and K. M. Abraham, ‘Preparation and characterization of poly (vinyl sulfone)-and poly (vinylidene fluoride)-based electrolytes’, *Electrochimica Acta*, vol. 40, no. 13–14, pp. 2289–2293, 1995.

[121] D. Kumar, M. Suleman, and S. A. Hashmi, ‘Studies on poly(vinylidene fluoride-co-hexafluoropropylene) based gel electrolyte nanocomposite for sodium–sulfur batteries’, *Solid State Ion.*, vol. 202, no. 1, pp. 45–53, Nov. 2011.

[122] D. Saikia and A. Kumar, ‘Ionic conduction in P(VDF-HFP)/PVDF–(PC + DEC)–$LiClO_4$ polymer gel electrolytes’, *Electrochimica Acta*, vol. 49, no. 16, pp. 2581–2589, Jul. 2004.

[123] H. Gao, B. Guo, J. Song, K. Park, and J. B. Goodenough, ‘A Composite Gel-Polymer/Glass-Fiber Electrolyte for Sodium-Ion Batteries’, *Adv. Energy Mater.*, vol. 5, no. 9, p. 1402235, May 2015.

[124] Y. Zhu, Y. Yang, L. Fu, and Y. Wu, ‘A porous gel-type composite membrane reinforced by nonwoven: promising polymer electrolyte with high performance for sodium ion batteries’, *Electrochimica Acta*, vol. 224, pp. 405–411, Jan. 2017.

[125] O. Krejza, J. Velická, M. Sedlaříková, and J. Vondrák, ‘The presence of nanostructured Al_2O_3 in PMMA-based gel electrolytes’, *J. Power Sources*, vol. 178, no. 2, pp. 774–778, Apr. 2008.

[126] D. Kumar and S. A. Hashmi, ‘Ion transport and ion–filler-polymer interaction in poly(methyl methacrylate)-based, sodium ion conducting, gel polymer electrolytes dispersed with silica nanoparticles’, *J. Power Sources*, vol. 195, no. 15, pp. 5101–5108, Aug. 2010.

[127] R. Che, W. Yang, J. Wang, and J. Lei, ‘Electrolyte-based antistatic plasticizer for soft poly(vinyl chloride) composites’, *J. Appl. Polym. Sci.*, p. NA-NA, 2010.

[128] Z. Zhang *et al.*, '$Na_{3.4}Zr_{1.8}Mg_{0.2}Si_2PO$ filled poly(ethylene oxide)/$Na(CF_3SO_2)_2N$ as flexible composite polymer electrolyte for solid-state sodium batteries', *J. Power Sources*, vol. 372, pp. 270–275, Dec. 2017.

[129] Y. L. Ni'mah, M.-Y. Cheng, J. H. Cheng, J. Rick, and B.-J. Hwang, 'Solid-state polymer nanocomposite electrolyte of TiO_2/PEO/$NaClO_4$ for sodium ion batteries', *J. Power Sources*, vol. 278, pp. 375–381, Mar. 2015.

[130] K. B. Hueso, V. Palomares, M. Armand, and T. Rojo, 'Challenges and perspectives on high and intermediate-temperature sodium batteries', *Nano Res.*, Jun. 2017.

[131] F. Colò, F. Bella, J. R. Nair, M. Destro, and C. Gerbaldi, 'Cellulose-based novel hybrid polymer electrolytes for green and efficient Na-ion batteries', *Electrochimica Acta*, vol. 174, pp. 185–190, Aug. 2015.

[132] J. R. Nair *et al.*, 'UV-cured methacrylic membranes as novel gel–polymer electrolyte for Li-ion batteries', *J. Power Sources*, vol. 178, no. 2, pp. 751–757, Apr. 2008.

[133] J. Evans, C. A. Vincent, and P. G. Bruce, 'Electrochemical measurement of transference numbers in polymer electrolytes', *Polymer*, vol. 28, no. 13, pp. 2324–2328, 1987.

[134] M. Watanabe, S. Nagano, K. Sanui, and N. Ogata, 'Estimation of Li+ transport number in polymer electrolytes by the combination of complex impedance and potentiostatic polarization measurements', *Solid State Ion.*, vol. 28, pp. 911–917, 1988.

[135] K. M. Abraham, Z. Jiang, and B. Carroll, 'Highly conductive PEO-like polymer electrolytes', *Chem. Mater.*, vol. 9, no. 9, pp. 1978–1988, 1997.

[136] H. Zhang *et al.*, 'Lithium bis(fluorosulfonyl)imide/poly(ethylene oxide) polymer electrolyte', *Electrochimica Acta*, vol. 133, pp. 529–538, Jul. 2014.

[137] M. Dahbi *et al.*, 'Sodium carboxymethyl cellulose as a potential binder for hard-carbon negative electrodes in sodium-ion batteries', *Electrochem. Commun.*, vol. 44, pp. 66–69, Jul. 2014.

[138] I. Hasa, J. Hassoun, Y.-K. Sun, and B. Scrosati, 'Sodium-Ion Battery based on an Electrochemically Converted $NaFePO_4$ Cathode and Nanostructured Tin-Carbon Anode', *ChemPhysChem*, vol. 15, no. 10, pp. 2152–2155, Jul. 2014.

[139] G. Meligrana, C. Gerbaldi, A. Tuel, S. Bodoardo, and N. Penazzi, 'Hydrothermal synthesis of high surface $LiFePO_4$ powders as cathode for Li-ion cells', *J. Power Sources*, vol. 160, no. 1, pp. 516–522, Sep. 2006.

[140] A. Sacco *et al.*, 'Electrodes/Electrolyte Interfaces in the Presence of a Surface-Modified Photopolymer Electrolyte: Application in Dye-Sensitized Solar Cells', *ChemPhysChem*, vol. 16, no. 5, pp. 960–969, Apr. 2015.

[141] C. Gerbaldi *et al.*, 'Innovative high performing metal organic framework (MOF)-laden nanocomposite polymer electrolytes for all-solid-state lithium batteries', *J Mater Chem A*, vol. 2, no. 26, pp. 9948–9954, 2014.

[142] M. Muszyńska, H. Wyciślik, and M. Siekierski, 'Composite polymeric electrolytes based on poly (ethylene oxide) matrix and metallic aluminum filler', *Solid State Ion.*, vol. 147, no. 3, pp. 281–287, 2002.

[143] N. A. Stolwijk, C. Heddier, M. Reschke, M. Wiencierz, J. Bokeloh, and G. Wilde, 'Salt-Concentration Dependence of the Glass Transition Temperature in PEO–NaI and PEO–LiTFSI Polymer Electrolytes', *Macromolecules*, vol. 46, no. 21, pp. 8580–8588, Nov. 2013.

[144] A. Chiappone *et al.*, 'Microfibrillated cellulose as reinforcement for Li-ion battery polymer electrolytes with excellent mechanical stability', *J. Power Sources*, vol. 196, no. 23, pp. 10280–10288, Dec. 2011.

[145] L. Wu, G. Becker, and L. Noels, 'Elastic damage to crack transition in a coupled non-local implicit discontinuous Galerkin/extrinsic cohesive law framework', *Comput. Methods Appl. Mech. Eng.*, vol. 279, pp. 379–409, Sep. 2014.

[146] F. Colò, F. Bella, J. R. Nair, and C. Gerbaldi, 'Light-cured polymer electrolytes for safe, low-cost and sustainable sodium-ion batteries', *J. Power Sources*, vol. 365, pp. 293–302, Oct. 2017.

[147] F. Bella, F. Colò, J. R. Nair, and C. Gerbaldi, 'Photopolymer Electrolytes for Sustainable, Upscalable, Safe, and Ambient-Temperature Sodium-Ion Secondary Batteries', *ChemSusChem*, vol. 8, no. 21, pp. 3668–3676, Nov. 2015.

[148] H. Zhang *et al.*, 'Lithium bis(fluorosulfonyl)imide/poly(ethylene oxide) polymer electrolyte', *Electrochimica Acta*, vol. 133, pp. 529–538, Jul. 2014.

[149] Y. Ma, M. Doyle, T. F. Fuller, M. M. Doeff, L. C. De Jonghe, and J. Newman, 'The measurement of a complete set of transport properties for a concentrated solid polymer electrolyte solution', *J. Electrochem. Soc.*, vol. 142, no. 6, pp. 1859–1868, 1995.

[150] L. Wu, D. Buchholz, D. Bresser, L. Gomes Chagas, and S. Passerini, 'Anatase TiO_2 nanoparticles for high power sodium-ion anodes', *J. Power Sources*, vol. 251, pp. 379–385, Apr. 2014.

[151] T. Uemura, R. Nakanishi, S. Mochizuki, Y. Murata, and S. Kitagawa, 'Radical polymerization of 2,3-dimethyl-1,3-butadiene in coordination nanochannels', *Chem. Commun.*, vol. 51, no. 48, pp. 9892–9895, 2015.

[152] L.-P. Lv *et al.*, 'Precursor-controlled and template-free synthesis of nitrogen-doped carbon nanoparticles for supercapacitors', *RSC Adv.*, vol. 5, no. 62, pp. 50063–50069, 2015.

[153] H. Gao, B. Guo, J. Song, K. Park, and J. B. Goodenough, 'A Composite Gel-Polymer/Glass-Fiber Electrolyte for Sodium-Ion Batteries', *Adv. Energy Mater.*, vol. 5, no. 9, p. 1402235, May 2015.

[154] S. A. Mohd Noor, H. Yoon, M. Forsyth, and D. R. MacFarlane, 'Gelled ionic liquid sodium ion conductors for sodium batteries', *Electrochimica Acta*, vol. 169, pp. 376–381, Jul. 2015.

[155] H. M. Ng, S. Ramesh, and K. Ramesh, 'Exploration on the P(VP-co-VAc) copolymer based gel polymer electrolytes doped with quaternary ammonium iodide salt for DSSC applications: Electrochemical behaviors and photovoltaic performances', *Org. Electron.*, vol. 22, pp. 132–139, Jul. 2015.

[156] C. Cao, W. Liu, L. Tan, X. Liao, and L. Li, 'Sodium-ion batteries using ion exchange membranes as electrolytes and separators', *Chem. Commun.*, vol. 49, no. 100, pp. 11740–11742, 2013.

[157] S. A. Mohd Noor, H. Yoon, M. Forsyth, and D. R. MacFarlane, 'Gelled ionic liquid sodium ion conductors for sodium batteries', *Electrochimica Acta*, vol. 169, pp. 376–381, Jul. 2015.

[158] K. M. Abraham, Z. Jiang, and B. Carroll, 'Highly conductive PEO-like polymer electrolytes', *Chem. Mater.*, vol. 9, no. 9, pp. 1978–1988, 1997.

[159] P. Hovington *et al.*, 'New Lithium Metal Polymer Solid State Battery for an Ultrahigh Energy: Nano C-$LiFePO_4$ versus Nano $Li_{1.2}V_3O_8$', *Nano Lett.*, vol. 15, no. 4, pp. 2671–2678, Apr. 2015.

[160] Y. Ma, M. Doyle, T. F. Fuller, M. M. Doeff, L. C. De Jonghe, and J. Newman, 'The measurement of a complete set of transport properties for a concentrated solid polymer electrolyte solution', *J. Electrochem. Soc.*, vol. 142, no. 6, pp. 1859–1868, 1995.

[161] L. Wu *et al.*, 'Unfolding the Mechanism of Sodium Insertion in Anatase TiO_2 Nanoparticles', *Adv. Energy Mater.*, vol. 5, no. 2, p. 1401142, Jan. 2015.

[162] Z. Bi *et al.*, 'Self-organized amorphous TiO_2 nanotube arrays on porous Ti foam for rechargeable lithium and sodium ion batteries', *J. Power Sources*, vol. 222, pp. 461–466, Jan. 2013.

[163] J. R. González, R. Alcántara, F. Nacimiento, G. F. Ortiz, and J. L. Tirado, 'Self-organized, anatase, double-walled nanotubes prepared by anodization under voltage ramp as negative electrode for aqueous sodium-ion batteries', *J. Electrochem. Soc.*, vol. 162, no. 2, pp. A3007–A3012, 2015.

[164] M. Peng *et al.*, 'Ruthenium-Oxide-Coated Sodium Vanadium Fluorophosphate Nanowires as High-Power Cathode Materials for Sodium-Ion Batteries', *Angew. Chem. Int. Ed.*, vol. 54, no. 22, pp. 6452–6456, May 2015.

[165] W. Huang *et al.*, 'A New Route Toward Improved Sodium Ion Batteries: A Multifunctional Fluffy $Na_{0.67}FePO_4$/CNT Nanocactus', *Small*, vol. 11, no. 18, pp. 2170–2176, May 2015.

[166] C. Gerbaldi, M. Destro, J. R. Nair, S. Ferrari, I. Quinzeni, and E. Quartarone, 'High-rate V_2O_5-based Li-ion thin film polymer cell with outstanding long-term cyclability', *Nano Energy*, vol. 2, no. 6, pp. 1279–1286, Nov. 2013.

[167] J. R. Nair, L. Porcarelli, F. Bella, and C. Gerbaldi, 'Newly Elaborated Multipurpose Polymer Electrolyte Encompassing RTILs for Smart Energy-Efficient Devices', *ACS Appl. Mater. Interfaces*, vol. 7, no. 23, pp. 12961–12971, Jun. 2015.

[168] Q. Ma *et al.*, 'A new Na[(FSO_2)(n-$C_4F_9SO_2$)N]-based polymer electrolyte for solid-state sodium batteries', *J. Mater. Chem. A*, vol. 5, no. 17, pp. 7738–7743, 2017.

[169] H. Che *et al.*, 'Electrolyte design strategies and research progress for room-temperature sodium-ion batteries', *Energy Environ. Sci.*, vol. 10, no. 5, pp. 1075–1101, 2017.

[170] X. Liu *et al.*, 'An interpenetrating network poly(diethylene glycol carbonate)-based polymer electrolyte for solid state lithium batteries', *J. Mater. Chem. A*, vol. 5, no. 22, pp. 11124–11130, 2017.

[171] Y. Zhou *et al.*, 'Cationic two-dimensional sheets for an ultralight electrostatic polysulfide trap toward high-performance lithium-sulfur batteries', *Energy Storage Mater.*, vol. 9, pp. 39–46, Oct. 2017.

[172] C. Berthier, W. Gorecki, M. Minier, M. B. Armand, J. M. Chabagno, and P. Rigaud, 'Microscopic investigation of ionic conductivity in alkali metal salts-poly (ethylene oxide) adducts', *Solid State Ion.*, vol. 11, no. 1, pp. 91–95, 1983.

[173] M. Armand, 'The history of polymer electrolytes', *Solid State Ion.*, vol. 69, no. 3–4, pp. 309–319, 1994.

[174] J. R. Nair, L. Porcarelli, F. Bella, and C. Gerbaldi, 'Newly Elaborated Multipurpose Polymer Electrolyte Encompassing RTILs for Smart Energy-Efficient Devices', *ACS Appl. Mater. Interfaces*, vol. 7, no. 23, pp. 12961–12971, Jun. 2015.

[175] V. P. Indran, A. S. Haji Saud, G. P. Maniam, M. M. Yusoff, Y. H. Taufiq-Yap, and M. H. Ab. Rahim, 'Versatile boiler ash containing potassium silicate for the synthesis of organic carbonates', *RSC Adv.*, vol. 6, no. 41, pp. 34877–34884, 2016.

[176] D. Bamford, A. Reiche, G. Dlubek, F. Alloin, J.-Y. Sanchez, and M. A. Alam, 'Ionic conductivity, glass transition, and local free volume in

poly(ethylene oxide) electrolytes: Single and mixed ion conductors', *J. Chem. Phys.*, vol. 118, no. 20, pp. 9420–9432, May 2003.

[177] M. Forsyth, P. Meakin, D. R. MacFarlane, and A. J. Hill, 'Free volume and conductivity of plasticized polyether-urethane solid polymer electrolytes', *J. Phys. Condens. Matter*, vol. 7, no. 39, p. 7601, 1995.

[178] M. Forsyth, J. Sun, D. R. MacFarlane, and A. J. Hill, 'Compositional dependence of free volume in PAN/$LiCF_3SO_3$ polymer-in-salt electrolytes and the effect on ionic conductivity', *J. Polym. Sci. Part B Polym. Phys.*, vol. 38, no. 2, pp. 341–350, 2000.

[179] J. R. Nair, L. Porcarelli, F. Bella, and C. Gerbaldi, 'Newly Elaborated Multipurpose Polymer Electrolyte Encompassing RTILs for Smart Energy-Efficient Devices', *ACS Appl. Mater. Interfaces*, vol. 7, no. 23, pp. 12961–12971, Jun. 2015.

[180] L. Porcarelli, C. Gerbaldi, F. Bella, and J. R. Nair, 'Super Soft All-Ethylene Oxide Polymer Electrolyte for Safe All-Solid Lithium Batteries', *Sci. Rep.*, vol. 6, no. 1, Apr. 2016.

[181] Q. Pan, Z. Li, W. Zhang, D. Zeng, Y. Sun, and H. Cheng, 'Single ion conducting sodium ion batteries enabled by a sodium ion exchanged poly(bis(4-carbonyl benzene sulfonyl)imide-co-2,5-diamino benzesulfonic acid) polymer electrolyte', *Solid State Ion.*, vol. 300, pp. 60–66, Feb. 2017.

[182] R. J. Sengwa, S. Sankhla, and S. Choudhary, 'Effect of melt compounding temperature on dielectric relaxation and ionic conduction in PEO–$NaClO_4$–MMT nanocomposite electrolytes', *Ionics*, vol. 16, no. 8, pp. 697–707, Nov. 2010.

[183] J. Mindemark, R. Mogensen, M. J. Smith, M. M. Silva, and D. Brandell, 'Polycarbonates as alternative electrolyte host materials for solid-state sodium batteries', *Electrochem. Commun.*, vol. 77, pp. 58–61, Apr. 2017.

[184] M. Stainer, L. C. Hardy, D. H. Whitmore, and D. F. Shriver, 'Stoichiometry of formation and conductivity response of amorphous and crystalline complexes formed between poly (ethylene oxide) and ammonium salts: PEOxNH_4SCN and PEOx$NH_4SO_3CF_3$', *J. Electrochem. Soc.*, vol. 131, no. 4, pp. 784–790, 1984.

[185] J. Evans, C. A. Vincent, and P. G. Bruce, 'Electrochemical measurement of transference numbers in polymer electrolytes', *Polymer*, vol. 28, no. 13, pp. 2324–2328, 1987.

[186] F. Bella, F. Colò, J. R. Nair, and C. Gerbaldi, 'Photopolymer Electrolytes for Sustainable, Upscalable, Safe, and Ambient-Temperature Sodium-Ion Secondary Batteries', *ChemSusChem*, vol. 8, no. 21, pp. 3668–3676, Nov. 2015.

[187] E. Quartarone and P. Mustarelli, ‘Electrolytes for solid-state lithium rechargeable batteries: recent advances and perspectives’, *Chem. Soc. Rev.*, vol. 40, no. 5, p. 2525, 2011.

[188] M. D. Slater, D. Kim, E. Lee, and C. S. Johnson, ‘Sodium-Ion Batteries’, *Adv. Funct. Mater.*, vol. 23, no. 8, pp. 947–958, Feb. 2013.

[189] G. Longoni *et al.*, ‘Shape-Controlled TiO_2 Nanocrystals for Na-Ion Battery Electrodes: The Role of Different Exposed Crystal Facets on the Electrochemical Properties’, *Nano Lett.*, vol. 17, no. 2, pp. 992–1000, Feb. 2017.

[190] M. N. Tahir *et al.*, ‘Extraordinary Performance of Carbon-Coated Anatase TiO_2 as Sodium-Ion Anode’, *Adv. Energy Mater.*, vol. 6, no. 4, p. 1501489, Feb. 2016.

[191] X. Zhu *et al.*, ‘Graphene-Modified TiO_2 Microspheres Synthesized by a Facile Spray-Drying Route for Enhanced Sodium-Ion Storage’, *Part. Part. Syst. Charact.*, vol. 33, no. 8, pp. 545–552, Aug. 2016.

[192] H. Tao, M. Zhou, K. Wang, S. Cheng, and K. Jiang, ‘Glycol Derived Carbon-TiO_2 as Low Cost and High Performance Anode Material for Sodium-Ion Batteries’, *Sci. Rep.*, vol. 7, p. 43895, Mar. 2017.

[193] S. Li *et al.*, ‘Alternating voltage induced ordered anatase TiO_2 nanopores: An electrochemical investigation of sodium storage’, *J. Power Sources*, vol. 336, pp. 196–202, Dec. 2016.

[194] A. Lamberti, N. Garino, A. Sacco, S. Bianco, A. Chiodoni, and C. Gerbaldi, ‘As-grown vertically aligned amorphous TiO_2 nanotube arrays as high-rate Li-based micro-battery anodes with improved long-term performance’, *Electrochimica Acta*, vol. 151, pp. 222–229, Jan. 2015.

[195] *DIRECTIVE 2006/66/EC OF THE EUROPEAN PARLIAMENT AND OF THE COUNCIL*. 2006, p. L 266/1-L 266/14.

[196] H. Chen, M. Armand, G. Demailly, F. Dolhem, P. Poizot, and J.-M. Tarascon, ‘From Biomass to a Renewable $Li_XC_6O_6$ Organic Electrode for Sustainable Li-Ion Batteries’, *ChemSusChem*, vol. 1, no. 4, pp. 348–355, Apr. 2008.

[197] D. L. Williams, J. J. Byrne, and J. S. Driscoll, ‘A High Energy Density Lithium/Dichloroisocyanuric Acid Battery System’, vol. 116, no. 1, pp. 2–4, 1969.

[198] Q. Zhao, Y. Lu, and J. Chen, ‘Advanced Organic Electrode Materials for Rechargeable Sodium-Ion Batteries’, *Adv. Energy Mater.*, vol. 7, no. 8, p. 1601792, Apr. 2017.

[199] F. Xu, J. Xia, and W. Shi, ‘Anthraquinone-based polyimide cathodes for sodium secondary batteries’, *Electrochem. Commun.*, vol. 60, pp. 117–120, Nov. 2015.

[200] W. Luo, M. Allen, V. Raju, and X. Ji, ‘An Organic Pigment as a High-Performance Cathode for Sodium-Ion Batteries’, *Adv. Energy Mater.*, vol. 4, no. 15, p. 1400554, Oct. 2014.

[201] E. Castillo-Martínez, J. Carretero-González, and M. Armand, ‘Polymeric Schiff Bases as Low-Voltage Redox Centers for Sodium-Ion Batteries’, *Angew. Chem. Int. Ed.*, vol. 53, no. 21, pp. 5341–5345, May 2014.

[202] C. Guo, K. Zhang, Q. Zhao, L. Pei, and J. Chen, ‘High-performance sodium batteries with the 9,10-anthraquinone/CMK-3 cathode and an ether-based electrolyte’, *Chem. Commun.*, vol. 51, no. 50, pp. 10244–10247, 2015.

[203] Z. Luo, L. Liu, Q. Zhao, F. Li, and J. Chen, ‘An Insoluble Benzoquinone-Based Organic Cathode for Use in Rechargeable Lithium-Ion Batteries’, *Angew. Chem. Int. Ed.*, vol. 56, no. 41, pp. 12561–12565, Oct. 2017.

[204] C. Luo *et al.*, ‘Graphene oxide wrapped croconic acid disodium salt for sodium ion battery electrodes’, *J. Power Sources*, vol. 250, pp. 372–378, Mar. 2014.

[205] K. Chihara, N. Chujo, A. Kitajou, and S. Okada, ‘Cathode properties of $Na_2C_6O_6$ for sodium-ion batteries’, *Electrochimica Acta*, vol. 110, pp. 240–246, Nov. 2013.

[206] S. Maiti, A. Pramanik, T. Dhawa, and S. Mahanty, ‘Redox-active organic molecular salt of 1,2,4-benzenetricarboxylic acid as lithium-ion battery anode’, *Mater. Lett.*, vol. 209, pp. 613–617, Dec. 2017.

[207] V. Medabalmi, G. Wang, V. K. Ramani, and K. Ramanujam, ‘Lithium salt of biphenyl tetracarboxylate as an anode material for Li/Na-ion batteries’, *Appl. Surf. Sci.*, vol. 418, pp. 9–16, Oct. 2017.

[208] F. Wan *et al.*, ‘Nanoeffects promote the electrochemical properties of organic $Na_2C_8H_4O_4$ as anode material for sodium-ion batteries’, *Nano Energy*, vol. 13, pp. 450–457, Apr. 2015.

[209] Z. Song, H. Zhan, and Y. Zhou, ‘Polyimides: Promising Energy-Storage Materials’, *Angew. Chem. Int. Ed.*, vol. 49, no. 45, pp. 8444–8448, Nov. 2010.

[210] S. Renault, J. Geng, F. Dolhem, and P. Poizot, ‘Evaluation of polyketones with N-cyclic structure as electrode material for electrochemical energy storage: case of pyromellitic diimide dilithium salt’, *Chem Commun*, vol. 47, no. 8, pp. 2414–2416, 2011.

[211] M. López-Herraiz, E. Castillo-Martínez, J. Carretero-González, J. Carrasco, T. Rojo, and M. Armand, ‘Oligomeric-Schiff bases as negative electrodes for

sodium ion batteries: unveiling the nature of their active redox centers', *Energy Environ. Sci.*, vol. 8, no. 11, pp. 3233–3241, 2015.

[212] K. Nakahara *et al.*, 'Rechargeable batteries with organic radical cathodes', *Chem. Phys. Lett.*, vol. 359, no. 5, pp. 351–354, 2002.

[213] Y. Dai, Y. Zhang, L. Gao, G. Xu, and J. Xie, 'A Sodium Ion Based Organic Radical Battery', *Electrochem. Solid-State Lett.*, vol. 13, no. 3, p. A22, 2010.

[214] J.-K. Kim, 'Micro-fibrous organic radical electrode to improve the electrochemical properties of organic rechargeable batteries', *J. Power Sources*, vol. 242, pp. 683–686, Nov. 2013.

[215] L. W. Shacklette, J. E. Toth, N. S. Murthy, and R. H. Baughman, 'Polyacetylene and polyphenylene as anode materials for nonaqueous secondary batteries', *J. Electrochem. Soc.*, vol. 132, no. 7, pp. 1529–1535, 1985.

[216] X. Chen *et al.*, 'The excellent cycling stability and superior rate capability of polypyrrole as the anode material for rechargeable sodium ion batteries', *RSC Adv.*, vol. 6, no. 3, pp. 2345–2351, 2016.

[217] D. Su, J. Zhang, S. Dou, and G. Wang, 'Polypyrrole hollow nanospheres: stable cathode materials for sodium-ion batteries', *Chem. Commun.*, vol. 51, no. 89, pp. 16092–16095, 2015.

[218] M. Zhou, J. Qian, X. Ai, and H. Yang, 'Redox-Active $Fe(CN)_6^{4-}$ -Doped Conducting Polymers with Greatly Enhanced Capacity as Cathode Materials for Li-Ion Batteries', *Adv. Mater.*, vol. 23, no. 42, pp. 4913–4917, Nov. 2011.

[219] Z. Song and H. Zhou, 'Towards sustainable and versatile energy storage devices: an overview of organic electrode materials', *Energy Environ. Sci.*, vol. 6, no. 8, pp. 2280–2301, Jul. 2013.

[220] Y. Park *et al.*, 'Sodium Terephthalate as an Organic Anode Material for Sodium Ion Batteries', *Adv. Mater.*, vol. 24, no. 26, pp. 3562–3567, Jul. 2012.

[221] V. A. Mihali, S. Renault, L. Nyholm, and D. Brandell, 'Benzenediacrylates as organic battery electrode materials: Na versus Li', *RSC Adv*, vol. 4, no. 72, pp. 38004–38011, 2014.

[222] V. A. Oltean, B. Philippe, S. Renault, R. Félix Duarte, H. Rensmo, and D. Brandell, 'Investigating the Interfacial Chemistry of Organic Electrodes in Li- and Na-Ion Batteries', *Chem. Mater.*, vol. 28, no. 23, pp. 8742–8751, Dec. 2016.

[223] C. Fongy, A.-C. Gaillot, S. Jouanneau, D. Guyomard, and B. Lestriez, 'Ionic vs electronic power limitations and analysis of the fraction of wired grains in $LiFePO_4$ composite electrodes', *J. Electrochem. Soc.*, vol. 157, no. 7, pp. A885–A891, 2010.

[224] V. A. Oltean, S. Renault, and D. Brandell, ‘Enhanced performance of organic materials for lithium-ion batteries using facile electrode calendaring techniques’, *Electrochem. Commun.*, vol. 68, pp. 45–48, Jul. 2016.